A New Optical Configuration for Flow Cytometric Sorting of Bovine Spermatozoa by Sex

A thesis submitted to the
University of Waikato
for the degree
of
Doctor of Philosophy in Physics
by

Johnathan Charles Sharpe

The
University
of Waikato
Te Whare Wānanga
o Waikato

Hamilton, New Zealand

April 1997

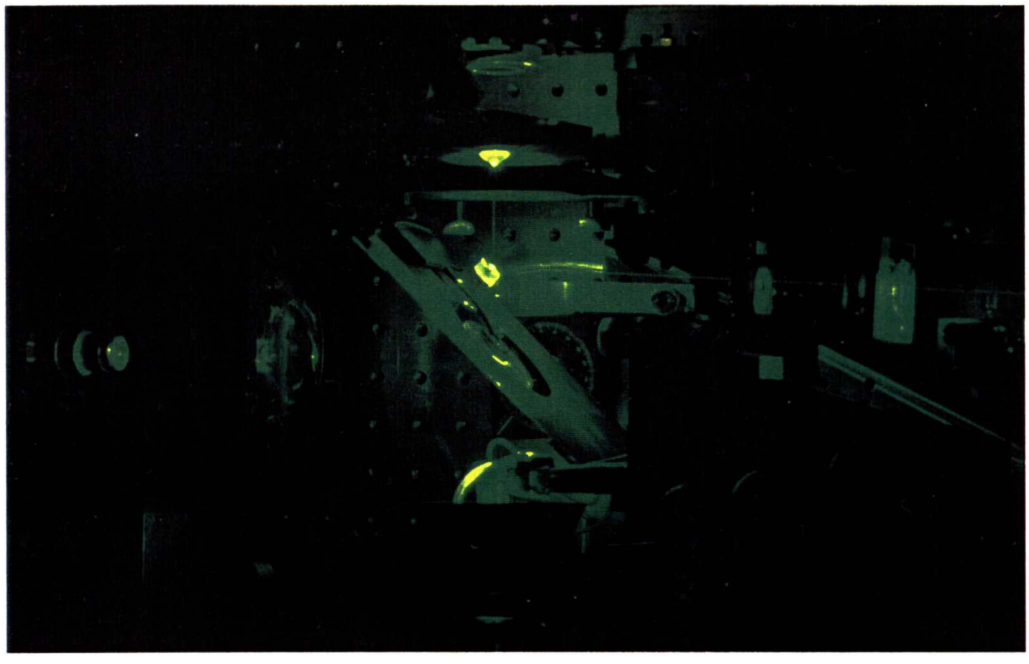

A photograph of the radially symmetric optics developed for sperm sexing.

Preface

Mankind's interest in predetermining the sex of offspring is an age old phenomenon. Fifth century Greek philosophers such as Hippocrates and Aristotle proposed a variety of pre-natal sex selection measures (Levin 1987). In the middle ages, a brew of wine and lion's blood, when consumed by the prospective mother prior to intercourse and during the appropriate lunar phase, was proposed to yield a male child. In the 18th century, it was believed that sperm from the right testis produced more male young, while sperm from the left testis produced more females. Another popular assumption of the early 20th century, not unlike a well-known nursery rhyme, was that boys would be conceived if expectant mothers ate bitter or sour food and red meat, while the consumption of sweets, cakes, and vegetables should guarantee the delivery of a girl.

Such practices as those outlined above were based less on empirical evidence than on the assumption that sex was determined 'not by inheritance but by the combined effect of external conditions' (Farley 1982). Recognition of the fact that in mammals fertilisation by X-chromosome-bearing sperm produces females, and Y-sperm males, has resulted in most of the recent (20th century) attempts at preconceptual sex selection involving the X:Y ratio in a sperm population.

The ability to resolve X- and Y-chromosome-bearing sperm populations has important applications for controlling the sex of offspring of agricultural animals. Any method which influences the sex ratio would provide a strong stimulus to genetic progress in animal husbandry, and should produce substantial economic benefits. The genetic pool of breeding stock could be rapidly and predictably altered, and undesirable or lethal sex-linked recessive traits might be eliminated or controlled.

A relatively new technology, flow cytometry, allows the laws of physics to be used through a combination of fluidics, optics and electronics to distinguish and sort mammalian sperm according to X or Y DNA content. If coupled with artificial insemination and embryo transfer, this technology provides a method for gender preselection. This method could be used to increase the efficiency of livestock production for an ever-growing world population.

Abstract

The orthogonal axes of illumination, flow, and detection in conventional sorting flow cytometers can limit accuracy or throughput when making fluorescence measurements on aspherical cells. We report a new radially symmetric optical configuration that has been designed to overcome these problems. This system has specifically been developed for high resolution DNA chromosome content measurement in cells with an ultimate goal to separate X- and Y-chromosome-bearing mammalian spermatozoa.

The new optics design provides radially symmetric illumination and detection of asymmetric particles while retaining the sort capability of a jet-in-air (or cylindrical cuvette) design. A paraboloidal reflector, symmetrical about the sample stream flow axis, both focuses a laser excitation beam and collects cell scatter and fluorescence from the inspection point.

The performance of the new optical configuration has been tested and compared to that of a conventional (orthogonal optical geometry) flow cytometer for a variety of particles and cells. For fluorescence measurements on calibration microspheres the new system produces histograms with similar coefficients of variation to those obtained with the conventional cytometer. Optical artifacts apparent in measurements on flat cells, such as blood cells and mammalian sperm, using conventional optics are overcome by the new configuration. Analysis of chinchilla sperm yields a dual-peaked histogram population that has a coefficient of variation and X-Y split which matches that for a gated (oriented) fraction of the sample as measured by the orthogonal system. Bovine sperm, which are larger and flatter than chinchilla sperm, also produce a single population which, when low sample to sheath differential pressures are used, has coefficients of variation matching those for an oriented subpopulation as measured by conventional optics.

Further modifications to the radial optics system have been carried out to study the effect of cell orientation (with respect to the excitation source) on fluorescence. A ray tracing model has been developed to explain the optical artifacts associated with the measurement of aspherical cells in orthogonal flow systems. This model has been used to verify the experimental findings from our cell orientation studies.

The radially symmetric optics we have described can be used to overcome the optical artifacts which decrease the accuracy of optical measurements on aspherical cells. With an added electrostatic sort capability, this system provides the high speed sort rates of conventional jet in air flow cytometers. The system presents an alternative, orientation-independent technique for measuring aspherical cells independent of their orientation. This optical configuration may provide a means for increasing throughput and accuracy for sperm sexing and other applications which require high resolution measurement and sorting of aspherical particles or cells.

Acknowledgements

There are numerous people to whom I am very grateful and without whose help the success of this research project would not have been possible.

First, I would like to thank my supervisors, Peter Schaare and Rainer Künnemeyer, for their guidance and stimulus throughout my research. I would particularly like to thank the staff of the Engineering Development Group for their encouragement and help, and I would also like to thank the staff and students of the Physics department for their friendship.

I am indebted to Sue Beaumont and Mike Gurnsey for their assistance and for many fruitful discussions. I am also grateful to AgResearch for allowing me access to an operational flow cytometer for the experimental work of this thesis. Thanks must also go to Graeme Bauchop of Becton Dickinson (Australia) for the loan of PC LYSIS software to analyse the HP format flow cytometer data.

I am very grateful to Larry Johnson, Glenn Welch, and Wim Rens of the United States Department of Agriculture for their assistance, and for many thought-provoking discussions.

Thanks must go to the University of Waikato and the Horticulture and Food Research Institute of New Zealand for financial assistance through scholarships. In addition, I would like to thank Howell Round and Kevin O'Donnel for providing financial support to present this research at the Photonics West '97 Symposium.

I am very grateful to Bob Jordan, Simon Barbour and Don Bond for their endless patience with computer advice and support. I would also like to thank the Physics Department of the University of Otago, and in particular, Rob Ballagh for providing me with resources to complete this thesis.

I would also like to thank the Eschmann family for their encouragement. I am also very appreciative to Heidi for sorting out numerous administrative requests.

Thanks must go to my friends, with whom I have enjoyed many stimulating evenings of wine and conversation. I would also like to thank Janine for proof-reading the final draft of this thesis.

I would like to thank my family, Mum, Dad, Geoff, Judy and Helen, for their support throughout my university studies.

Above all, I would like to thank Andrea for her endless encouragement, patience and support.

Table of Contents

List of Figures

List of Tables

Acronyms

AI	artificial insemination
ADC	analogue to digital conversion
CCD	charge coupled device
CRBC	chicken red blood cells
CV	coefficient of variation
DNA	deoxyribonucleic acid
DPBS	Dulbeccos's Phosphate Buffered Saline
FACS	fluorescence activated cell sorter
FWHM	full width half maximum
MACS	magnetic cell sorting
NA	numerical aperture
OFCM	orienting flow cytometer
PI	propidium iodide
PMT	photomultiplier tube
TEM	transverse excitation mode
USDA	United States Department of Agriculture
UV	ultra-violet
X	X-chromosome-bearing
Y	Y-chromosome-bearing

1. Introduction

The capability of sorting domestic animal sperm into two sub-populations, one containing the X- and the other the Y-bearing-chromosome, is of great scientific and economic interest. More specifically, the capability to artificially inseminate dairy or beef herds with sexed semen would be of considerable economic advantage to the farmer. With a natural sex ratio of 1 male to 1 female, a dairy farmer would inseminate the best half of a dairy herd with dairy bull semen to obtain a sufficient number of heifer calves, assuming a herd replacement rate of 25% per year. However, using a sexed straw of sperm, the required number of cattle to be inseminated with dairy bull sperm would be reduced to one quarter. The remaining 75% of cows in the herd could then be inseminated with semen from beef bulls which would produce calves suitable for meat production. This breeding technique would then reduce the genetic wastage faced at present by farmers who have no option but to send male (bobby) calves to the freezing works, and would double the rate of genetic gain in the herd, as only the top 25%, rather than the top 50%, of the herd would be used for breeding replacements. Other areas in which sex selection would be beneficial include the rapid upgrading of stock, the husbandry of single sex groups, and the management of endangered species or rare breeds of mammals.

Flow cytometry is a tool that has recently (over the last ten years) been used in the analysis and separation of mammalian spermatozoa - a branch of biology and genetics often termed 'sperm sexing'. Flow cytometry is currently the only scientifically proven means for viable sperm sexing, where sperm retain their ability to fertilise an egg. This method seems to be the most promising for separating sperm by sex for commercial artificial insemination (AI).

Flow cytometry uses specific measurable characteristics to tag a cell. One characteristic used is the uptake of stain by the deoxyribonucleic acid (DNA) material within a cell. When the stained cell, carried by a microscopic jet of fluid, passes through an intensely focused excitation light, the stain will fluoresce with an intensity proportional to the DNA content. This fluorescent light can be detected and processed electronically to characterise a particular cell, and the information can then be used to electrostatically separate cells into sub-populations according to certain desired characteristics.

The commercial flow cytometer draws on a number of physical disciplines including fluidics, optics, analogue and digital electronics, and data acquisition. Several properties of each cell, such as size, structure and internal cellular content can be detected as the cells pass through the illuminated observation point. Particles as small in size as 0.1μm are detectable and the accuracy of measurement for commercial flow cytometers can reach the precision of a few percent at analysis rates of several thousand cells per second.

The progress of accurate flow cytometric analysis of sperm has been hindered by several inherent cellular properties and technical difficulties as detailed in Chapter 3. As a result of these difficulties, sort rates of

sperm have been limited to a maximum of less than two hundred per second (Rens 1996). This figure may seem impressive at first glance, however two to ten million cells are required for a single straw of viable semen for AI. This means an operation time of 4 to 20 hours would be required for the separation of one straw for the insemination of one cow. Besides making cytometric separation an uneconomic option for the farmer, times of this duration make the process unfeasible because of the short and fragile lifetime of sperm under flow cytometric sorting conditions (approximately 48 hours).

The research that has been carried out to date is part of an objective to improve the maximum sperm sorting rates of a flow cytometer with specific application to gender preselection of bovine spermatozoa by DNA content. The work contained in this thesis was carried out by introducing a new optical configuration to overcome many of the problems that presently limit maximum sort rates. The research for this thesis has principally been concerned with development of a new flow cytometer optical configuration for the analysis of asymmetric cells such as bovine sperm.

The sperm sexing project was funded by the Foundation for Research Science and Technology as part of the 'Innovative Engineering in Pastoral Research' program being undertaken at the Technology Development Group (TDG), Ruakura. TDG is a science group of The Horticulture and Food Research Institute of New Zealand (HortResearch).

1.1 Thesis Outline

This thesis is divided into eight Chapters. In Chapter 2 a historical account of the development of flow cytometry, from early beginnings to the research tool used in laboratories today is presented. The flow cytometric components of fluidics, optics, electronics and analysis are also described, and the sequential operation of these physical aspects in order to analyse and sort cells in a non-destructive manner is discussed. Several clinical and research applications of flow cytometry are outlined.

The role of sperm in sex determination for mammals is described in Chapter 3. The morphology and physical characteristics of bull sperm cells, and how these characteristics have complicated the measurement of X- and Y-bearing sperm are also discussed. The historical attempts to overcome these complications, and the current method of sorting sperm by DNA sex content, are also outlined.

In Chapter 4 a new optical configuration is presented that has been designed and built specifically for the measurement of fluorescence from DNA-stained aspherical cells such as bull sperm. The operation and performance of this system is measured and compared to a conventional, orthogonal optical geometry.

Chapter 5 presents data from our experimentation of fluorescence measurements for several particles and cells. Several experiments were performed on a comparative basis between the radial and orthogonal optics of a commercial flow cytometer.

A mathematical model is presented in Chapter 6 to explain the optical artifacts which are associated with the measurement of bull sperm DNA content using flow cytometry. This model is extended to confirm our experimental findings. Further experiments have been carried out to test the validity of the model with regard to cell illumination effects.

The prospects for using the radial optics for sperm sexing in a commercial sense are outlined in Chapter 7. Performance of the system is evaluated and compared to that for conventional flow cytometric techniques.

In Chapter 8 we conclude with final remarks of the performance of the system, and how the objectives of this research have been met.

2. An Introduction to Flow Cytometry

The flow cytometer is an instrument that measures cells or other particles as they flow in single file through a sensing region. The addition of sorting capabilities to a flow cytometer makes possible the isolation of highly enriched populations of cells with precisely defined characteristics. The sorting flow cytometer systematically combines fluidics, optics, electronics, and computer software to analyse and sort biological cells or other particles in a non-destructive manner. It is this technology which is used to separate sperm by sex, based on total DNA content.

This chapter details the history of flow cytometry, from initial methods using a microscope, to current multi-wavelength instrument technology (Section 2.1). The process that an individual cell undergoes as it flows through a cytometer before being sorted is described (Section 2.2), and subsequently each component which serves the cytometer process is outlined in more detail (Sections 2.3-2.7). Finally, several clinical and research applications of flow cytometry are discussed (Section 2.8).

2.1 History of Flow Cytometry

Flow cytometry has developed over the last 25 years from an instrument initially intended to count and size particles, into a sophisticated analytical tool for rapidly quantifying chemical and physical properties of individual cells or cellular constituents of inhomogeneous populations. Much of the early work in flow cytometry development was stimulated by efforts to automate the detection of cancer cells in clinical specimens.

Automated flow analysis of single cells had its beginning in the early 1930s when Moldavan (Melamed 1991) reported a bright-field photoelectric method for counting individual cells on a microscope stage. However, this capillary flow cell design was limited in sensitivity and standardised measurements were difficult to obtain.

Early instruments were plagued with frequent obstruction of the required narrow flow channels by large cells or large clusters of particles. In 1953, Crosland-Tayor used the classical Reynolds laminar sheath flow principle to count red blood cells. This permitted a wide diameter flow channel to be used with a narrow, centrally injected aqueous suspension of cells. Thus, the basis of hydrodynamic focusing was established. Hydrodynamic focusing served two purposes; it virtually eliminated any possibility of flow channel blockage, and it allowed precise centering of the sample stream. Essentially all flow cytometers use this technique today.

Modern flow-system instrumentation development began in the 1950s with Coulter's design (Coulter 1956) of an instrument that measured the volume of cells by means of electrical resistance changes as they passed through a small orifice suspended in a conducting electrolyte solution.

A photoelectric particle counter was developed by Bernie and Hutcheon (1957) which, in principle, was similar to that of Moldavan. Suspended particles were drawn through a capillary under the objective of a microscope. A photomultiplier was mounted above the microscope eyepiece and produced electrical impulses corresponding to the extinction of light by particles. Particle size distributions could also be obtained from conductivity measurements, and mean particle size from counts of the number of particles per gram.

Two concepts which extended the potential applications of flow cytometry were introduced by Kamentsky *et al.* (1967): one was the use of spectrophotometry to quantify specific cellular constituents, and the other was that of cell classification by a combination of several simultaneous measurements of different cellular features. They reported a flow system for measuring UV absorption of nucleic acid and visible light scatter simultaneously on unstained cells at rates of up to 500 cells s^{-1}. Kamentsky *et al.* were the first to display and analyse multiparameter flow cytometry data by means of a two-dimensional histogram. Subsequently, Kamentsky (1969) reported a flow cytometer capable of carrying out up to four simultaneous measurements per cell, and were the first to use an interfaced computer for recording and analysis.

In 1968, Dittrich and Ghöde developed a system which used a high numerical aperture objective to measure fluorescence and phosphorescence of particles moving through the focal plane in a flow stream parallel to the optical axis. The same objective could then be used both for fluorescence excitation with Köhler illumination, and for collecting emitted fluorescence (Melamed 1991). The high numerical aperture of this system meant conventional xenon or high pressure mercury arc sources would provide sufficient illumination, and excitation wavelength bands would be available from ultra-violet into the visible spectrum.

Van Dilla *et al.* (1969) developed the first instrument having orthogonal axes of flow, illumination and detection. This system used a laminar flow chamber design and introduced the argon-ion laser as a light source for flow cytometry. The orthogonal system promoted further development of fluorescence and scatter sensors, and resulted in the first DNA histograms that clearly defined different phases of the cell cycle.

High speed separation of cells was first reported by Fulwyler (1965). Fulwyler adapted the electrostatic ink jet droplet deflection technique of Sweet (1965), which is essentially the same technology as that used in bubble jet printers today. Several alternative techniques such as pneumatic, hydraulic and fluidic methods for sorting cells have been investigated. However, the fastest and most efficient sorting device which remains in use on commercial flow cytometers is the technique of electrostatic deflection of cell-containing droplets described by Fulwyler. Operation of the sorter was simplified by Bonner *et al.* (1972a,b) and improved by carrying out cell measurement in the fluid stream, beyond the nozzle of the

flow chamber but before droplet formation occurred. The sorting of X- and Y-bearing sperm for sperm sexing is achieved by this process.

During the early years of instrument development, most of the studies carried out in cytometry were connected with characterisation of blood cells and cancer cell identification. While much engineering development continued in flow cytometer optics and multiple light sources, today's commercial sorting flow cytometers use the same basic principles of fluorescence measurement and electrostatic deflection. Technological advances in microprocessor and software capabilities has provided powerful data acquisition and analysis systems. Flow cytometric development now focuses on cell preparation, new fluorescent dyes, and markers of cell properties, which lead to an ever increasing number of biological and biomedical applications. Flow cytometers are employed in applications from routine clinical analysis of blood specimens, to AIDs research, oceanography, mapping the human genome, and now genetic selection through sperm sexing.

2.2 Sorting Flow Cytometer Operation

The operation of a sorting flow cytometer combines the technologies of optics, fluidics, electronics, and electrostatics to differentiate and sort a fraction of cells from a population. Cells are forced through an intense light source for illumination and any stain that is bound to the cells is excited and fluoresces. This fluorescence, along with any light scattered, can be detected and used to characterise each cell. Cells of interest can then be sorted from the main population using electrostatic droplet deflection. Figure 2-1 illustrates the key features of a sorting flow cytometer. A description of each of the components follows.

1. Particles which are suspended in a carrier fluid, are forced through a nozzle to form the liquid into a continuous jet.
2. Particles travel through an observation region in single file where they are illuminated by an intense source.
3. The particles scatter and absorb the incident light and fluoresce. Photons from the particles are collected on two or more photodetectors located behind and at right angles to the incident beam.
4. Electronic circuitry uses the photodetector signals to perform particle classification according to the optical characteristics of individual particles.
5. A piezoceramic crystal applies a mechanical oscillation to the jet which causes the formation of droplets with uniform size and spacing.
6. When a particle that is to be deflected becomes contained within a forming droplet, an electric potential is applied via the conductive filter to the jet fluid. As the droplet breaks free from the jet, it retains a net surface charge.

7. The droplet passes through an electric field perpendicular to its direction of travel and, if charged, is caused to deviate by electrostatic force.

8. The droplet exits the field with a lateral velocity component that will continue to displace it from its original vertical trajectory until it is collected

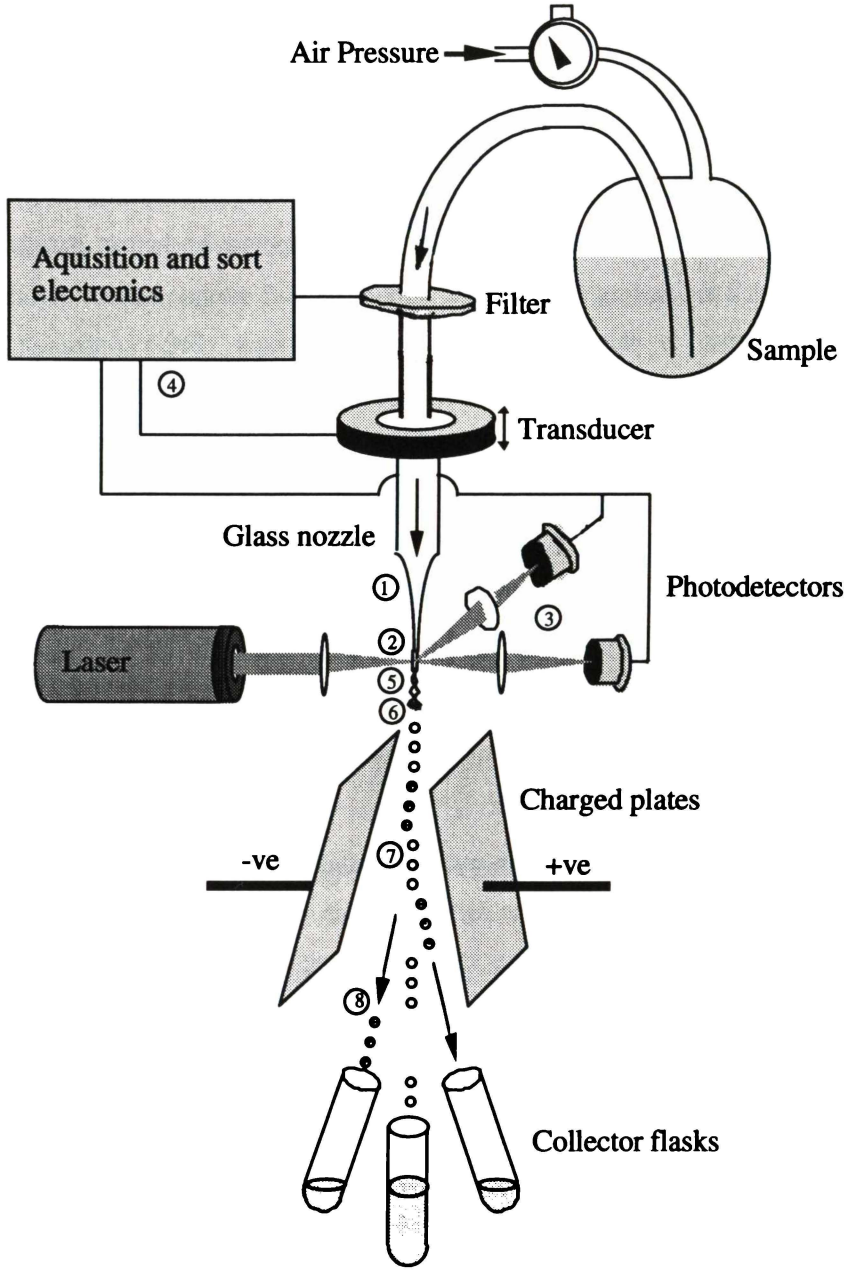

Figure 2-1. Fluorescence activated sorting flow cytometer operation. A suspension of stained cells is presented in single file to an intense light source for measurement of inherent cellular features. As each cell is characterised, it may be deflected from the main population by electrostatic droplet deflection. Numbers refer to features explained in text.

2.3 Optics

Optics are central to flow cytometry, in both the illumination of stained cells with an intense source and the detection of scatter and fluorescent light signals by a photodetector. The optical configuration of a flow cytometer must meet several requirements. The optical geometry must collect at least some of the light emitted (fluorescent and/or scattered) by the cells. The optics must provide sufficient spatial resolution to collect as much cell-emitted light as possible, while minimising the collection of stray light. Optical filters are used to provide spectral resolution, and to discriminate between scatter and fluorescent light. Finally, the photodetectors which are used for conversion of the light energy into electrical signals, must be sensitive and responsive enough to detect these relatively low light levels.

2.3.1 Light Source

The two types of light sources commonly used in flow cytometers are arc lamps and lasers. While arc lamps are relatively cheap and emit light across a spectrum ranging from ultra-violet to infra-red, their intrinsic intensity noise, limited lifetime and finite arc dimensions limit their use in flow cytometry.

The laser, which provides a coherent and intense parallel beam of light at a specific wavelength is more commonly used in flow cytometry than the arc lamp. A variety of laser types used in flow cytometers include gas (e.g. helium neon and argon ion), solid-state (e.g. ruby), semiconductor (e.g. laser diode), or dye lasers (e.g. rhodamine-6G).

2.3.2 Light Delivery

In flow cytometry, single transverse excitation mode (TEM_{00}) laser operation is usually desired. For such modes, the laser forms a Gaussian distribution of light intensity across its transverse axis. Beam shaping optics are required to obtain an ellipsoid intensity profile, desirable because the vertical profile is shorter than that of the cell to be analysed, while the horizontal profile is broadened to provide uniform light intensity across the jet to minimise cell to cell illumination variations (Figure 2-2). An elliptical beam shape is formed by using a combination of crossed cylindrical lenses.

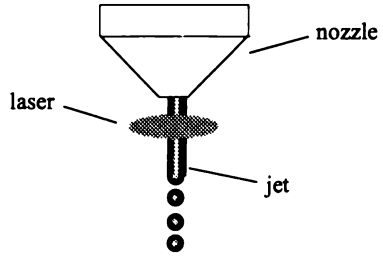

Figure 2-2. Elliptical shaped laser beam projected onto jet (beam axis into page).

In jet-in-air flow cytometers the illuminating beam must have a low numerical aperture to minimise spherical aberration caused by the stream acting as a second half-cylindrical lens in the light path of the image. A beam wider than the jet may also produce unacceptable noise at the detectors due to

perturbations on the jet surface produced by the piezo-electric transducer during sorting, which lead to scatter off the jet. Jet-in-air cytometers use beam shaping optics to deliver typical elliptical spot dimensions of between 20μm and 200μm. Alternatively, long focal length lenses producing circular-profiled spots of 30μm to 50μm in diameter are used to simplify the optical design at the expense of resolution.

2.3.3 Cell Fluorescence

Most commercial flow cytometers measure cell scatter and fluorescence. Optically excited fluorescence occurs when a molecule excited by light of one wavelength returns to a lower state by emitting light of a longer wavelength. The excitation and emission light, being of different wavelengths, can be blocked or differentiated by optical filtering. The wavelength of fluorescence must be sufficiently removed (detuned) from that of the exciting laser light to allow easy separation of the two wavelengths. In addition, several cellular constituents can be measured simultaneously by using several excitation sources at different wavelengths and cell stains which are sensitive to, and emit at, different wavelengths. The ability to detect fluorescence simultaneously from several different compounds bound to one or many cells has enabled flow cytometry to be used for mutiparameter analysis. For studies where several stains are employed, careful choice of cellular stains is essential to avoid overlap of fluorescent wavelengths.

In fluorescence, decay from the excited state generally obeys first order exponential kinetics. If fluorescence were the only process by which molecules returned to the ground state, the mean lifetime of molecules in the excited state would be $1/k_f$, where k_f is the rate of fluorescence emission. This quantity is defined as the intrinsic lifetime, τ_0. In reality, there are other processes competing with fluorescence to de-excite the molecule. The actual excited lifetime τ will therefore be shorter. The quantum efficiency, or quantum yield of a fluorescent material ϕ, is equal to the ratio of the number of photons emitted to the number of photons absorbed, and can be represented as

$$\phi = \frac{\tau}{\tau_0} = \frac{k_f}{\left(k_f + \sum k_i\right)}, \tag{2-1}$$

where Σk_i is the sum of rate constants for the competing non-radiative de-excitation processes. The total fluorescence emission obtained from a material is the product of the number of photons absorbed and the quantum efficiency.

The possible effects of quenching, photobleaching, and saturation, must be considered when exciting and measuring fluorescent particles. Quenching results when excited molecules relax to the ground state by non-radiative paths which provide an alternative to fluorescence. Such processes include loss of energy by vibration and collision, or by energy transfer. Polar solvents such as water can quench fluorescence since such molecules reorient around excited state dipoles. Under conditions of high-intensity illumination, such as those experienced by a cell as it passes through the laser focus of a flow cytometer, the

irreversible destruction or photobleaching of the excited fluorophore becomes a factor which limits fluorescence intensity. The saturation of the bound dye in a stained cell occurs when the number of dye molecules in the excited state becomes equal to the number of dye molecules in the ground state. At this point further net transition between the ground state and the first excited state is not possible. An increase in incident excitation light will only increase the rate of bleaching. The effect of saturation on the sperm sexing process is investigated experimentally in Chapter 5.

2.3.4 Light Collection

In conventional orthogonal axis flow cytometers, light is collected by two lenses of high numerical aperture (NA). These are termed the forward and side collection lenses depending on their orientation as viewed from the entering excitation (laser) beam, and are used for scatter and fluorescence collection respectively.

The forward collection lens gathers scattered light over a solid angle of up to 0.56sr (NA = 0.32, or 7% of a sphere) centred on the laser beam axis. Light scatter in the forward direction can be used to obtain information of particle size.

The side collection lens typically has a higher NA than the forward lens. Fluorescence collection efficiency increases with NA. However, while the numerical aperture increases, the focal length of the lens decreases, requiring that the lens be positioned closer to the jet. In most commercial jet-in-air cytometers NAs are limited to 0.6 or less (1.05sr, or 14% of a sphere).

2.3.5 Spectral Filters

In a flow cytometer, the purpose of the optical filters is to separate the mixture of scattered and fluorescent light collected from stained particles so that correlated measurements (over several wavelength parameters) can be made on a particle or cell. The separation of different wavelengths is achieved by the use of dichroic mirrors, interference, and absorption filters.

Delivery

For flow cytometers which employ arc lamp sources, filters are required to select the wavelength of the exciting light. For instruments employing lasers which output monochromatic light, optical filtration is unnecessary.

Collection

Once the fluorescence light from a cell has been captured by the collection optics, the spectral component of interest for each stain must be separated for detection. A combination of filters and beam splitters are used to achieve this separation. Figure 2-3 illustrates a typical filter configuration which progressively cuts out longer wavelengths from the entire fluorescence light signal from a stained cell. One of the following types of filters may be used to achieve this separation.

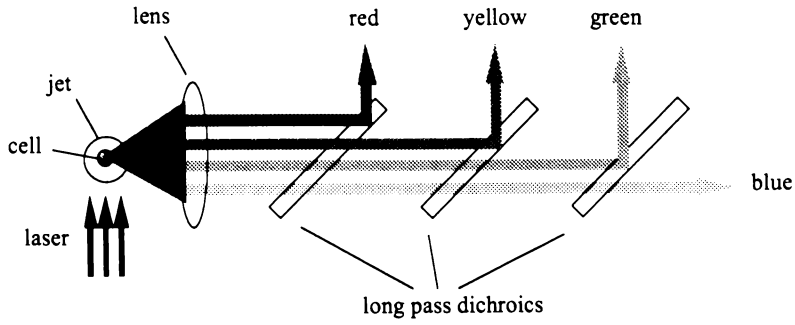

Figure 2-3. A diagram of wavelength separation using a series of filters (cell flow axis is into the page).

Coloured glass filters

Coloured glass filters attenuate light by ionic absorption and colloidal scatter. Ionically coloured glass follows Beer's law of absorption because absorption is proportional to the logarithm of the concentration of the absorbing species. Colloidal scatter induces dispersion and absorption of unwanted wavelengths while allowing the desired wavelengths to pass through the filter unattenuated. Since flow cytometry involves the Stokes shift (which sees emitted fluorescence at a longer wavelength than that of the incident, exciting beam), long-pass filters must be used to transmit fluorescent emissions. Such filters are available with cut-off wavelengths in the range 250nm to 1000nm.

The absorption of coloured glass filters will increase with thickness or as they are tilted, but otherwise their optical properties are almost invariant for different ray geometries. Some coloured glass filters fluoresce slightly under UV illumination, which must be considered when using stains which have low quantum efficiencies. Band-pass filters in coloured glass seldom have sufficient discrimination to be of use in flow cytometry.

Interference filters

Interference filters, also known as dichroic, dielectric, or reflective filters, consist of dielectric layers deposited on a glass or quartz substrate. Constructive and destructive interference causes different wavelengths of light to be transmitted or reflected.

The spectral response of these filters is heavily dependent on light incidence angle since the path length will vary with filter angle. Interference filters produce sharper transition regions from cut-on to cut-off regions than coloured glass. However, their rejection of unwanted wavelength light is usually lower than that of coloured glass filters.

Bandpass filters transmit light of interest over a narrow wavelength band. Edge filters (shortpass or longpass) are often used as dichroic mirrors at an angle of 45° to the incoming fluorescence to provide a similar sharp cut-off to bandpass filters. In flow cytometers, this type of filter is used to reflect a particular wavelength band of interest to one photodetector while allowing the remaining light to be transmitted for detection at other wavelengths.

To take advantage of both coloured glass and interference filters, a combination of dielectric layers with absorptive materials can be used to produce hybrid filters with improved spectral discrimination characteristics. The absorptive material can be used to allow high transmission of desired pass-wavelengths, while blocking unwanted wavelengths. These filters also have sharp cut-off characteristics.

2.3.6 Spatial Filters

The intensity of fluorescence from a stained cell is considerably less than that of the excitation source. As a result, in many situations, the spectral discrimination of optical filters is insufficient for scatter removal and reliable fluorescence detection.

In jet-in-air flow cytometers, the jet acts as a cylindrical lens by reflecting and refracting light in a plane around the inspection point. Most of this light can be removed by placing a beam stop or obscuration bar in the plane perpendicular to the jet. Further scatter removal can be performed by placing a pinhole in the image plane of the collection lens to restrict the field of view at the inspection point, allowing only light from a small region around the cell to continue through spectral filters to the photodetectors.

2.3.7 Photodetectors

Once the photons of interest (which are emitted or scattered by a stained cell) have been separated from those photons that are not of interest (background and stray light) using filters, they may be detected and converted to electronic signals. The two main photodetector types used in flow cytometry are silicon photodiodes and photomultiplier tubes (PMTs). Electronic analysis of photodiode and PMT photodetector signals is discussed in Section 2.7.

The silicon photodiode detector consists of a junction between p- (hole-rich) and n- (electron-rich) type semiconductor materials. In the depletion layer between the materials, a local electric field exists as a consequence of current equilibrium. When photons are absorbed in the vicinity of this region, the electron-hole pairs are separated by the field, causing a change in voltage. This is termed the photovoltaic effect. Silicon photodiodes have a broad spectrum and fast response, but are relatively low in sensitivity. This lack of sensitivity limits their use in flow cytometry to the measurement of scatter, absorption, and extinction measurements at the illuminating or excitation wavelength.

PMTs operate by transporting electrons from a photoemissive material (cathode) to an electrode (anode) thereby producing an electric current which is proportional to the incident photon flux. The photoemitted electrons are accelerated by a series of electrodes (dynodes), which emit a greater number of electrons through secondary emission, thereby amplifying the circuit current. PMTs have high gain and therefore sensitivity, with good signal to noise characteristics and restricted spectral response. Their high sensitivity means PMTs are suitable for the detection of weak fluorescence, such as the signals generated in flow cytometers. In selecting a PMT for a specific application, the spectral response over the wavelength region of interest must be matched to the emission spectrum of the fluorescent dye.

2.4 Fluidics

The fluidic system of a flow cytometer is used to deliver particles in a random three-dimensional suspension one by one to a specific point in space intersected by the illuminating beam. Fluidic transportation in flow cytometers usually involves the laminar, or non-turbulent, flow of cells or particles in an electrically conductive carrier fluid. This fluid flow is affected by flow tube lengths, and by the sizes and behaviour of particles both inside and outside the flow chamber, and can have a marked effect on the accuracy of data obtained from the flow cytometer.

This section describes the hydrodynamic properties of the carrier fluid as it flows into a fine nozzle, where it forms a jet which subsequently disintegrates into droplets. The review of Kachel *et al.* (1991) comprehensively describes hydrodynamic properties of flow cytometers.

2.4.1 Sorting Mechanisms

Two main sorting mechanisms have been utilised in sorting flow cytometers. The method of fluidic switching (Kamentsky *et al.* 1967, Göhde *et al.* 1987) uses a mechanical or acoustic force to divert a volume of fluid, which contains a cell of interest, away from the main flow channel. Maximum sort rates of this technique are limited to 500 cells s^{-1} due to cell coincidence restrictions (which are further discussed in Section 2.5.6) and maximum mechanical switching rates. The low throughput of this technique has limited its use for flow cytometry.

The flow sorting technique in most widespread use for flow cytometry uses electrostatics to charge and deflect a cell containing droplet as it passes through a perpendicular electric field (Fulwyler 1965). The cell carrier fluid is conductive and forms a jet as it exits the nozzle chamber. A mechanical oscillation is applied through a piezo-electric transducer, thus perturbing the jet surface as it travels. The natural tendency of the jet to break up into droplets due to surface tension is stabilised and regulated by the transducer. Each individual droplet can be charged just prior to break-off through application of a voltage to the carrier fluid. The charged droplet continues its path through an electric field, which is produced by a pair of oppositely charged plates, and is deflected from its original trajectory into one of several collection vessels beneath the apparatus.

Electrostatic deflection of particle-containing droplets is a simple, fast, and efficient method of separation since no mechanical parts are required. While not as fast as bulk sorting methods such as centrifugation, sedimentation, filtration, or magnetic separation, the electrostatic sort technique enables the vital sorting of cells which require high resolution measurement for differentiation. To date, this technique has been the fastest method for sorting vital bovine sperm based on X or Y DNA content.

2.4.2 Cytometer Fluidic System

A diagram of a typical sorting flow cytometer fluidic system is shown in Figure 2-4. The fluidic system relies on air pressure regulation for operation, and consists of two fluid lines feeding the flow chamber. Both the sheath and sample lines are controlled by a differential pressure regulator to ensure stable and constant flow conditions.

On entering the nozzle chamber, the sheath fluid hydrodynamically focuses the sample cells into single file (see Section 2.5.3). This injected sheath then exits the nozzle through a circular orifice (typically 50μm to 100μm in diameter) and produces a jet. The jet passes through the excitation beam at the inspection point prior to droplet formation and charging. Droplets which are not electrostatically deflected from the central path, are collected directly below and flushed to waste. To facilitate instrument start-up, removal of bubbles and debris, or clearance when unstable jet formation or blockages occur, a vacuum line is provided for purging the nozzle chamber.

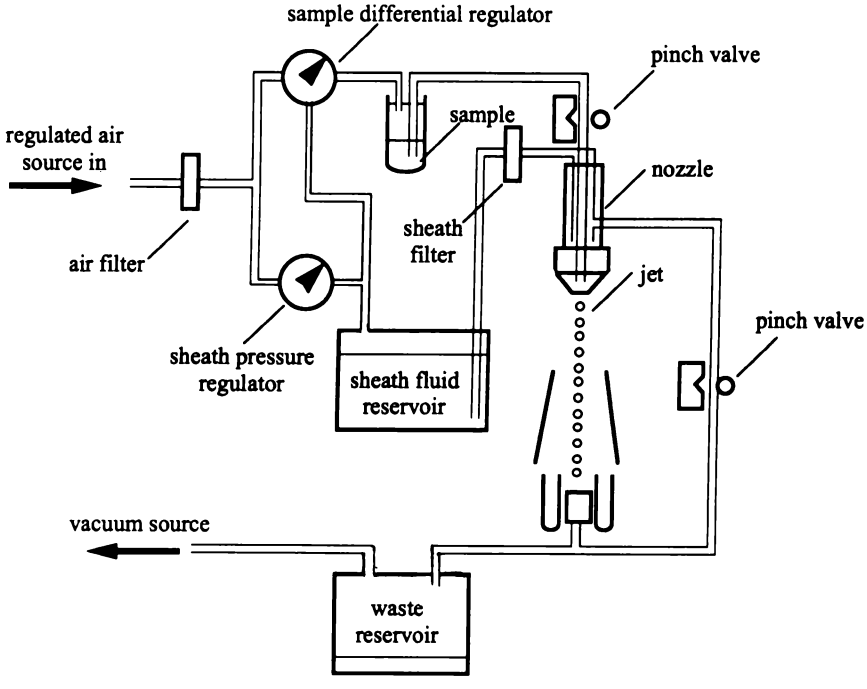

Figure 2-4. Schematic of a typical flow cytometer fluidic system. Air pressure regulators are used to control the flow and rate of sample cells through the flow cytometer sensing region. Vacuum is used to dispose of waste.

Several operational factors must be taken into account with fluidics systems. Measurement uncertainty can be caused by fluctuations in fluidic pressure. Thus, stable air pressure must be delivered by the sample and sheath pressure regulators. The sample flow line should be kept as short as possible to reduce sample introduction time lags and waste due to dead volume. In addition, connectors and other devices where cells can be trapped, should be avoided.

2.4.3 Sheath Fluid Selection

The sheath carrier fluid must meet several requirements so that live cells can be analysed and sorted with a minimum of disturbance. These requirements include:

Biological Suitability - For live cell analysis in particular, the carrier fluid must not affect cell viability through toxicity or contamination.

Sedimentation - The specific gravity of the carrier fluid must be similar in value to that of the particles investigated to ensure uniform suspension density throughout.

Isotonicity - The carrier fluid must be at constant pressure as it flows through the fluidic system to avoid membranous damage through implosion or expansion (explosion).

Surface Tension - The surface tension of the carrier fluid must be sufficient to promote stable droplet generation.

Conductivity - The carrier fluid must be electrically conductive, so that droplets can be charged for sorting by electrostatic deflection.

Dulbeccos's Phosphate Buffered Saline (DPBS) (Sigma Biosciences, St. Louis, MO) adequately meets these requirements and is a common sheath fluid used for flow cytometry.

2.5 Flow Sorting

In this section, the process of cell sorting using electrostatic droplet deflection is described. Operational factors which affect the efficiency and ultimate enrichment of collected cells using this technique are also discussed.

2.5.1 Jet Characteristics and Droplet Formation

The formation of jets and droplets in flow cytometers is crucial to stable particle flow, optical sensing and accurate particle separation. To form a stable jet exiting the nozzle orifice, the rate of fluidic energy flow into the jet must be greater than that of surface tension forces. Figure 2-5 shows jet perturbation followed by droplet formation.

When the cylindrical jet of fluid travelling in air becomes unstable due to surface tension, the jet will disintegrate into droplets. By mechanically coupling an oscillatory force to the jet such as that provided by a piezoelectric transducer, this instability can be controlled to a point where droplets of uniform size, spacing, and most importantly rate, can be formed. By controlling the droplet formation rate it is possible to determine when a particular cell breaks free and becomes encapsulated in a droplet (as outlined in Section 2.5.4). With a suitable sorting mechanism, such as electrostatic deflection, such a droplet can be drafted to one side of the main population.

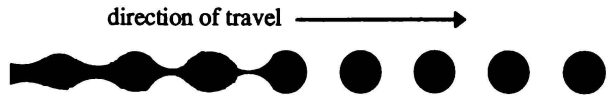

Figure 2-5. Illustration of jet perturbation and droplet formation.

2.5.2 Flow Nozzle Design

In a flow cytometer the flow system, and in particular the flow nozzle, must deliver cells along almost identical trajectories at constant velocity if satisfactory data is to be obtained from the measurement process. A suitably designed flow nozzle must therefore be used to ensure stable jet formation. Three jet-in-air nozzle designs were used for this research; a Becton Dickinson FACStar jet-in-air, a Coulter EPICS V jet-in-air, and a custom drawn-glass observation in thin-walled cavity (Figure 2-6).

*Figure 2-6. Three nozzle designs used: **A:** BD FACStar jet-in-air, **B:** EPICS V jet-in-air, and **C:** a custom glass nozzle.*

2.5.3 Fluid Flow and Cell Interaction

As cells are injected into the outer, faster flowing, sheath fluid in the nozzle of a flow cytometer, they are subjected to forces that extend them (in single file) in the direction of flow. Non-spherical cells tend to become aligned with their long axis parallel to flow, and deformable cells can become elongated in the direction of flow (Kachel *et al.* 1977). As the cells emerge (contained in a jet) from the nozzle, they can interfere with normal droplet generation if they are large with respect to the jet diameter. This leads to increased uncertainty in transit time between observation and when the droplet carrying the cell

separates. The transit time uncertainty can be minimised by increasing the amplitude of the transducer-induced perturbations on the jet, or by increasing the nozzle (and therefore jet) diameter.

In an attempt to reduce cell blockage and increase the precision of cellular fluorescence measurement, most modern flow cytometers use hydrodynamic focusing as illustrated in Figure 2-7. The cell-laden sample fluid is presented at a low rate compared to the outer, laminar flowing, sheath fluid which draws the cells into single file within a narrow core region within the jet for consistent positioning at the laser observation point.

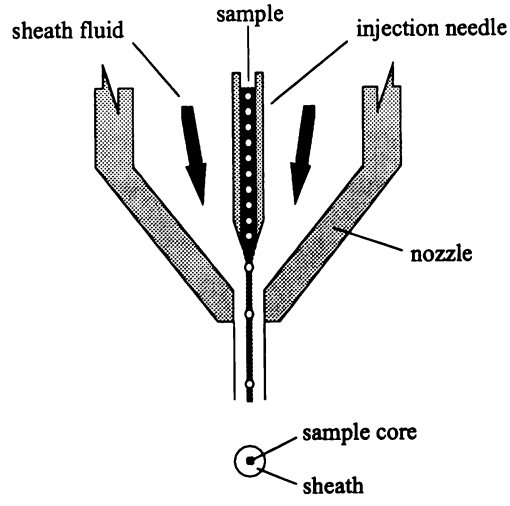

Figure 2-7. Hydrodynamic focusing in a flow cytometer nozzle head.

The technique of hydrodynamic focusing has been further improved for the purpose of orienting flat cells as they pass through the inspection point of a flow cytometer (Stovel *et al.* 1978, Johnson *et al.* 1986). This technique is discussed further in Chapter 3.

2.5.4 Charging and Deflecting Droplets

The physical sorting mechanism in flow cytometry is similar to that of an ink-jet printer where droplets are deflected electrostatically. Droplets are charged by applying a positive or negative voltage to the carrier fluid stream in synchrony with the vibrating-transducer oscillation clock. If a droplet separates from the stream while such a charge is applied, it will retain a surface charge proportional to the applied voltage. The charged droplet passes through an electric field created by two high-voltage plates of opposite polarity. This charge causes the droplet to experience an electrostatic force and a resultant acceleration when it passes through the electric field. The droplet charge, volume, mass, density, permittivity, velocity, and the time spent in the electric field will determine the distance it is deflected from its original path when it is collected a certain distance below the deflector plates. If the droplet has a positive net charge it will be electrostatically attracted towards the negative plate, while a negatively

charged droplet will be attracted towards the positive plate. A droplet that has no charge with respect to ground will travel an undeflected path. The particle flow rate must be less than the droplet generation frequency to minimise the likelihood that more than one particle is contained within an individual droplet.

The charging and separation of droplets serves as the particle sorting mechanism. Each deflected stream of droplets may be collected in a different flask. If the charge-inducing voltage on the sample stream can be varied, the number of deflected droplet streams is limited only by the accuracy of the deflection mechanism and the size of, and distance to, the collection vessels.

2.5.5 Droplet Charge Timing

The timing of droplet charging in flow cytometric sorting is crucial for accurate sorting. The number of particles actually found in a sorted fraction relative to the number of activated sort events is termed recovery. Ideally a recovery of 100% is desired when sorting particles, however, this figure is usually lower in practice (Section 2.6.1).

The correct charge delay setting is achieved first by estimating the delay setting, and second by confirming the appropriate setting by test sorting. The delay setting is estimated by measuring the distance from the illumination focus to the droplet break-off point. This measurement is performed by counting the number of transducer-produced perturbations on the jet surface. Since the oscillation frequency is known, the number of perturbations (transducer oscillation periods) can be used to determine the time taken for a particle to travel from the laser focus to the break-off point. The estimated charge delay can be verified by sorting test particles and varying the delay setting until a maximum particle recovery occurs.

2.5.6 Coincidence Detection

When cells are spaced too closely for separate optical interrogation, or isolation into separate groups of deflected droplets, coincidence detection circuitry is required. This circuitry is often used to ensure a high purity of the cell sorting process, to avoid contamination of the sorted fractions, or to sort an exact number of cells. Coincidence circuitry aborts any sort decision if a nearby cell is likely to be deflected along with the desired cell.

2.6 Operational Characteristics of Flow Sorting

Electrostatic flow sorting provides an accurate and efficient method for separating cells according to pre-defined characteristics. However, when applying this technique consideration must be given to factors such as sorting efficiency, recovery, and purity of cells before estimates of the final sort rate can be made.

2.6.1 Recovery

Often expressed as a percentage, the recovery of a sort is the fraction of particles found in the sorted fraction at the end of a run (usually a predetermined trigger or event count), relative to the number of activated sort (or droplet charge) events. An ideal recovery of 100% is not achieved due to either charged droplets not reaching the collection vessel, or, droplets that do reach the collection vessel not containing the desired cell.

One factor which can prevent charged droplets from reaching the collection vessel is incorrect charge voltage. This will result in unexpected deflection trajectories of the droplets. Electrostatic build-up of isolated instrument components can also result in deviation from the deflected droplet path. These problems can be detected by comparing the expected mass of liquid sorted for a certain number of events with the amount of liquid recovered.

When droplets do reach the flask, but do not contain the desired cell, the correct timing of the droplet charging pulse relative to the time of sensing at the observation point must be considered. Any variation in flow velocity between cells will result in a corresponding variation in the distance between the observation point and the droplet break-off. The extent of these effects can be determined by performing test sorts using calibration particles.

2.6.2 Purity

The purity or enrichment of a sorted fraction is often defined as the fraction of sorted cells which match the criteria by which they were sorted. For high concentration samples where the probability that a nearby cell is deflected together with the desired cell is increased, purity is highly dependent on the effectiveness of coincidence circuitry. The importance of sort purity is discussed further with specific application to sperm sexing in Chapter 7.

2.6.3 Efficiency

Sort efficiency relates the sample input rate to the probability that a particle will be sorted as classified by the electronics. For applications where a high sort rate is required, the random nature of the arrival of cells at the observation point must be considered. This cell occurrence can be treated as a Poisson process (Melamed 1991).

The sorting efficiency (E), can be represented as

$$E = e^{-mnT} \tag{2-2}$$

where m is the average analysis input rate, n is the number of droplets deflected for each sort event, and T denotes the time interval required (for which no other cell can be analysed) for each sort event. If it is of importance to obtain as many desired cells as possible of a particular sample (thereby minimising sample waste), sorting should be performed at a low input rate, so that the rejection rate due to coincidences will be low. If a is the fraction of wanted cells in the unsorted sample, ma will be the detection rate for wanted cells. The rate of wanted cells sorted (R_s) can be determined from Equation (2-2)

$$R_s = ma\, e^{-mnT} \tag{2-3}$$

which has a maximum at $m = 1/nT$ corresponding on average to the analysis of one cell within the time interval used for coincidence detection.

2.7 Electronics and Data Acquisition

The role of the electronics is to monitor and control the operation of the flow cytometer, from detection of a cell event as it passes through the laser focus, to physical deflection of that particle into a collection flask, and the archival storage of the individual measured pulse information.

In the previous sections of this chapter, descriptions have been given for the process of optical excitation of a stained particle along with considerations that must be made to ensure reliable detection. The fluidic system has been outlined, as have the operational characteristics of the electrostatic flow sort process.

In this section, the main electronic elements are described. These include the main signal processing elements, timing circuitry, and software analysis and display. Methods for interpretation of cytometer-generated data and histograms are also outlined.

2.7.1 Signal Processing

As a particle of interest passes through the focus, fluoresces and is detected by a photodetector, an electrical pulse is generated and presented to the signal processing electronics. The signal from the photodetector is fed into a filtering preamplifier for initial smoothing. The preamplifier output voltage signal, proportional to the number of photons reaching the detector, typically lies in the range 0 - 10V. The particular pulse characteristics are determined by the particle speed and size, the width of the illumination beam, and in the case of fluorescence, the distribution of fluorochrome within the particle.

The output signal from the preamplifier typically contains some background noise. This noise may be at a high frequency and may mask true pulses. Therefore, a system threshold, set at a pre-set voltage, is used to ensure that a signal which contains only noise will not be processed. Measuring circuits for electronic processing are triggered only by pulses which surpass this threshold.

The short duration of pulses (of the order of 1-5μs) and the short latency before droplet break-off (approximately 10-50μs) make the digital processing of pulses difficult. Pulse processing circuitry provides an analogue voltage memory of the signal which is held long enough for further processing to take place. The sustained voltage output from this sample-and-hold circuit can be made proportional to the height (peak height), area (integral), or width (time of flight) of the pulse. The sample-and-hold circuits maintain their voltage output for a fixed period (typically between 15 to 120μs) and are triggered when the signal voltage rises above the pre-set threshold level. Various pulse processing modes enable different measurements to be made from the same signal. During the period of sample-and-hold circuit operation, the electronics is not available for further pulse processing. During this dead time, any further cells and associated pulses presented by the preamplifier will pass undetected. A large system dead time has less serious consequences for analysis than for sorting. The cells which pass undetected during the system dead time will be taken randomly from the population of cells being analysed and no bias of final statistical results will be evident. However, the time taken to acquire a specific number of events and therefore sorted cells will be increased.

Digital Conversion

For analysis and display by computer systems or pulse height analysers, the sample-and-hold voltages from the analogue circuitry are digitised. The analogue to digital converter (ADC) translates the continuous analogue signal with a resolution dependent upon the scale interval of the conversion. The 10 bit ADC supplied with the FACStar Plus used for this research gives a resolution of 1024 elements (10mV per division, full scale 10.24V).

2.7.2 Drop Drive Clock Signal and Sorting

The master, or drop drive clock signal provides uniform rate generation of droplets and serves as the reference timing signal for all sort events. A particle is detected as it passes through the laser inspection point, and the information contained in its pulse is processed. Reliable droplet charge timing is achieved by applying a charge to the entire stream at a measured multiple of the droplet charge period according to the distance, and therefore time taken for a cell to transit from the inspection point to the break-off point.

2.7.3 Software Analysis and Display

The result of voltage pulses from a population of cells is a stream of numbers between channel 0 and 1024 of the ADC. Original flow cytometers used an oscilloscope for simple pulse height display and analysis. Today, most instruments use some form of computer for data acquisition, analysis and display.

The most common display methods used in flow cytometry are frequency histograms and, when more than one detector is used, dual parameter correlated plots, which are often termed cytograms or dot plots. The frequency histogram is a direct graphical representation of the number of events occurring for each ADC channel (i.e. number of events, or cells as a function of intensity). The acquisition memory is

mapped to each channel of the ADC to act as a series of counters. Each memory location corresponds to a specific ADC output value and is incremented for each corresponding event level. Information from each detector for a given cell will be stored by the acquisition electronics. This information is then stored to a hard-disk for subsequent analysis.

The dot plot is a two-dimensional extension of the frequency histogram. The locations in memory correspond to a two-dimensional array of the channels of one ADC correlated against the channels of a second ADC. Each location on the dot plot corresponds to the co-ordinates of the first ADC versus the second ADC for a given cell. For a large number of cells, the dot plot can be extended to a third frequency histogram dimension where each (x,y) co-ordinate pair is binned. This graphical representation is often termed a 3D contour or isometric plot. For dual-stained cells, the dot plot can be used to monitor the extent to which a pair of molecular probes fluoresce for each individual cell of a population. For multiparameter analysis, where several spectral characteristics of a cell are studied at once, data can be presented on a polyhedral plot surface.

Typical graphical representations of fluorescence histograms, dot and contour plots are shown in Figure 2-8. These results were produced using Hoechst 33342 impregnated latex microspheres (Flow Cytometry Standards Corporation, NC). The fluorescence histograms display fluorescence intensity of the microspheres against the number of events in two detectors; the forward (at 0° with respect to the laser source) detector, and the side (90°) detector. The distribution of the fluorescence within the population is bell shaped on both histograms.

Statistical analysis of these displays is achieved using computer software. Dot and contour plots are usually analysed by setting boxes or polygons around areas of interest for statistical evaluation. Further restrictions on defined regions can be set by arranging gates or windows on defined parameters across several detectors. Only cells which fall within the gates are acquired and analysed further. This method is used in sperm sexing where the intensity of fluorescent light pulses from one photodetector are used to gate out those nuclei which are deemed to be misaligned and unresolvable for X or Y DNA chromosome content measurement. The gating techniques for sperm sexing are outlined in Chapter 3. Gating can increase efficiency, reduce processing and storage requirements, and can be used to investigate populations with minor variations in structure.

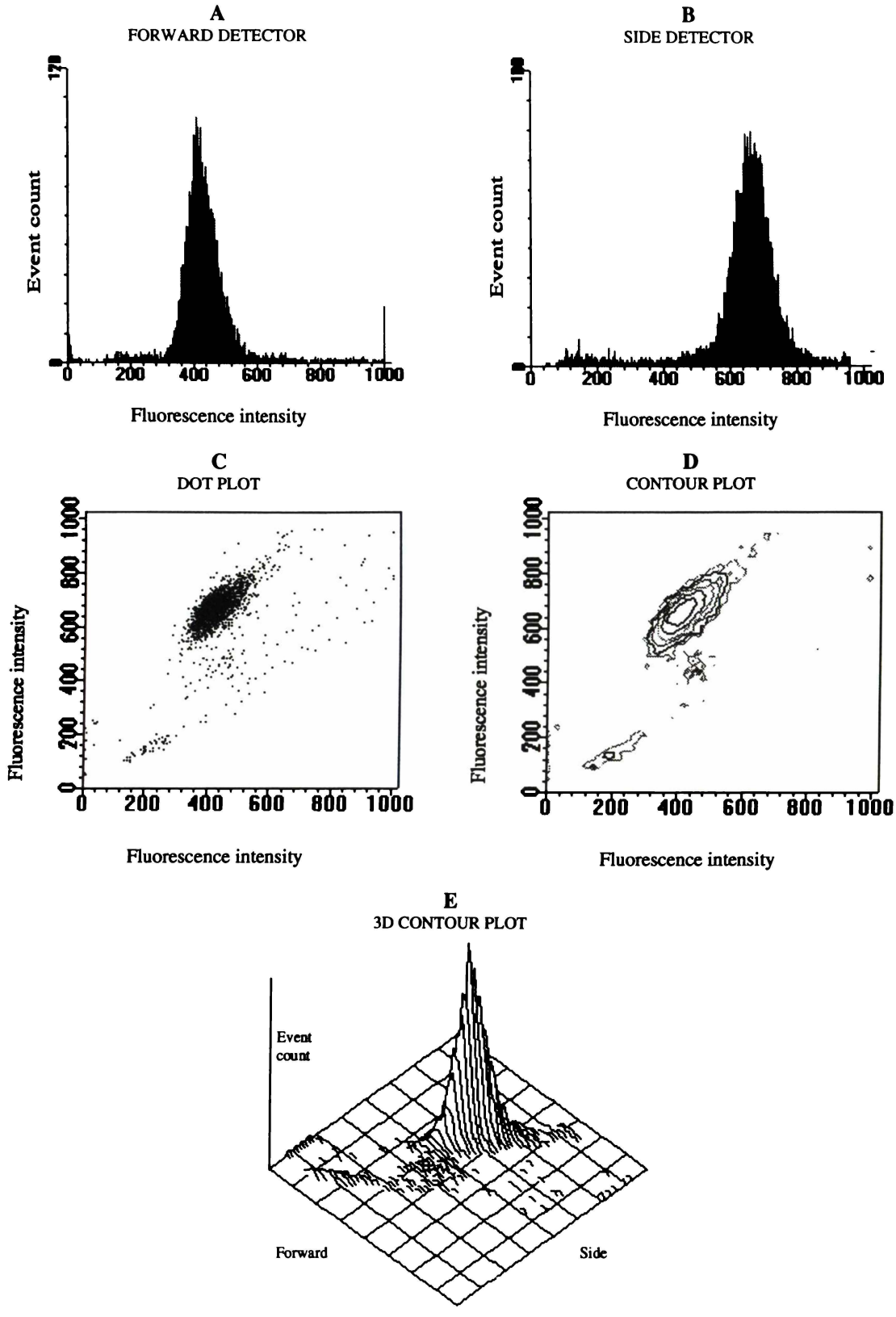

*Figure 2-8. Flow cytometer data representations for a population of fluorescent microspheres; **A:** forward detector frequency histogram, **B:** side detector frequency histogram, **C:** forward vs. side detector dot plot, **D:** 2D contour plot, and **E:** 3D contour plot.*

Flow cytometer data can be processed immediately into histograms on screen, or individual correlated measurements can be stored on disk as list mode data. While storing cytometer data is useful for analysis later, much storage space is required if all information from anywhere up to 20 000 events per second is to be acquired, each comprising several detector parameters.

2.7.4 Interpretation of Acquired Data

Interpretation of data generated by flow cytometry is statistical in nature. Measurements are performed for a population of cells from the fluorescent signal intensity levels they emit. These measurements are plotted on histograms for quantitative measurement and for differentiation of cell groups. When analysing the cells of a particular group, it is often the case that a measurement of variance in this cell subpopulation is required. A common measurement which is made in flow cytometry is the coefficient of variation (CV), or kurtosis, which is defined as the standard deviation of a population divided by the mean. The CV, expressed as a percentage, defines the tightness of population. Figure 2-9 illustrates fluorescence intensity distributions for two calibration microsphere populations. Each histogram contains fluorescence intensity data from 10 000 particles. The Fluorescebrite calibration microspheres are measured to have a channel mean of $x = 745.1$, a standard deviation of $\sigma = 16.14$, and a coefficient of variation $CV = 2.16\%$. The Hoechst microspheres have corresponding values of $x = 669.3$, $\sigma = 50.5$, and $CV = 7.54\%$.

Flow cytometric analysis, although capable of measurements with high precision, is prone to the introduction of systematic errors. Sources of measurement degradation can include poor sample preparation and staining, non-specific and non-homogeneous staining, fluorochrome emission variations with pH and temperature, optical and electronic noise, laser noise, and fluidic instability. Any degradation in the accuracy of measurements can be detected rapidly if standard particles such as fluorescent microspheres are used routinely. Such particles can be used for optical alignment and reproduction of parameter settings for a particular specimen.

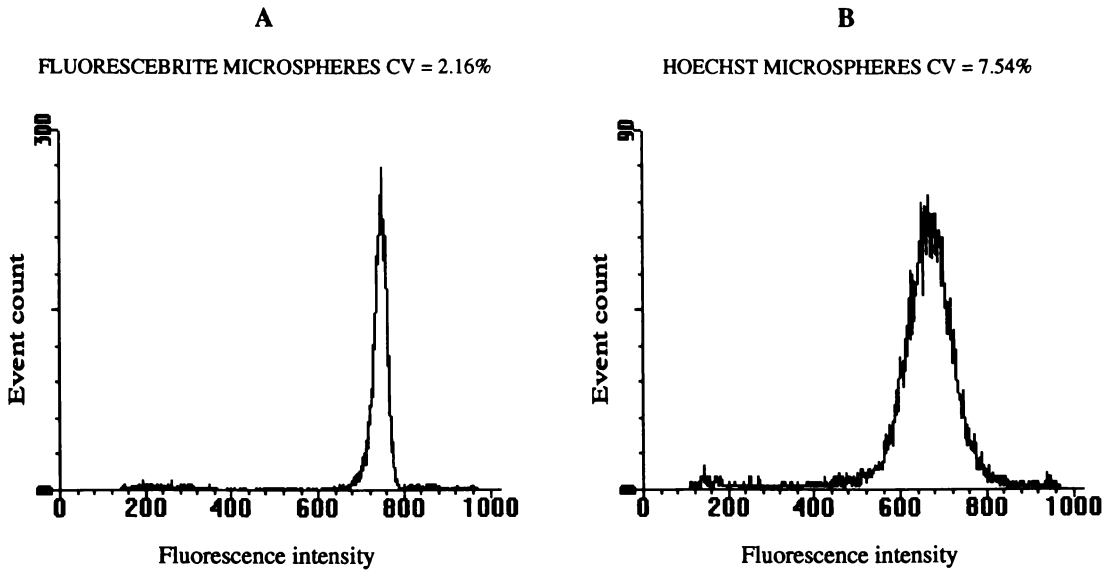

Figure 2-9. Interpretation of coefficient of variation for two different particles; A: Fluorescebrite calibration spheres, and B: Hoechst 33342 microspheres.

2.8 Applications of Flow Cytometry

Flow cytometry is used in a variety of research fields and clinical applications. This section briefly discusses a selection of several major areas of flow cytometry application. New applications of flow cytometry are continually being found.

DNA Analysis

Recently, an important task of flow cytometry has been to map the human genome (the haploid set or number of chromosomes). The process, which is underway at present at the Lawrence Livermore Laboratory (Lawrence, CA), will determine the base sequence of every gene in the human genome, map the location of these genes and produce a DNA library.

Marine Biology

Flow cytometric analysis is performed on aquatic organisms such as bacteria, algae, and plankton. Many of these studies are focused on particle concentration and abundance.

Veterinary Medicine

In veterinary medicine, studies have been conducted on sperm fertility and milk quality. The scope of veterinary medicine also encompasses the topic of this thesis, sperm sexing research. Molecular techniques include quantitative flow cytometric detection of specific micro-organisms in soil samples.

Cell Biology

Application of flow cytometry to cell biology includes determination of DNA and RNA content, cell viability, chromosome analysis, cell function, structure, activity, and toxicity. Measurements of dynamic cellular events such as cell cycle analysis (e.g. apoptosis - programmed cell death) can also be performed.

Bacteria

Flow cytometric analysis of micro-organisms stained with fluorescent dyes is used for bacterial detection and differentiation. Cytometry has also been used for studies of bacterial viability and antibiotic sensitivity measurements.

Food Industry

Flow cytometry is used in food microbiology for the detection of food-borne pathogens, and for characterisation of food bacteria such as *Escherichia coli*.

Oncology

Cytometry can be used in the prognosis of cancers for monitoring therapy and patient progress (e.g. bone marrow cells), leukaemic cell detection and typing.

Immunology

Immunological applications include the study of cell surface structure, the immune system, and possible predisposition to diseases. Cytometry is routinely used in cell measurement for the HIV disease through assessment of disease progress (by lymphocyte enumeration).

Sorting Flow Cytometry

The addition of the electrostatic sort function to flow cytometry has introduced many opportunities for cell enrichment. This includes sorting sperm by X or Y DNA chromosome sex content. Flow sorting is an important preparative tool in many areas related to genetics and developmental biology.

3. Sperm Sexing

Many attempts have been made to predict or control the sex of animal offspring. With very few exceptions, information for sex determination in mammals is carried in the spermatozoa (sperm), so most sex control schemes have concentrated on semen manipulations. The term sperm sexing describes a method by which the spermatozoa of a given species may be differentiated by sex and physically separated.

The role that spermatozoa play in sex determination is outlined in Section 3.1. Section 3.2 describes the morphology, dimensions, and physical and optical characteristics of bovine spermatozoa and several other mammalian species. In Section 3.3 methods of verification of sperm sexing success are discussed. Various historical and current (scientific) sperm sexing attempts are outlined in Section 3.4. Section 3.5 examines approaches to sperm sexing using flow cytometry and discusses associated problems. The flow cytometric method of sperm sexing, its commercial limitations, and the stains used, are described in Sections 3.6, 3.7 and 3.8 respectively. Section 3.9 discusses the conditions required for sperm longevity and the effects of environment on vitality, and therefore, viability of sperm.

3.1 What Determines Sex?

Every living being has a set chromosomes which carry all the genetic material necessary to maintain and propagate life. All but one chromosome are called autosomes and carry genes for all the characteristics of the body, such as skin type, hair and eye colour, mature size, and other body characteristics. The remaining sex chromosome includes the genetic material that specifies gender. One sex chromosome is called X, the other Y.

A sperm from the male, or an egg from the female, each contains a set of autosomes. In mammals, the egg always contains an X chromosome, while the sperm carries either an X or Y chromosome. When a sperm and egg unite and the sperm carries a Y chromosome, the offspring is male (XY). Conversely, if the sperm carries an X chromosome when it fertilises the egg, the resulting offspring is female (XX).

The only scientifically established means of differentiating vital X and Y sperm is a difference in deoxyribonucleic acid (DNA) content. The X chromosome is larger and contains slightly more DNA than the Y chromosome. The difference in total DNA between X- and Y-chromosome bearing sperm is 3.4% in boar, 3.9% in bull, and 4.2% in ram sperm. Table 3-1 lists the X-Y DNA content differences for several mammalian species. The amount of DNA in a sperm cell, as in most normal body cells, is stable. Therefore, the DNA content of individual sperm can be monitored and used to differentiate X- and Y-chromosome-bearing sperm.

Table 3-1. Percentage difference between X- and Y-chromosome bearing sperm from several species (Johnson 1992a)

Species	X-Y Difference (%)
Turkey	0
Human	2.9
Rabbit	3.0
Swine	3.6
Cattle	3.8
Dog	3.9
Horse	4.1
Sheep	4.2
Dorcus gazelle	4.3
Muntjac	6.3
Chinchilla	7.5
Creeping Vole	12.5

3.2 Characteristics and Function of Bovine Sperm

3.2.1 Morphology

The principal morphological features of the bull spermatozoa are illustrated in Figure 3-1. Optical photomicrographs are shown in Figure 3-2. The heads of spermatozoa consist essentially of a haploid, or single nucleus, surrounded by a cell membrane. This haploid amount of DNA is very uniform in mature normal sperm of a given species. The variability in mean value is measured to be less than 1% for human sperm (Sarkar 1974). A cap-like structure (*Galea capitis*) covers the front half of the head. It contains the acrosome (responsible for egg penetration) and is thus often termed the acrosomal cap. The mid-piece of the sperm contains a helix of mitochondria that surround a set of fibres which continue to the tail. The flagellum or tail of the sperm is very fibrillar and is responsible for motility.

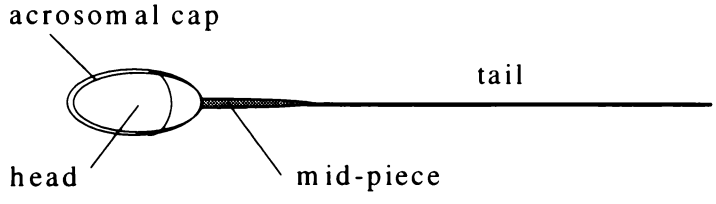

Figure 3-1. Diagram of the principal features of a bull sperm cell.

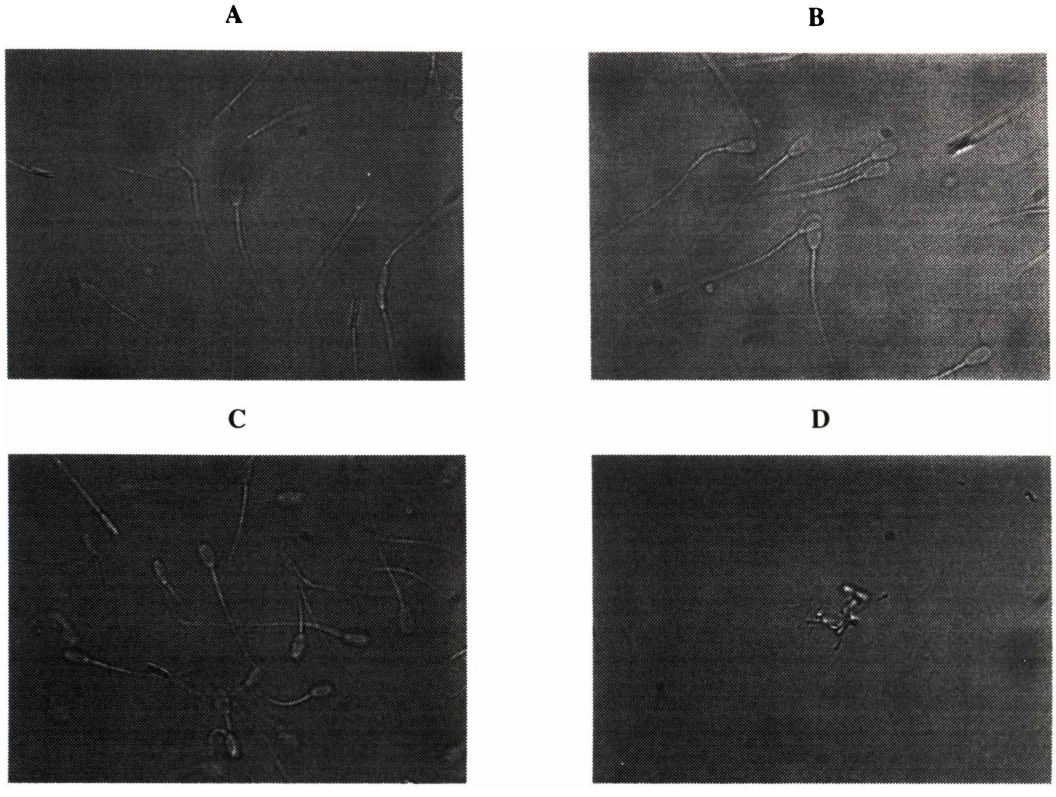

*Figure 3-2. Photomicrographs of **A:** bull, **B:** ram, **C:** deer, and **D:** chinchilla spermatozoa.*

3.2.2 Dimensions

The geometry of sperm is highly variable between mammalian species. The size and shape do not only differ between, but also within individual animals of a species (Van Duijn 1971). There may be variations as a function of the age of the animal, and environmental factors including season and nutrition. The dimensions of spermatozoa also change after death (Baker 1962). Ageing *in vitro* induces dimensional changes depending on the composition of the diluent, light irradiation, and temperature. Staining procedures can also alter the dimensions of spermatozoa (Mukherjee 1960).

Bull sperm are ellipsoidal in shape, as is demonstrated by the microscope image of Figure 3-2. Several studies including optical and electron microscopy techniques have been performed to determine the length (l), width (w), thickness (t), and cross-sectional area (A) of bull sperm. Mukherjee (1960) measured head length and breadth of live sperm heads as observed under a microscope for five different bulls (of two species). Mean head length and width measurements were 9.27μm and 4.97μm respectively. Rahlmann (1961) used electron microscopy to measure a mean bull sperm head thickness at between 0.65μm and 0.70μm.

Baker and Salisbury (1963) used the eosin differentiation method, where dye is taken up only by dead sperm, to measure nuclear dimensions of live sperm. They found l, w, and A to be $8.5 \pm 0.5\mu m$, $4.0 \pm 0.3\mu m$, and $27.5 \pm 2.1\mu m^2$ respectively. Base width was measured to be $1.80 \pm 0.24\mu m$, however,

this measurement was taken across a point at which the head joins the mid-section, and so is expected to be greater than a measurement taken across the broadest part of the sperm head.

Van Duijn *et al.* (1971) measured the length, width, thickness and area of bull sperm heads by an optical technique which utilised an image splitting eyepiece to yield resolution of measurement to 0.02μm. The mean dimensions measured were $l = 9.08\mu m$, $w = 4.66\mu m$, $A = 34.2\mu m^2$. Interference microscopy was used to determine a thickness measurement of $t = 1.03 \pm 0.005\mu m$. Later, Van Duijn (1974) reviewed measurement techniques of sperm. This review included the methods for measuring linear dimensions of sperm using a micrometer eye-piece. The difficulties of thickness determination were also discussed, along with the methods of phase contrast and microscopic interferometry. More recently, Chandler *et al.* (1990) used videomicroscopy to obtain measurements of live sperm yielding dimensions of $l = 8.9\mu m$, $w = 5.3\mu m$ and $t = 0.3$ to $0.5\mu m$.

Using a Nikon video fluorescence microscope, we measured mean dimensions of $l = 9.0 \pm 0.2\mu m$, $w = 4.6 \pm 0.2\mu m$, $t = 1.0 \pm 0.2\mu m$ (for 20 sperm).

3.2.3 Refractive Index

By using interferometry, Van Duijn (1971) measured the refractive index, n, of bull sperm heads to be $n = 1.42 \pm 0.01$. Mukherjee (1960) measured a value of $n = 1.481$. The disparity between measurements may have been due to any of the environmental factors outlined in Section 3.2.2. In addition, a further optical property of sperm heads is that they are slightly birefringent (Van Duijn 1971). This may affect the propagation of light through the cell material because different polarisations of incident light will lead to different values of the refractive index.

3.2.4 Optical Density

Baker *et al.* (1963) performed a study on profiling the optical density of Feulgen-stained bovine sperm nuclei. Measurements were taken along the length and width of the sperm head. Results showed uniform density across the nucleus surface with a decrease near the edges. The optical density varied between 0.2 and 0.4 which corresponds to a transmittance of 63% and 39% of the $\lambda = 570nm$ light used over an average head thickness of 2μm. Consequences of this effect may lead to variations in detected fluorescence intensity for varying cell orientations (with respect to photodetectors) in a flow cytometer.

3.3 Verification of X and Y Sperm Separation

The ultimate test for gender preselection is, of course, live births. However, the time and expense required to determine the sex of offspring becomes intractable in any comprehensive experimental programme. Therefore, a number of alternative methods have been developed to demonstrate successful X or Y sperm enrichment. These methods include quinacrine staining (Windsor *et al.* 1993), DNA probes

(van Vliet *et al.* 1989), *in vitro* fusion (Rudak *et al.* 1978), the polymerase chain reaction (PCR) (Johnson 1995), and re-analysis using flow cytometry (Pinkel 1985).

3.4 Gender Preselection - Principle Scientific Options

Numerous reviews have been published documenting the existence and use of a variety of sperm sexing methods (Amann and Seidel 1982, Gledhill 1988, Windsor *et al.* 1993, Jafar and Flint 1996). The following survey outlines several scientific sex selective techniques which rely on physical differences between X- and Y-chromosome-bearing sperm.

3.4.1 Size and Mass

Evidence that the X chromosome is larger than the Y chromosome would suggest that an X chromosome-bearing sperm will be larger than a Y chromosome-bearing sperm (Roberts 1972). The closest to a measurable difference in sperm head size was made by Chandler *et al.* (1990) who performed a video-microscopic comparison of bull sperm related to gender. Chromosomal area in the head was calculated using this method and a discriminant analysis technique was successful in categorising spermatozoa corresponding to the presence of the X or Y chromosome with a difference of 2.6% between the peak sperm head area frequencies of each category. Chandler indicated that a relationship existed between the sum of the corrected chromosome areas and the sperm head areas, and that discrimination was due to the presence of the respective sex chromosome area in the discriminant function.

Separation of sperm using a method based on a mass difference would require a technique with extremely high resolution, since, if it could be assumed that nucleoprotein content is proportional to DNA content, a human or bovine Y chromosome-bearing sperm would be at most only 1% smaller in total cellular dry mass than an X sperm (Gledhill 1988).

3.4.2 H-Y Antigen Immunomagnetic Cell Sorting

An immunomagnetic method (which used super-magnetised polymer beads coated with antibodies) was developed (Peter *et al.* 1993) for removal of sperm that bind to anti-H-Y IgG. Assuming that only Y chromosome-bearing sperm had cell surface H-Y antigens, this fractionation method would remove almost all of the Y sperm, leaving a population that was greater than 98% X sperm.

This procedure was validated with a flow cytometer which indicated this immunomagnetic technique produces an effective and practical separation of X and Y sperm. Further studies such as *in vitro* fertilisation and subsequent embryo sexing are required to provide further validation of this technique. Morphological changes and fertilising capacity of the immunomagnetically sorted sperm are not known. Experiments are now under way to determine this ability.

3.4.3 Electrophoresis

The technique of electrophoresis relies on a difference of net surface charge between X- and Y-bearing sperm. There seems to be no reason why X- and Y-bearing sperm should differ in surface charge. However, in an electric field, some sperm do move towards the anode and some toward the cathode. Kaneko *et al.* (Gledhill 1988) used free-flow electrophoresis to separate a population into two groups. The difference in charge between the subpopulations was attributed to the X sperm having a greater net negative charge than the Y sperm. However, sperm motility is lost following electrophoresis.

3.4.4 Flow Fractionation

Bhattacharya (1977) devised a technique which combined thermal convection, centrifugation and galvanisation. Bhattacharya proposed that the lighter Y sperm would lag behind the X sperm in flow. If the two classes of sperm contained opposite charges on their surface then a suitable current (μA) would attract Y sperm to the anode and X sperm to the cathode. This method has not yet gained widespread acceptance.

Sarkar (1984) modified a laminar flow fractionation method for enrichment of X and Y sperm. It was proposed that swimming behaviour is a phenotypic characteristic of the two types of sperm, and when a velocity gradient is applied to sperm swimming in a suspension, the X sperm move in a straighter pattern than the Y sperm. Up to 80% enrichment was claimed using this method. However, the success of this technique has not been confirmed by other workers or validated by other methods.

3.4.5 Separation Based on Cell Density and Sedimentation Rates

Most separation procedures involving sedimentation rely on the assumption that the X and Y sperm differ in density due to a difference in DNA content. The density of sperm is heavily dependent on its water content and not its chromosomal constitution. Live sperm volume is dependent on the osmotic nature of the surrounding media. Meistrich (1982) estimated that the 2.1% difference in DNA content of X and Y bull sperm resulted in a difference of 0.0007 g cm^{-3} or 0.06% of the density of an X sperm. Separation on the basis of density therefore requires techniques with very high levels of density measurement resolution.

Separation is further complicated by the fact that sperm volume and therefore density may be modified by relative maturity of sperm (O'Donnell 1969, Laufer *et al.* 1979). Separation according to density may also be inhibited by differences in sperm motility characteristics, leading to various rates of sedimentation. While there have been several reports of separation of X- and Y-bearing sperm by density based methods, the technique is yet to gain widespread acceptance.

3.4.6 Adherence of Sperm to Sephadex / Sephadex Gel Filtration

Steeno *et al.* (1975) observed a significant decrease in the proportion of sperm bearing an F-body (a fluorescent spot found in the interphase nuclei of male sperm) of 3% to 9% after passage through a Sephadex chromatography column. Most of the sperm released from the Sephadex by washing after filtration exhibited F-bodies. Adimoelja *et al.* (1977) reported a 95% enrichment of F-body negative sperm. However, using this technique Henriet and Jaumotte (Windsor *et al.* 1993) found that cows inseminated with filtered semen did not yield an altered sex ratio of calves born. The Sephadex gel filtration method causes a marked reduction in sperm numbers and has the potential to cause low fertility rates.

3.4.7 Albumium Centrifugation

Ericsson and colleagues (Ericsson *et al.* 1973) used the human, salt-poor, water soluble, protein albumin as a gradient. This procedure takes 4 to 5 hours with less than 10% of the original fresh specimen remaining. Those sperm remaining display very high motility and strong swim velocity. Limited trials of this technique in domestic animals have given contradictory results, with some claiming enrichment (Zavos 1985) and others failing to alter sex ratio (Beal *et al.* 1984).

3.4.8 Separation using Flow Cytometry

Chromosome measurements have shown, that depending on the species examined, X sperm contain between 0% and 12.5% (Section 3.1) more DNA than Y sperm. X-bearing sperm consequently display a greater level of DNA linked fluorescence when stained with DNA-specific fluorochromes.

The first flow cytometric analysis of the DNA content of sperm to determine the ratio of X to Y chromosome-bearing sperm was successfully carried out by Gledhill (1976) and Van Dilla (1977). Early attempts to apply the flow cytometric technique to bull sperm were complicated by the flattened shape of the sperm head, and the highly condensed state of sperm DNA. These problems have largely been overcome by cytometers which align the sperm uniformly (Dean *et al.* 1978) or employ epi-illumination (Otto *et al.* 1979). The combination of these factors has produced an accurate method for measuring sperm DNA content which can be used to determine the X:Y ratios of sperm populations (Pinkel *et al.* 1982, Garner *et al.* 1983), and to assess the success of sperm separation techniques (Pinkel *et al.* 1982,1985). The physical separation of sperm according to DNA content was accomplished by Johnson (1986) on a modified commercial flow cytometer. The first live births from animals (rabbits) surgically inseminated with sorted sperm were subsequently reported by Morrell *et al.* in 1988.

While the method of sorting flow cytometry gives an X:Y enrichment ratio exceeding 90% (Johnson *et al.* 1995), it does so at a rate greatly limited by the sperm head shape and high refractive index. The maximum sort rate achieved for spherical cells currently approaches twenty thousand per second. Routine sorting of bull sperm is limited to less than 200 sorted X or Y sperm per second. The advancement of sperm sexing procedures using new developments for flow cytometry is considered in Section 3.5.

3.5 Sperm Sexing using Flow Cytometry

The use and development of flow cytometry for sperm sexing is now described, including methods used to overcome the problems associated with high resolution measurement of flat cells such as bovine sperm.

3.5.1 First Studies on Sperm

The first reported studies on sperm using flow cytometry were by Gledhill *et al.* (1976), and Van Dilla *et al.* (1977). Flat sperm from six eurethian species were stained with acriflavine and produced histogram distributions, each having a peak corresponding to a low fluorescence with a lateral extension to higher fluorescence intensity values (Figure 3-3). When radially symmetric (cylindrical or spherical) sperm such as abalone sperm were analysed, a second type of fluorescence distribution with none of the lateral extension was observed.

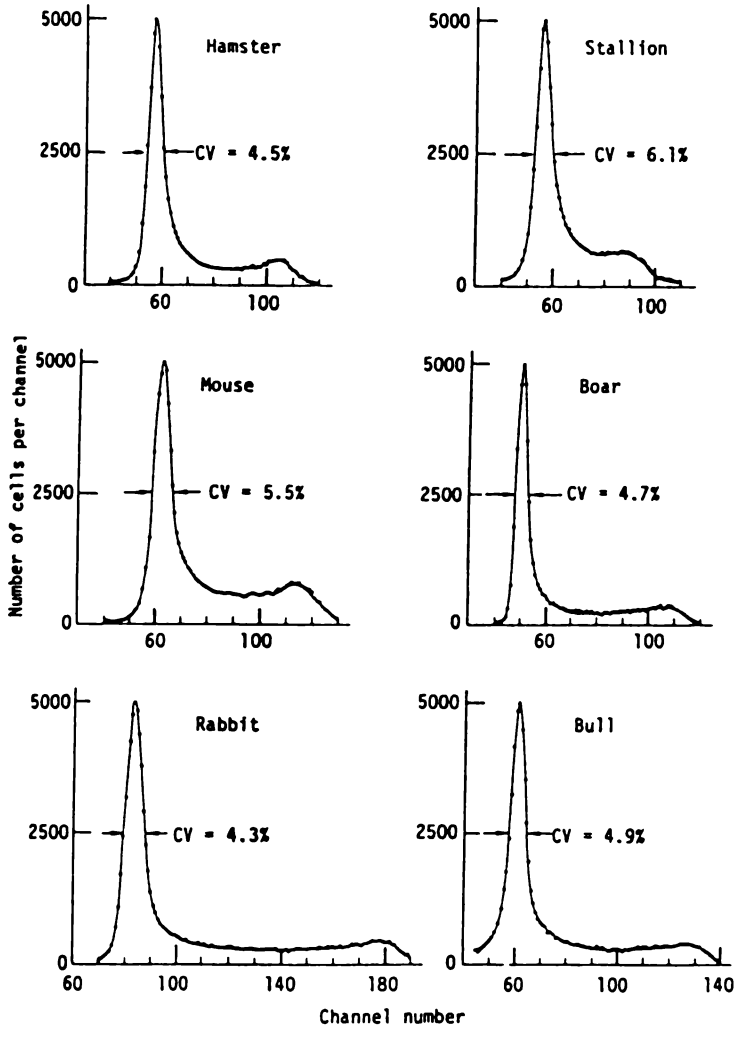

Figure 3-3. Frequency distributions of acriflavine-stained eutherian sperm from six species illustrating a lateral extension to higher intensity values (Gledhill et al. 1976).

If those sperm which fell within the main peak of the fluorescence distribution were sorted from the suspended solution of sperm and reanalysed, the complete distribution was obtained once more. Matching the refractive index of the suspending fluid in the cytometer (from $n = 1.33$) with that of the stained sperm ($n = 1.55$) was found to decrease the overall width of the distribution, however the lateral extension could not be entirely removed. It was also found that alternative fixtures and stains had no significant effect on the distribution. Reducing the effective fluorescence detection angle from 30° to 4°, to overcome any integrating or smoothing effect of the light emission from around the sperm surface resulted in no significant change in the fluorescence distribution.

Gledhill (1976) proposed that fluorescent light emission near the surface of the cell is favoured over light emission perpendicular to the surface because light is bent away from the normal by the cell-fluid refractive index mismatch. Thus, more light would exit the cell edge-wise than through the flat face of the sperm. When the cell edge pointed towards the fluorescence sensor, a maximum sized pulse resulted, but when at 90° to the detector axis, a minimum sized pulse resulted. With orientation at an arbitrary angle with respect to the z (flow) axis, intermediate sized pulses would result and the detailed shape of the observed fluorescence distribution depended on the angular distribution of the emitted fluorescence around the sperm axis. A two-dimensional model was proposed to confirm this hypothesis. This model is described in Chapter 6 and has been extended to include other physical effects which further explain the nature of histogram data for sperm studies.

Van Dilla *et al.* (1977) investigated the distorted fluorescence intensity distribution further by making several variations to flow cytometer optics. An epi-illumination flow system developed by Göhde (1973), where sperm were aligned parallel to the flow axis, yielded a measurement of DNA with a single frequency distribution peak. This system was not capable of sorting cells, due to constraints on the fluidic path within the instrument. Coefficients of variation (CVs) in the region of 4% - 5% were obtained with this method, however, CVs of less than 1.5% are generally required to measure the 3.9% difference between X- and Y-chromosome-bearing bull sperm (Chapter 7).

3.5.2 High Efficiency Flow Cytometer

A high efficiency flow cytometer was developed by Skogen-Hagenson *et al.* (1977) which employed an ellipsoidal flow chamber with a large effective numerical aperture (NA) and, therefore, a high fluorescent light collection efficiency (Figure 3-4). It was claimed that approximately 60% of the fluorescent light emitted by a cell passing through the chamber was captured, avoiding the orientation problem for fluorescence emitted by flat sperm. Any orientation problem related to the delivery of the illuminating light was still present, as illumination was from one direction only.

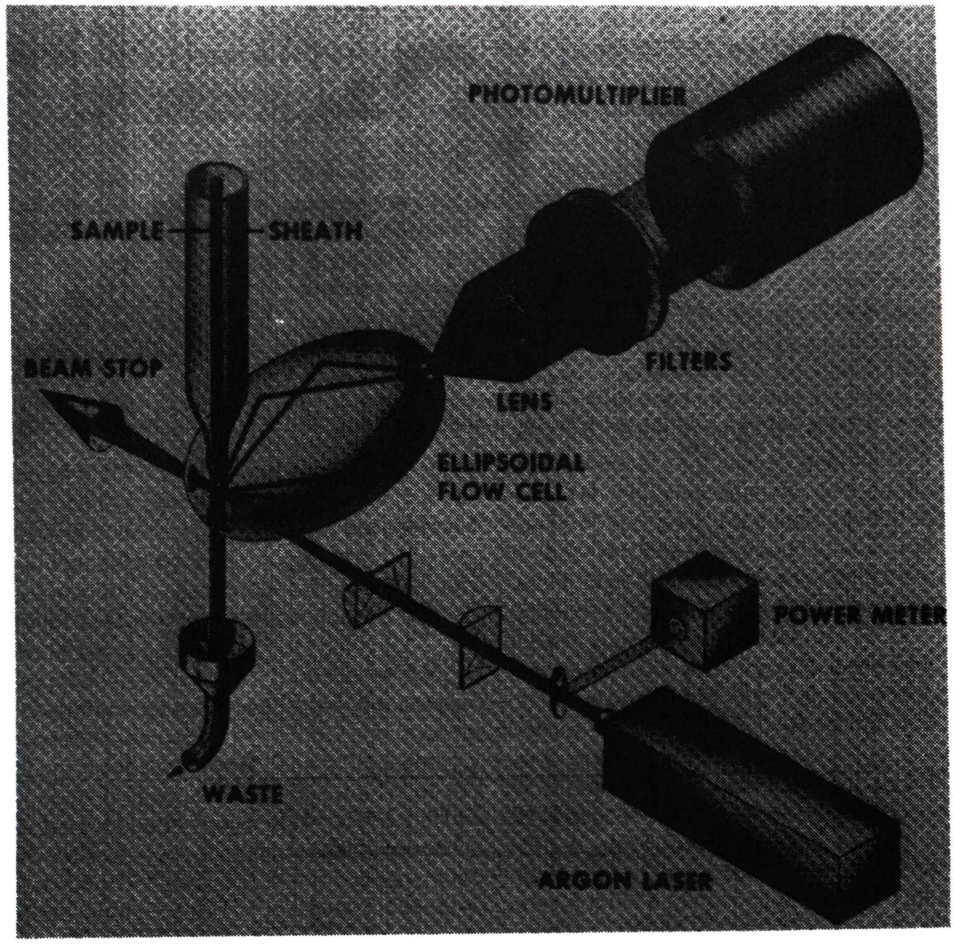

Figure 3-4. The high efficiency flow cytometer of Skogen-Hagenson et al. (1977) which uses an ellipsoidal reflector for fluorescence collection.

Coefficients of variation of 2.2% and 4% - 5% were reported for abalone (cylindrical), and bull sperm, respectively. The difference in CV between the two types of sperm suggest this system was unable to overcome the problem of uniform illumination with cell orientation, therefore increasing the error in measurement between cylindrical and flat sperm. Skogen-Hagenson noted that orientation-independent illumination of the fluorochrome may be a problem for all flow systems using a focused laser beam for excitation. This variation in illumination may cause a corresponding variation in fluorescence emission, thereby contributing to a broadened coefficient of variation. This effect is investigated in the modelling work of Chapter 6.

3.5.3 Sperm Orientation

Dean (1978) accomplished cell orientation by subjecting sperm to planar hydrodynamic forces achieved with a bevelled sample tube. By rotating the bevelled nozzle, Dean was able to obtain fluorescence distributions for a range of sperm orientations with respect to the laser beam and detector. The observed fluorescence intensity was found to vary considerably with cell orientation. The uniformity of

fluorescence intensity measured from the flat face of sperm heads was affected minimally by cell morphology. Measurements made on oriented sperm yielded CVs as low as 2%. Effective orientation and therefore low CVs required low flow rates, thus limiting analysis (input) rates to a few hundred cells per second.

Pinkel *et al.* (1982) demonstrated that the optical problems associated with sperm could be overcome using the commercial ICP22 epi-illumination flow cytometer (see Figure 3-5), or a specially built orienting flow cytometer. Using acriflavine stained rabbit sperm, Pinkel showed it was possible to orient sperm with a tolerance of ± 7°. Success was also achieved using sperm from bull, ram, and boar. Reliable results with human sperm could not be obtained. Both instruments were limited to analysis capacity only due to constraints imposed by the fluidics.

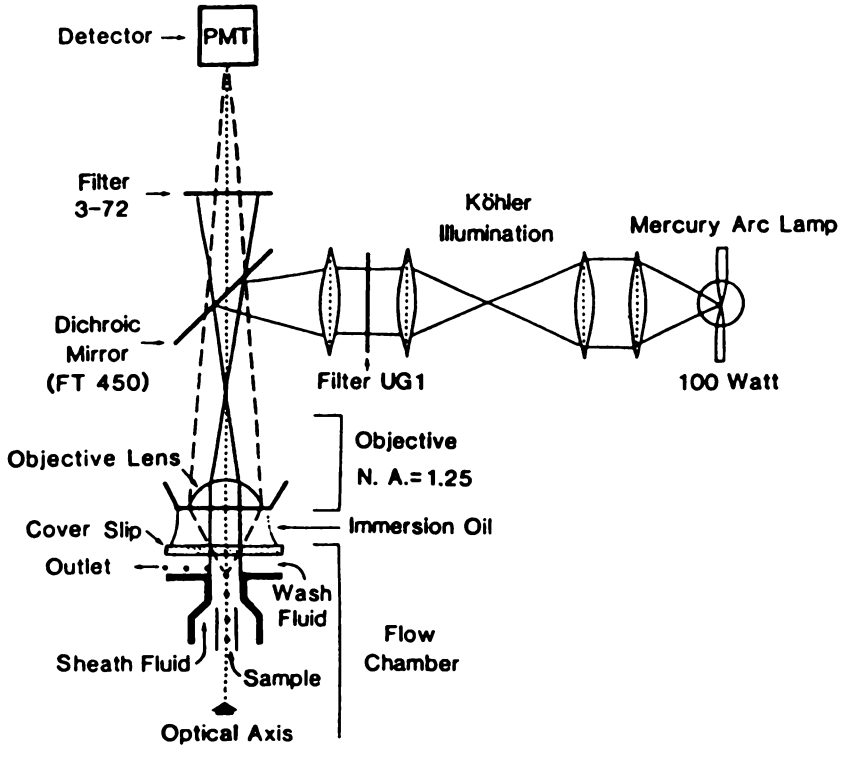

Figure 3-5. Flow chamber and optics of the epi-illumination flow cytometer. Sample flows toward the focus of the microscope objective for interrogation before being forced through the outlet (Garner et al. 1983).

Another approach to the problem of measuring flat cells such as sperm was to sense orientation by light scattering methods and to accept only those cells at an appropriate angle to the sensor (Métézeau 1991). While this method did eliminate the lateral (histogram) extension to higher intensity values, the

coefficient of variation was unacceptably large (5% - 10%), with half of the sperm rendered as waste since they were not at a measurable angle.

3.5.4 Measuring the Difference in DNA Content Between X and Y Sperm

Further work on the analysis of bull sperm was carried out by Garner *et al.* (1983) using an epi-illumination flow cytometer. Analysis of the bimodal fluorescence histograms by fitting two Gaussian distributions to the data showed the means of the peaks differed by 3.9%, 3.7%, 4.1%, and 3.9% for bulls, boars, rams, and rabbits respectively. Several bull breeds were studied and the X:Y sperm ratios measured for each. The evidence obtained in these studies suggested flow cytometry is a useful method for validating the effectiveness of spermatozoa X-Y enrichment techniques.

3.5.5 Sperm Separation using Flow Cytometry

Johnson and Pinkel (1986) modified an EPICS V orthogonal flow cytometer by introducing a forward fluorescence detector along the beam axis to complement the 90° detector. A bevelled tube was used to orient the sperm of the bull, boar and ram. The modified instrument was able to resolve X and Y sperm histogram peaks with equivalent accuracy to the epi-illumination design. This method initiated the first possibility of a successful method of sperm separation according to DNA sex content, since the modified jet-in-air flow cytometer was capable of droplet sorting by electrostatic deflection.

Johnson and colleagues carried out further analysis using a vital staining procedure to sort chinchilla (for which the 7.5% X-Y DNA difference is more easily distinguishable) and bull sperm (3.9% X-Y difference). On re-analysis of sorted sperm through the flow cytometer, relative X and Y purities of greater than 90% were measured.

The first conclusive evidence of sperm sorting success was obtained when sorted sperm were microinjected into hamster oocytes. Johnson and Clarke (1988) reported the first separation of bull, boar and ram X and Y chromosome-bearing sperm populations followed by proof of the viability of the sperm.

3.5.6 Live Births

Morrell *et al.* (1988) also carried out separation of X and Y chromosome-bearing sperm using a sorting flow cytometer and these were used for insemination of females. A breeding study, involving several generations of rabbits derived from sexed sperm, did not reveal any mutagenetic properties of the staining or sexing process. However, it was noted that such a study might have to be continued over many generations with different species before potential problems become apparent.

Johnson *et al.* (1989) also reported live births in rabbits surgically inseminated with sexed sperm, with accurate sex prediction of offspring. Later, Cran *et al.* (1993) demonstrated that viable bovine sperm can be sorted into X- and Y-bearing populations at reasonably high purity using a flow cytometer, that they

retain their capacity for *in vitro* fertilisation, that the sex of the resultant embryos is markedly skewed, and normal progeny can be produced with the birth of live calves.

Further studies have been performed to increase the resolution of the measurement of sperm DNA content using slit-scan methods (Rens 1996). These tests have provided an insight into orientation effects caused by the flat geometry and tails of intact sperm as they pass through the inspection point of the flow cytometer so that resolution of measurement may be improved.

3.5.7 Patents

Two patents exist for the technique of sperm sexing:

1) Sorting Living Spermatozoa (Dresser and Keeler 1985)

Dresser describes a method by which mammalian spermatozoa are stained with a fluorochrome dye, which, when analysed by a flow cytometer, result in a bimodal fluorescence profile. This enables the spermatozoa to be sorted into two distinct (X- and Y-chromosome-bearing) populations of motile spermatozoa.

2) Method to Preselect the Sex of Offspring (Johnson 1992b)

Johnson outlines the separation process according to DNA content using a modified flow cytometer. Sorted sperm are surgically inseminated into rabbits or swine. The subsequent birth of sexed offspring with a phenotypic sex ratio is consistent with predictions based on the relative DNA content of the sorted sperm populations.

3.5.8 Extension to Humans

The first human birth (a baby girl) involving flow cytometry recently resulted from the combined clinical development of flow cytometric sperm separation with pre-implantation genetic testing for the prevention of X-linked hydrocephalus, a recessive mutation carried by the mother (Levinson *et al.* 1995).

3.6 Sperm Sexing - Method of Johnson et al.

The method of Johnson *et al.* (1986, 1995) for sperm sexing histogram interpretation and gating is briefly described below. The fluorochrome which is used to stain the sperm is outlined in Section 3.7.

This method uses a combination of fluidic orientation of the sperm heads, which biases the orientation of sperm heads to lie in one plane, and orientation sensing, by detecting the bright flash of sperm which are edge-on to the side fluorescence photodetector. Fluidic orientation is achieved by a bevelled sample injection needle, that generates a ribbon flow of the sample core as the sheath draws the cells into single file. Orientation is sensed by monitoring the intensity of cellular fluorescence as sperm heads pass the side detector. Only those cells which are shown to be oriented, by their high-intensity edge emission, are considered for sorting. Figure 3-6 displays a typical histogram set for a population of Hoechst-stained bull

sperm as measured by the forward and side fluorescence detectors of a flow cytometer with an orthogonal optical geometry.

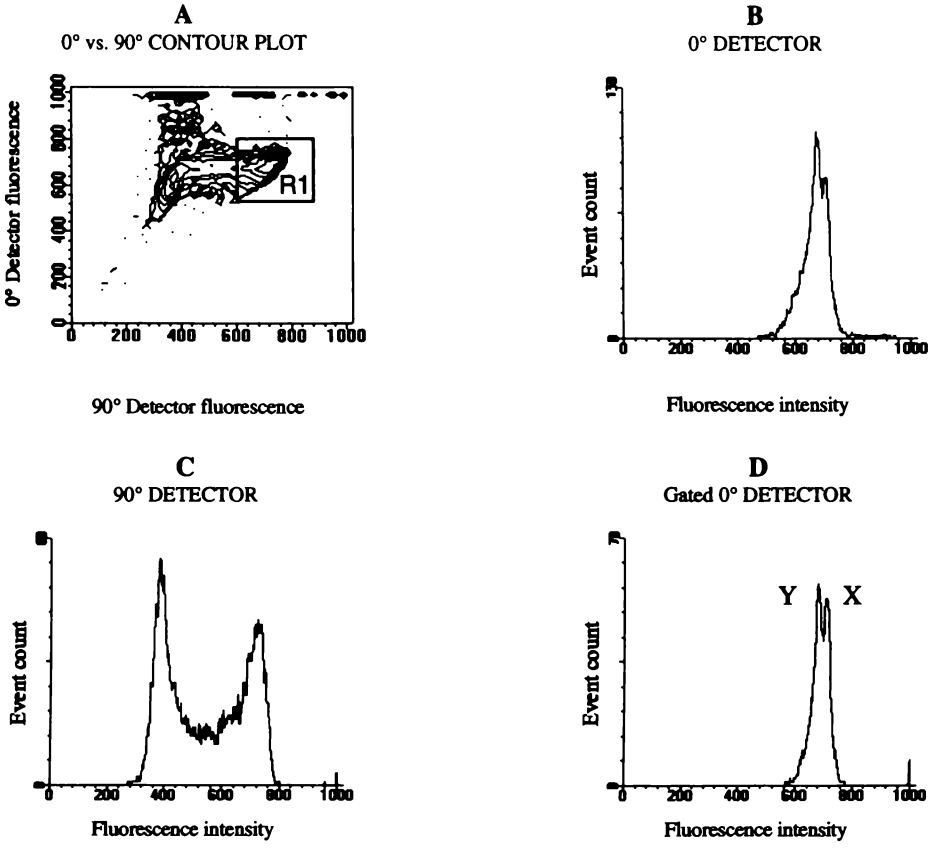

Figure 3-6. Hoechst 33342 stained bull sperm fluorescence histograms displaying A: contour plot, and histograms of B: forward (0°) detector, C: side (90°) detector, and D: R1 gated side detector for oriented cells.

The difference of 3.9% in DNA content between the X- and Y-bearing sperm is expected to produce a corresponding difference in Hoechst stain uptake and therefore difference in fluorescence intensity. The contour plot of side vs. forward fluorescence (Figure 3-6A) displays an L-shaped distribution characteristic of that produced for flat cells in an orthogonal laser-detector optical arrangement. Those sperm which are measured as having high fluorescence intensity by the side detector (Figure 3-6C) but low intensity at the forward detector (Figure 3-6B), thereby falling on the lower right region of the L, are assumed to be aligned edge-on with respect to the side detector. Sperm which are oriented face-on to the side detector fall within the intensity values of the upper left region of the L, with intermediate orientations lying between the two extremes. The modified flow cytometer uses a bevelled sample tube to bias the orientation of cells in the sample stream. The effect of this on the contour plot is to increase the proportion of cells in the lower right region and decrease those in the upper left region compared with measurements obtained with randomly oriented cells. A gate (R1) is positioned over the oriented cells which lie in the lower right region of the L (Figure 3-6A). The X and Y sperm populations can be distinguished in this figure as two overlapping Gaussian-like curves separated by approximately 3.9% in intensity (Figure 3-6D).

3.7 Fluorescent Stains for Sperm Sexing

A fluorescent stain used for sorting sperm with retention of viability must be sufficiently stoichiometric and, therefore, homogeneous at low concentrations to allow good resolution of the X and Y sperm populations. Flow cytometric sperm sexing relies on the staining of cells with a light-sensitive stain which, when illuminated, will fluoresce. The key feature of DNA probes (stains) is that they are stoichiometric. Thus, the number of molecules of stain bound is equivalent to the number of molecules of DNA. Depending on the number of bond sites available to the stain, the difference in uptake will yield a difference in the number of molecules available for excitation and fluorescence. For the case of sperm, the difference between X and Y DNA content will correspond to an equivalent measurable difference in fluorescence light incident on a photodetector.

The primary stain which is used for sperm sexing is Hoechst 33342, which is of the bis-benzimidazole family. The molecular stucture of Hoechst 33342 is given in Figure 3-7. The bis-benzimidazoles bind preferentially to AT-rich regions in the small groove of DNA and fluoresce blue when excited. Hoechst 33342 has an excitation peak at 365nm with peak emission at 450nm, and so the 365nm UV line from an Ar^+ laser is well suited to this stain. Hoechst 33342 is also actively transported into, and out of cells, so that the concentration of dye in a cell and its fluorescent spectrum will depend on conditions of incubation. A typical concentration for this stain, for a sperm concentration of 10^6 ml^{-1} as used in our research, was 9µl ml^{-1} Hoechst 33342. Sperm samples were incubated at 35°C for 60 minutes prior to analysis.

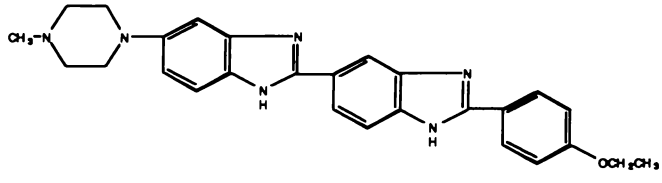

Figure 3-7. Molecular structure of Hoechst 33342.

DAPI, or 4-6-diamidino-2-phenylindole, is a dye which has similar properties to Hoechst 33342 in that it is AT-specific and has been used for DNA content analysis. However this stain is non-vital and so is only useful for re-analysis of other X-Y separation methods.

Many other DNA stains (including SYBR-14 and the TOTO series) have been trialed in the hope of finding a possible replacement for the Hoechst stain which is visible rather than UV wavelength excitable. This quest is for two reasons: to reduce the effect of UV irradiation damage to the DNA, and to reduce the relative expense of having a UV laser on hand. To date, this search has not provided a fluorophore replacement for live cells which consistently produces the X-Y differential resolution of Hoechst 33342.

3.8 Operational Considerations - Sperm Vitality and Viability

As mentioned earlier in Section 3.2.2, different environmental factors can greatly affect sample morphology. In the case of sperm sexing, it is essential that these environmental conditions be optimised to ensure the vitality, longevity, and viability for successful fertilisation.

Lifetime Under Optimum Conditions

By using appropriate buffer extension mediums and by storing samples at suitable temperatures, sperm remain motile and viable for up to several days. Dilution of a sperm sample in a biologically unsuitable medium can reduce viability, as can temperature shock. Samples which contain a high proportion of dead cells are also susceptible to loss of vitality.

Stains

The vital stain Hoechst 33342 used for sperm sexing binds between the A-T base pairs of the DNA chain. Traces of this stain can be detected several divisions into the development of an embryo, however live births have not shown signs of mutagenetic damage and reproductive integrity is retained (Kissane 1982, Morrell *et al.* 1988, Johnson 1995).

Laser Irradiation Effects on Viability

UV laser irradiation in the flow cytometric analysis of DNA for sperm introduces a possibility of genetic damage. Exposure to high laser power levels (exceeding 100mW) appears to decrease survival (Kissane *et al.* 1982). Laser power levels must be minimised to reduce mutagenetic effects.

Pressure Variations in Flow

The pressure variations that a cell experiences as it travels through the nozzle of a flow cytometer can be extreme, causing cell implosion or explosion. Sample and sheath pressure must be at a level which does not allow these extremes to damage the spermatozoa.

Optical Artifacts of Sperm Fluorescence Measurement

The combination of the size, shape, geometry, high refractive index, and the small relative difference between the size and therefore uptake of fluorescent stains by bovine (and many other mammalian) sperm heads produces optical artifacts in measurement when using a flow cytometer with orthogonal axes of illumination, flow and detection. These artifacts have hindered the ability for high resolution measurement to differentiate the 3.9% fluorescence intensity difference between X- or Y-chromosome-bearing sperm. This is discussed further in Chapter 6, in conjunction with an optical model which we have developed to simulate, quantify and explain these effects.

Swimming Motions

Mammalian spermatozoa rely on an oscillatory motion of the flagellum for transportation prior to fertilisation with an egg. This motion produces velocities of up to 200 $\mu m\ s^{-1}$ with average head flip frequencies of 9.1 Hz at 37°C (Beaumont 1997) which, for fluorescent measurements, could pose

resolution difficulties. These values decrease considerably with temperature. For the case of flow cytometric measurement, where cells are presented to the laser for measurement over a period of less than 5μs, these swimming motions are unlikely to have any effect.

3.9 Commercial Application

If sperm sexing in domestic animals is to become commercially viable, a method must be found to produce higher volumes of sorted viable X or Y sperm at a higher rate than that of current techniques. The low sort rates of the orthogonal optics method precludes the use of sexed sperm for commercial-scale *in vivo* fertilisation. The method of *in vitro* fertilisation following flow cytometric sperm sorting is currently the only procedure available to produce embryos of a predetermined sex.

A modified orienting flow cytometer can differentiate and sort approximately 10% of sperm passed through the instrument. This low efficiency is caused first by the requirement of the system that only those sperm in a known orientation can be reliably analysed for X-Y differentiation. Second, due to X and Y population histogram overlap, only one quarter of those sperm which are considered oriented can be reliably considered to be X or Y chromosome bearing sperm. For a sperm input rate of 3000 s^{-1}, 600 will typically be oriented with a resultant output of 300 (approximately 150 X and 150 Y) sorted sperm per second (Chapter 7).

To put these figures into perspective, in cattle, approximately ten thousand sperm are required for *in vitro* fertilisation of one egg for the birth of one animal. This requires a few minutes of sorting at current sort rates. If *in vivo* fertilisation by artificial insemination were to be made possible, between two and ten million sperm are needed for one straw for the insemination of one cow, requiring 4 to 20 hours of instrument sort time. An increase in throughput would yield the possibility of fertilisation through *in vivo* (in the female tract) rather than the more laborious *in vitro* techniques.

4. A New Optical Configuration for Sperm Sexing

One of the principle objectives of our research was to design a new optical configuration which could remedy optical artifacts experienced when measuring fluorescence from aspherical or flat cells such as bovine sperm. In an attempt to meet this objective, a radially symmetric optical system has been designed which overcomes the effects of cell orientation in flow cytometry. This chapter describes the optical system (radially symmetric optics) that we have developed.

Section 4.1 gives the background and describes the motivation for a new optical system. In Section 4.2, a general description of the optical elements and associated mounting hardware is given, and in Sections 4.3 and 4.4, each of the key optical components is described. In Section 4.5, measurements and comparisons are made between the focal volume of the radial configuration, and that for a conventional orthogonal optical geometry. The efficiency of the radial configuration built is considered in Section 4.6. Finally, operational considerations of the radial optics configuration are summarised in Section 4.7.

4.1 Motivation For A New Optical System

There are several problems in flow cytometry for sperm sexing which limit the accuracy of analysis and ultimate sort rates. The goal of the sperm sexing process is to sort X- and Y-chromosome bearing sperm and, following artificial fertilisation, to enable gender preselection of offspring for mammalian species of agricultural importance. With this aim in mind, an ideal flow cytometer optical system must be able to measure the difference between X and Y bearing sperm, independent of the cell orientation with respect to the illumination and collection optics. It must do so at maximum sort rates, purity, efficiency, and with minimal sample damage and waste. The primary goal of our research was to obtain accurate fluorescence measurements on flat particles without compromising speed. An additional goal of the work was to increase collection efficiency in an effort to reduce UV power. Before presenting the design of the new optical configuration we discuss the objectives of the system.

It was proposed that orientation-independent illumination of the sperm cells could be used to overcome variations in the amount of light incident on the DNA stain. These variations are due to effects such as cell absorption, total internal reflection, or the cross-sectional area presented to the uni-directional laser illumination used in a conventional system. Fluorescence collection which is independent of cell orientation was also desired. Such an optical system would eliminate the need to gate appropriately oriented cells in order to achieve reliable measurement of DNA content. In addition, hydrodynamic alignment of cells would no longer be required, releasing the constraints on flow rate associated with hydrodynamic orientation and consequently increasing flow and therefore analysis rates.

A further objective was to increase illumination efficiency. UV irradiation of DNA must be minimised to reduce possible genetic damage. A more efficient light delivery system would minimise required laser

power levels, and therefore the level of UV irradiation to cells, by for example, illuminating around the cell flow axis. In addition, lower power requirements could lead to the implementation of inexpensive light sources such as air-cooled lasers or arc lamp sources rather than the expensive water-cooled devices, such as argon ion lasers, which have been required to date. Secondly, maximisation of light collection efficiency was desired in order to capture as much of the fluorescence emitted from the stained sperm as possible. An improvement in collection efficiency could further reduce the laser power required to obtain a detectable amount of fluorescence and thus reduce UV irradiation to cells.

A further objective was to provide an optical configuration capable of being fitted to an electrostatic droplet deflection sort mechanism. Electrostatic droplet deflection is the fastest flow cytometric technique for sorting single cells to date. Electrostatic deflection required that the new optical configuration operates as a jet-in-air system.

4.2 Description of Optics

A new radial flow cytometer optical configuration has been designed (Sharpe and Schaare 1997) to meet the objectives outlined in Section 4.1. This geometry combines 360° radial illumination and radially symmetric collection of fluorescence from particles or cells as they pass through the inspection point. Schematic diagrams of side, and isometric views of the radial optics are shown in Figures 4-1 and 4-2 respectively. The photograph of Figure 4-3 illustrates the experimental set-up of the radial optics configuration.

The key elements are a custom-made glass cone (axicon), and a paraboloidal reflector (POF10-1, Opti-Forms Inc.,Temecula, CA), which are aligned coaxial with the flow cell. An argon ion (Ar^+) laser (Coherent Innova 500 series) delivering 150mW (TEM_{00}) in multi-line UV is used as the excitation source. The optical beam of the Ar^+ laser is reflected by a front surface mirror (02MPG006, Melles Griot, Irvine, CA) onto the point of the axicon. The beam refracts into a divergent cone of light which propagates through the rear face of the axicon. The light is then reflected by a planar mirror (02MPG009, Melles Griot, Irvine, CA) back through the cone to refract again at the front face, producing a cylinder of laser light which encircles, and is anti-parallel to, the input beam. The cone angle and mirror placement are calculated so that the radius of the cylinder of light is 20.4mm.

The paraboloidal reflector has a focal length of 10.2mm and a 22mm hole in the base through which the sample stream exits, and where a droplet sorting mechanism may be situated. The cylindrical beam is incident on the 45° section of the reflector and forms a convergent disk perpendicular to and focused on the sample stream. The size and shape of the beam focus was measured by shading off all but a 60° sector of the cylindrical illuminating beam and placing a two-dimensional charge coupled device (CCD) array (TC211, Texas Instruments Inc., Dallas, TX) at the parabola focus to measure light intensity at 13.75μm by 16μm grid spacings. The radial focus region has a three-dimensional ellipsoid intensity profile, with a

96.7μm vertical dimension and a 58.5μm horizontal diameter (beam waist at 1/e intensity, see Section 4.5.2 for details). Stained cells are carried by the sample stream through the radial excitation focus and fluoresce. Much of the fluorescence is collected by the paraboloidal reflector and projected out in a collimated beam. The solid angle subtended at the focus by the reflector is 8.67 sr, equivalent to approximately 60% of a sphere surrounding the focus. For applications where maximum fluorescence collection is desired, this collection efficiency compares favorably with a typical microscope objective employed in an orthogonal flow cytometer which has a solid angle of approximately 1.77 sr, or 14% of a sphere centred at the focus.

A pair of 45° mirrors direct the fluorescent light from the reflector regions above and below the radial excitation path onto a 95mm focal length aspheric condensing lens (17.1301, Rolyn Optics Company, Covina, CA). Light emitted forwards and backwards with respect to the direction of flow of the jet will be reflected by the paraboloidal reflector to the inner and outer mirrors, respectively, and can be focused to different detectors (see Section 4.2.1). The aspheric lens focuses the fluorescent light to a 1mm spot which is then imaged by a conventional flow cytometer microscope objective (H32x/0.60 NA Quartzgl, Leitz, Germany) and standard BDIS FACs photomultiplier tube (PMT) housing. Light signals can then be split or passed through suitable dichroic, interference, or glass filters before falling on the PMTs.

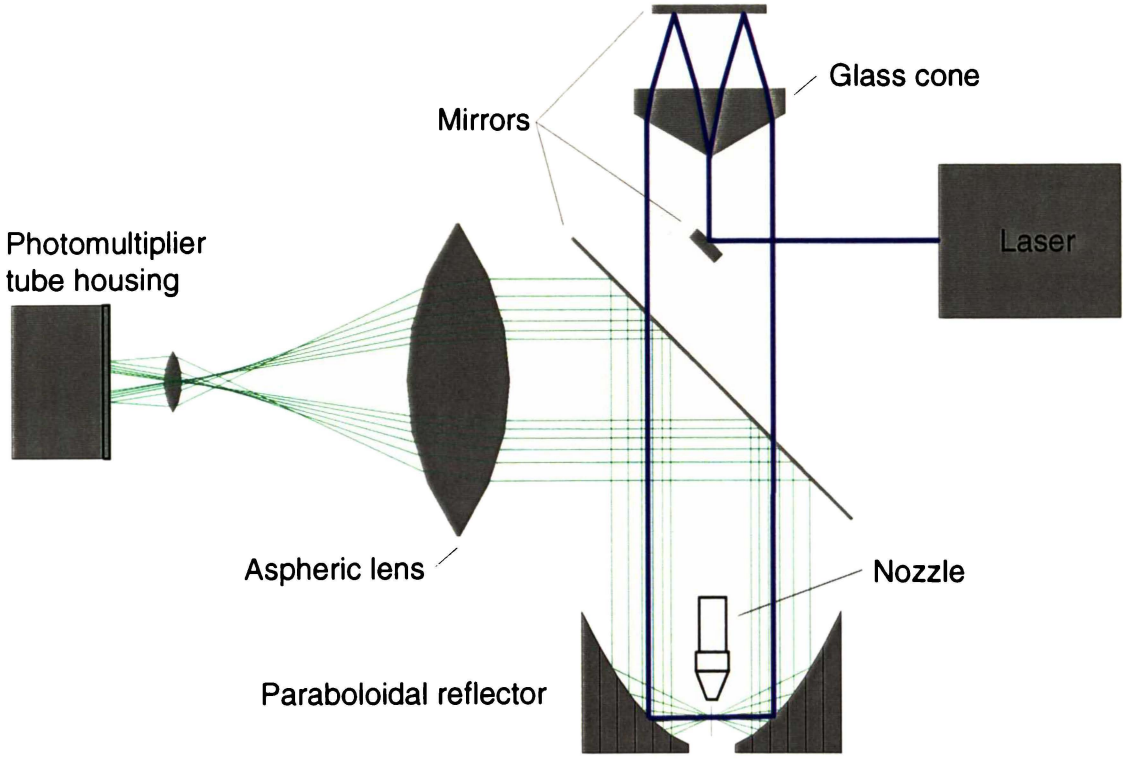

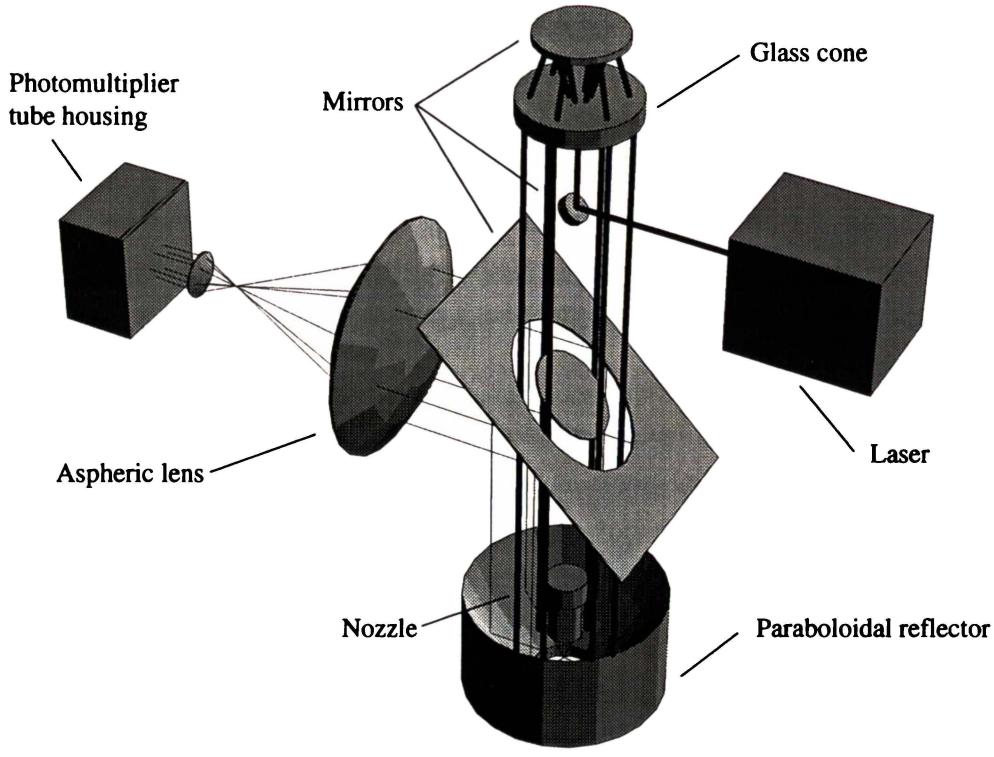

Figure 4-2. Isometric view of the key optical components.

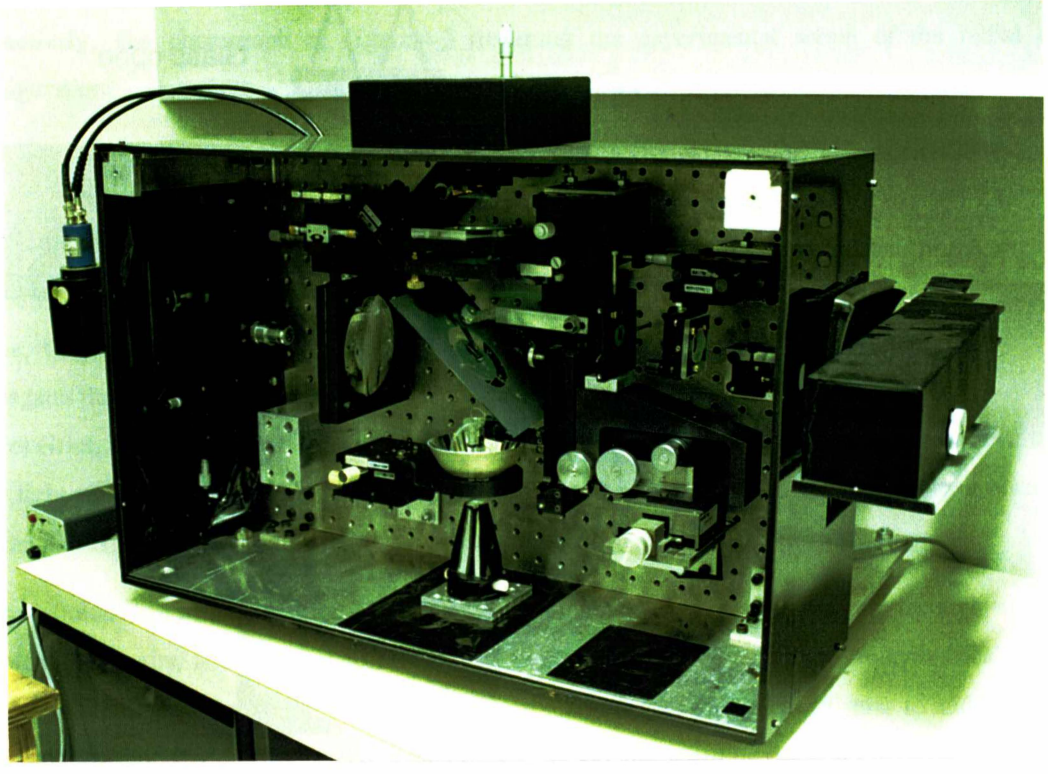

Figure 4-3. Photograph of the experimental layout of the radial optics.

No beam stop is required for this configuration since most of the excitation wavelength light which is reflected, scattered or refracted by the jet retraces the path of the illuminating beam and will exit the fluorescence collection optics through the elliptical aperture in the collection mirrors.

This optical geometry provides 360° radial illumination and omni-directional cell scatter and fluorescence collection around the sample flow axis while allowing for the incorporation of conventional jet-in-air electrostatic droplet sorting.

4.2.1 Radial Optics Modifications

Two modifications were carried out on the radial optics in order to simulate the light collection geometry of a conventional flow cytometer (see Chapter 5 for experimentation). First, the radial optics collection geometry was modified to provide fluorescence collection by two independent detectors. The radial optics were partitioned to provide lower hemisphere, or fore (in front of the focus relative to direction of flow), and upper hemisphere, or aft (behind the focus relative to direction of flow) detection of the light as the cells flowed through the inspection point. This situation is illustrated in Figure 4-4. A mirror was positioned (at 45° to the optical axis) between the aspheric collection lens and the original PMT housing. A second (fore) PMT housing (and objective) was introduced to collect the fluorescence from this mirror. Thus, fluorescence originating from the focus and collected by the lower hemisphere of the paraboloidal reflector, could then be detected, while fluorescence from the upper hemisphere was projected into the original (aft) PMT housing.

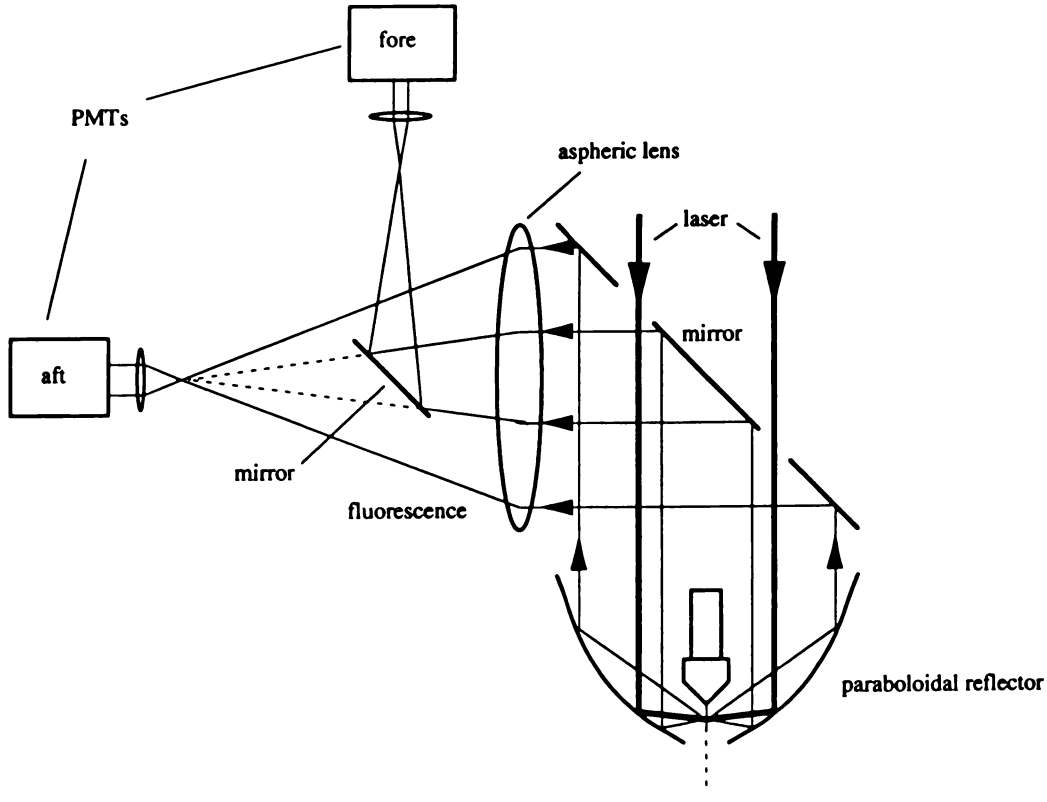

Figure 4-4. Fore-aft detector modification to collect fluorescence above and below cells as they pass through the inspection point.

The second modification enabled the orthogonal collection geometry of a conventional flow cytometer to be reproduced, while retaining radial illumination. This modification was made to investigate the effect of cell orientation with respect to the excitation source, on the accuracy of fluorescence measurement using orthogonal optics. The fore-aft detection system was modified by positioning a (60°) wedge-shaped aperture in front of each PMT housing (Figure 4-5). The first aperture element was located in front of the fore PMT housing. The second aperture element, rotated 90° about the optical axis, was located in front of the aft PMT housing. Thus, the radial sector of light reaching each detector from cells at the inspection point was restricted to an angle of 60° (the collection angle of a conventional orthogonal detector). This sectored fore-aft detector arrangement was used to reproduce the forward and side light collection geometry of an orthogonal flow cytometer arrangement, while preserving the radial (orientation independent) light delivery system of the radial optics design.

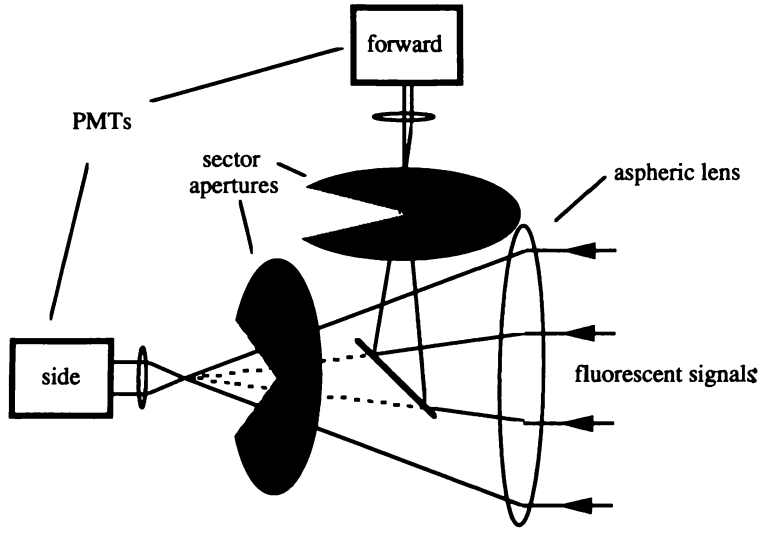

Figure 4-5. Modified radial optics with two sector apertures rotated 90° about the optical (and flow) axis relative to each other to obtain an orthogonal collection geometry.

4.2.2 Comparison with Other Optical Systems

Numerous methods have been developed to overcome optical artifacts associated with sperm DNA content measurement using flow cytometry (Chapter 3). The merits of several such optical geometries are outlined in Table 4-1 and are now compared with those of the radial system.

High NA fluorescence collection can be used to overcome orientation effects due to fluorescence emission, by encircling the laser cell excitation focus (inspection point) with an ellipsoidal reflector (Skogen-Hagenson *et al.* 1977). However, such systems are still prone to orientation effects because of uni-directional illumination. An epi-illumination flow cytometer provides a means for overcoming the effects of orientation on both illumination and fluorescence collection of flat cells (Garner *et al.* 1983). However, the fluidic design of these instruments inhibits jet-in-air sorting, restricting their use to analysis only. The only method which consistently achieves high resolution flow cytometric measurements of sperm uses

modified fluidics and orthogonal optical geometry to align cells and monitor their orientation (Johnson *et al.* 1986). Using this technique it is possible to resolve the 3.9% X-Y difference for those bull sperm (10% - 40%) which are oriented appropriately and to subsequently sort the cells. However, this technique is sort-rate limited by fluidic constraints required to produce successful orientation, and efficiency limited due to sample waste of all non-aligned cells.

The radial optics provides orientation independent illumination and fluorescence collection of cells as they pass through the inspection point, and thus does not require hydrodynamic orientation of cells in one plane. From Table 4-1 the value for the solid angle shows that fluorescence collection efficiency is increased for this system. A low power UV light source may then be used to replace the Ar^+ laser which is required in the orthogonal geometry. Most importantly, the radial system can easily be fitted with an electrostatic sort mechanism for high speed cell sorting.

Table 4-1. Comparison between various optical geometries for sperm sexing. The solid angle of collection is expressed as the percentage of a full sphere (4π steradians) subtended from the inspection point.

Optical system	Orientation independent illumination	Orientation independent collection	Electrostatic sort capability	Hydrodynamic orientation requirement	Solid angle of collection (% sphere)
Ellipsoidal Collection (Skogen-Hagenson, 1977)	No	Yes	No	-	75%
Epi-illumination (Garner, 1983)	Yes	Yes	No	-	< 50%
Orthogonal Optics (Johnson, 1986)	No	No	Yes	Yes	7% + 14% (two detectors)
Radial Optics	Yes	Yes	Yes	No	60%

4.2.3 Radial Optics Alignment Procedure

Reproducible alignment of the optical train of a flow cytometer is crucial to obtain repeatable measurements on a day to day basis. The following series of steps outlines the method for aligning the radial optics prior to cell analysis.

- The laser beam is steered onto the point of the axicon lens. The trajectory of this beam defines the optical system *z*-axis.
- A fixed diameter retro-reflected (partial internal reflection off back surface of axicon) ring of light will emerge. This ring must be oriented anti-parallel to the *z*-axis. This alignment is performed by adjusting tilt and yaw with a kinematic mount, by centering the in-coming beam with respect to the out-going light ring.

- The retro-reflection mirror must then be aligned with the z-axis. The mirror is located close to, and parallel with, the axicon back surface. Introduction of this mirror will yield a brighter, second output ring which must be aligned concentrically with the faint ring from the axicon. This is achieved using pitch and yaw kinematic mount adjustment. Once aligned, the z position of this mirror can be adjusted to alter the output ring diameter to its appropriate size.
- The paraboloidal reflector must be coaxial with the axicon to minimise focal broadening. Initial alignment is performed by centering the light ring with respect to the aperture of the paraboloidal reflector by adjusting x and y translation stages. Once centred on the z-axis, the retro-reflection of the incoming ring is used to adjust yaw and tilt for concentric alignment of the parabola and z axes.
- The z translation stage of the retro-reflector mirror is adjusted to produce a ring of 40.8mm diameter which will result in 45° reflection off the parabola surface, producing a horizontal disk of light which converges to the focus.
- Preliminary nozzle alignment is performed by locating the jet in a position that scatters the incoming light back onto the reflector in a radially symmetric fashion. At this point, the illumination optics are coarsely aligned.
- Fine adjustment of the collection optics must then be performed. The fluorescence collection mirror pair are located at 45° to the z-axis in order to project cellular fluorescence away from the excitation beam for detection. The inner mirror yaw and tilt is adjustable. Some jet-scattered and stray excitation light is also collected and used for further visual alignment of the collection lenses.
- The light is projected onto the aspherical lens which produces a dim image of the scattered light at its focus. The microscope objective is mounted onto, and is aligned with, the PMT detector housing. This unit is adjustable in three dimensions and is located one objective focal distance from the aspheric lens image.
- Fine adjustment is then performed by introducing fluorescent calibration particles to the jet. Two position adjustments are performed iteratively to maximize the height of fluorescent signals from the calibration particles. The x, y, z position of the objective and the x, y position of the nozzle are adjusted alternately until fluorescent pulses have been maximized.

4.3 Axicon Design Considerations

4.3.1 Background

A key operational requirement of the radial optics design was to deliver excitation light to the cells at the inspection point of the flow cytometer in a radially symmetric manner. A paraboloidal reflector performed this function. The use of a paraboloidal reflector required that the input light source (laser beam) be in the

form of a collimated, cylindrical tube of light. An axicon element was chosen to produce this cylinder of light.

The name axicon means axis image, and in optics, describes a figure of revolution. The axicon was first described by McLeod (1954) as an optical element of circular symmetry which focuses a point source on the axis into a continuous series of point sources. There are many forms of axicon, such as rings, cylinders and cones. A common axicon form is a flat cone lens which was used in the radial optics design, and is displayed in Figure 4-6.

Figure 4-6. Schematic of the flat cone lens (axicon) used in the radial optics configuration.

4.3.2 Operation

For application to the radial optics, an axicon was used to transform a laser beam into a ring of light with a variable diameter. The planar surfaces of this element allow refraction to be used to split the laser beam, which is incident on the apex of the cone, into a radially symmetric diverging cone of light. By locating a variable z-position mirror behind the axicon (the z-axis being the axis of rotational symmetry of the axicon), this light cone can be intercepted and projected back through the same refractive path to produce a cylinder of light which is anti-parallel to the incoming laser beam.

4.3.3 Other Component Options

Other light-cylinder-generating optical components were considered for the radial optics design. These components included ring diffractive elements and crystal structures. Diffractive elements produce a divergent light-cone profile that would require further modification to produce a light cylinder. Sperm sexing requires that UV grade (i.e. low absorption) optical materials be used. Commercially available diffractive elements are produced only with plastic materials which are not suitable for UV transmission (due to high absorption). Crystal structures such as Aragonite ($CaCO_3$) exhibit internal conical refraction, however the length of such a material required to produce a 40.8mm light cylinder is prohibitive.

4.3.4 Design

Two refractive cone lens configurations, and one reflective element, each of which produces a cylinder of light from a laser beam, are presented in Figure 4-7. The single element axicon has its rear surface mirror coated (Figure 4-7A). The two element design has a shorter axicon in combination with a front surface

mirror which is mounted parallel to, and at a variable distance from, the rear surface (Figure 4-7B). The reflective element consists of a pair of (convex, and concave) axicons that are mounted coaxially (Figure 4-7C).

Operational advantages of the single element design are its fixed alignment and minimum number of interface surfaces, thus corresponding to low reflection losses. The two element design provides relatively low transmission losses due to absorption (because of a shorter internal path length of the light), and the capability to adjust ring diameter. Both refractive designs, however, exhibit losses due to absorption and multiple interface reflection losses. It is envisaged that later designs of the radial optics will incorporate a reflective axicon element as illustrated in Figure 4-7C. The reflective element would not be susceptible to absorption losses (as are the refractive elements), would reduce the number of interaction surfaces (where reflection losses come into effect), and would be insensitive to wavelength variations (i.e. changing the laser excitation line).

For our research, an initial single-element design was modified to the two element configuration to provide variable light cylinder diameter. The variable diameter design was useful for applying the cone lens to various paraboloidal reflectors and for alignment and fine adjustment of the light cylinder. Financial and manufacturing constraints prevented us from using a reflective axicon. However, future work will investigate its possible incorporation into the optics.

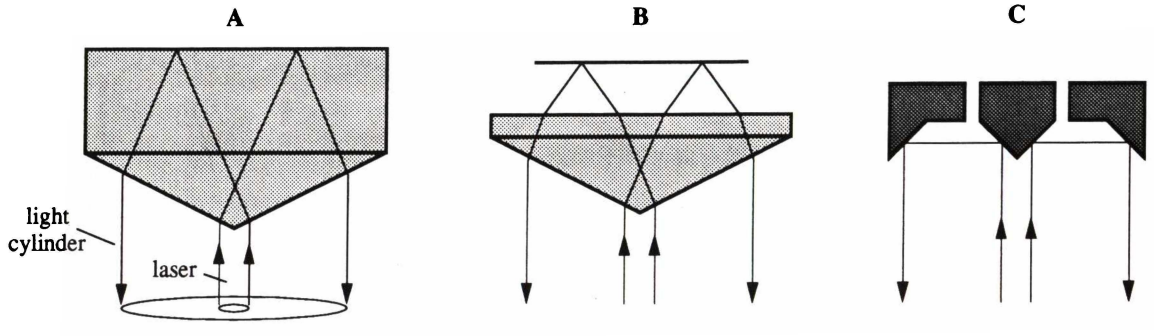

*Figure 4-7. Three axicon configurations which generate a light cylinder from an incident laser beam. **A:** A single, rear-surface-mirrored axicon, **B:** axicon and rear mirror combination, and **C:** reflective axicon.*

Single Element Axicon Design

We will now determine the cone geometry required to produce a light cylinder of given radius for the single element design (Figure 4-8). For this analysis the cone is coaxial with the z-axis, has a pitch angle ϕ, length l, and refractive index n_2. An incoming ray of light propagates through air (n_1) parallel to the z-axis, and is incident on the cone near the tip. The incidence angle the ray makes with the axicon, θ_1, is equal to the pitch angle ϕ.

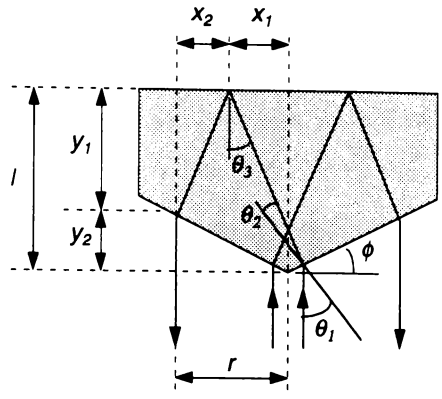

Figure 4-8. Geometry of the single element axicon design.

Using Snell's law of refraction $n_1 sin\theta_1 = n_2 sin\theta_2$, we can determine the angle of refraction θ_2, which is related to the axicon back surface incidence angle θ_3 by

$$\theta_3 = \theta_1 - \theta_2 \tag{4-1}$$

$$= \phi - \sin^{-1}\left(\frac{n_1 \sin\phi}{n_2}\right). \tag{4-2}$$

From the diagram the following holds

$$x_1 = l\tan\theta_3 \tag{4-3}$$

$$x_2 = y_1 \tan\theta_3 \tag{4-4}$$

$$y_1 = l - y_2 \tag{4-5}$$

$$y_2 = r\tan\phi \tag{4-6}$$

$$r = x_1 + x_2 . \tag{4-7}$$

Using these expressions we obtain

$$r = (2l - r\tan\phi)\tan\theta_3 . \tag{4-8}$$

Re-arranging this equation for l, the final expression for the cone length is obtained

$$l = \frac{r}{2}\left(\frac{1}{\tan\theta_3} + \tan\phi\right). \tag{4-9}$$

Variable Output Axicon - Rear Reflector Design

For the two element design in Figure 4-9 a similar geometrical analysis to the single element case can be applied to obtain an expression for the axicon-mirror separation d, required to achieve an output light cylinder radius r, for a given cone length l, and pitch ϕ.

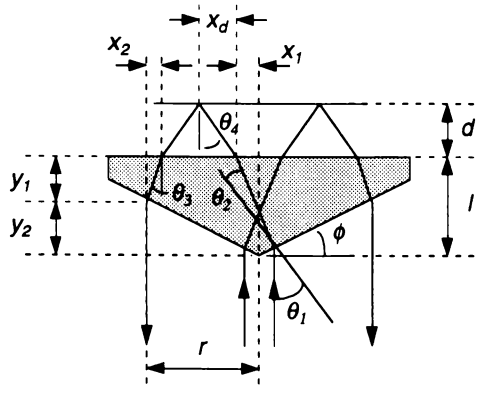

Figure 4-9. Geometry of the two element axicon-rear mirror design.

Once again, $\theta_1 = \phi$ and we have the same expression for θ_3 above. From Snell's law of refraction the retro-reflector incidence angle can be calculated from

$$\theta_4 = \sin^{-1}\left(\frac{n_2 \sin\theta_3}{n_1}\right). \tag{4-10}$$

In addition, we have

$$x_d = d\tan\theta_4. \tag{4-11}$$

On substituting Equations (4-3) to (4-6) and (4-11) into (4-7) we obtain an expression for the light cylinder radius as a function of d

$$r = (2l - r\tan\phi)\tan\theta_3 + 2d\tan\theta_4. \tag{4-12}$$

Solving for d gives

$$d = \frac{1}{2}\frac{r - \tan\theta_3(2l - r\tan\phi)}{\tan\theta_4}. \tag{4-13}$$

4.3.5 Specifications for Manufacture

A single element axicon was manufactured to our specifications by Light Standards, Industrial Research Ltd., New Zealand, and was later modified to the two element design. The material used for manufacture was optical glass (BK7, n=1.53648 at 363.8nm). The axicon cone pitch was 30° ± 0.1° with the rear surface perpendicular to the mechanical axis within ± 0.5°. The pitch angle was chosen to maximise the effect of refractive divergence at the tip (thereby reducing the overall path length of light within the

element and the total absorption), while minimising effects of incidence angle on reflection losses at air-glass interfaces. The overall length of the (two element) axicon was 25 ± 0.2 mm.

4.3.6 Performance

Absorption and Reflection Losses

The material used for manufacture of the axicon was BK7 optical glass. Reflection losses of this material are typically 4% for both external (i.e. air-glass interface) and internal (i.e. glass-air interface) boundaries. The rear surface mirror used to provide retro-reflection has approximately 85% reflection efficiency. The axicon air-gap configuration has two air-glass interfaces, two glass-air interfaces, and the rear reflector interface. There are also absorption losses to consider with the refractive axicon design since BK7 is not specifically suited to UV transmission. Internal transmittance of 365nm light is stated to be 96% over a 25mm path length (Melles Griot 1990). The final transmission efficiency of the axicon-rear reflector design due to reflection and absorption losses is 69%. By manufacturing this component from a UV-suitable material such as fused silica, utilising increased transmission coatings, and by using a UV-grade retro-reflector mirror, the transmission efficiency of the axicon-reflector system would be significantly increased.

Machining of Axicon Tip

While investigating the quality of the output light cylinder, a problem was found with the axicon. Light was found to converge radially towards the light cylinder axis. It was discovered that this was caused by the polishing method used in the manufacturing process. An uneven pressure distribution across the axicon surface results in the cone tip becoming blunt. The incident laser beam, due to its small dimension relative to the tip, is extremely sensitive to geometrical variations over the area of the cone tip. This results in a deviation of the path of the laser beam from that incident on a perfect cone tip. Re-manufacture of the axicon with this consideration in mind significantly reduced the problem.

Fresnel Diffraction

Analysis of the light cylinder using a CCD element (TCK211 Evaluation Board, Texas Instruments, Dallas, TX) revealed further detail of the structure of the light cylinder. The CCD element was located at a distance of 160mm from the axicon tip and used to obtain a profile over a 2.6mm by 2.6mm section of the light cylinder. Close inspection of the profile revealed an intensity variation along the radial dimension of the cylinder (Figure 4-10). This effect can be explained by diffraction theory (Heavens *et al.* 1991), which states that if a light source, such as a laser, is incident on a straight edge, and viewed in the far-field, fringes are observed. For a laser incident on the tip of the axicon, there is an analogous straight edge of revolution which acts on the central region of the beam. The effect of the Fresnel diffraction is to produce a series of fringes which, after retro-reflection through the axicon, decay in intensity towards the optical axis. Such fringes are not seen at the focus of the paraboloidal reflector (Section 4.5), and furthermore, the fluorescent signals produced as cells pass through the inspection point do not display

intensity fluctuations. The only visible sign of the diffracted light is a tail in the intensity profile (Section 4.5.1). Thus, the effect of Fresnel diffraction does not seem to limit the use of an axicon in producing a light cylinder for radially symmetric delivery to the cells.

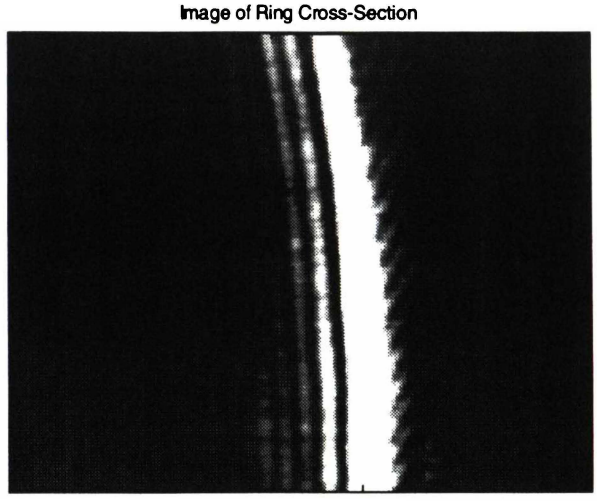

Figure 4-10. Intensity profile for a 2.6mm by 2.6mm section of the light cylinder produced by the axicon. Fresnel diffraction is observed in a radial direction with fringe intensity decaying towards the optical axis.

4.4 Paraboloidal Reflector

4.4.1 Background

Concave paraboloidal reflectors are used for a variety of high efficiency illumination, light collection, and light concentration systems. High efficiency is achieved by collecting light over a large solid angle around the focus. Any light which leaves the focus of a paraboloidal reflector, and becomes incident on the reflector surface will be projected out of the reflector parallel to the optical axis. Likewise, when light which is parallel to the optical axis enters and hits the reflector surface, it will be projected toward and through the focus. The equation relating the radial r, and vertical z, coordinates on the surface of a reflector positioned at the origin with focal length f, is $r = z^2/4f$. A schematic diagram of a paraboloidal reflector is shown in Figure 4-11.

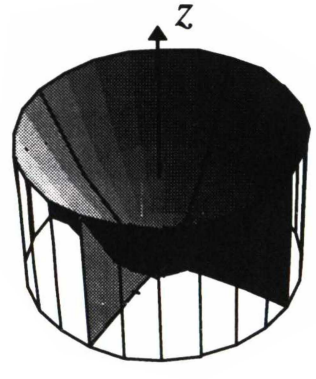

Figure 4-11. A schematic of the paraboloidal reflector that was used for radially symmetric illumination and fluorescence collection in the radial optics configuration.

4.4.2 Other Component Options

Both paraboloidal and ellipsoidal reflector forms were considered for radial illumination and fluorescence collection since these elements provide similar collection efficiencies. The paraboloidal reflector was chosen because it allowed the arbitrary positioning of components along the optical axis. The arbitrary positioning of components is possible because of the collimated properties of the paraboloidal system. Fibre optic geometries were also investigated. However, the low delivery and fluorescence collection efficiencies, coupled with mechanical assembly and alignment difficulties, made their use impractical.

4.4.3 Specifications

Two paraboloidal reflectors were used in the radial optics, each with focal length 10.2mm. The first reflector had a rhodium reflective surface. The second reflector was coated with $AlSiO_2$ for enhanced UV reflection. Both elements were formed from a nickel substrate. The rhodium element was used in most of the experimentation (rather than the enhanced UV reflector) because of its superior durability to the corrosive environment introduced by the saline sheath solution. Manufacturer specifications for surface specularity were 80-50 scratch and dig with surface slope error not exceeding ± 30 arc seconds.

4.4.4 Performance

Reflection Losses

The reflective surfaces of the rhodium and UV enhanced ($AlSiO_2$) elements provided (manufacturer specified) reflectance values of 75% and 88% (at 365nm) respectively. In a system optimised for sperm sexing, this loss would have to be minimised by using a coating with increased durability and high UV reflectance.

Focal Volume

Comparisons between the focal region produced by the paraboloidal reflector (in conjunction with the ring of light) and the focus of a conventional flow cytometer are presented in Section 4.5.

4.5 Focal Volume Determination

4.5.1 Intensity Profile at Inspection Point

In this study, intensity profiles were determined at the inspection point of both orthogonal and radial optical configurations to compare the relative cell irradiation (illumination) of each system.

Figure 4-12 displays the experimental layout for this study. A HeNe (543nm) laser was used for the analysis of both optical configurations. A 5μm diameter pinhole (04PIP003, Melles Griot, Irvine, CA) was used to approximate the cross-sectional (surface) area that a cell (such as a bull sperm) would present to the incident light at the inspection point. The pinhole was translated through the flow axis direction of the inspection point in a similar fashion to the propagation of a cell in a flow cytometer. Light transmitted through the pinhole aperture was measured by a silicon photodiode detector (BPX65 Philips, Radio

Spares, New Zealand) for each z-axis position. The photodiode was operated in photovoltaic mode to provide a linear output voltage response as a function of light intensity.

A standard EPICS V crossed cylinder lens pair (Coulter Corporation, Hialeah, FL) was used to generate the uni-directional beam (with an elliptical cross-section), providing simple measurement of the intensity profile using the pinhole-detector.

For a radially symmetric system, reliable measurement of the three-dimensional focus with a two-dimensional detector is not possible. To overcome this problem a wedge-shaped aperture was positioned in the path of the light cylinder to block all but a 60° sector from reaching the focus. Since this system is radially symmetric, we would expect that the light detected at the pinhole (which is located along the optical axis) would be one sixth of the intensity recorded by a detection device that could collect light from the entire sphere surrounding the focus. Thus, if a cell was to travel through the optical axis, it too would experience a light intensity six times greater than that measured by the pinhole detector arrangement. This statement assumes that the cell area is small with respect to intensity variations across the centre of the focus, and that the detector responds equally to light with angles of incidence varying over ±30°.

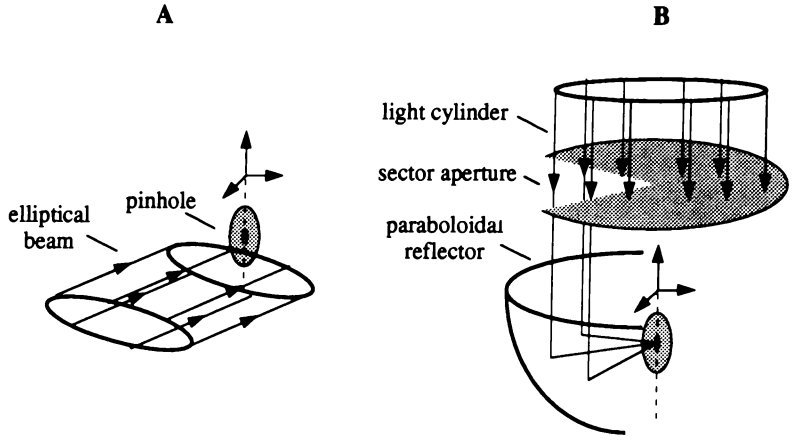

Figure 4-12. Experimental layout of the pinhole detector assembly which was used to determine the intensity profile that a cell would experience as it flowed through ***A****: the uni-directional focus, and* ***B****: the radial focus.*

Measured intensity profiles for the uni-directional, and radially symmetric foci are presented in Figure 4-13. The x-axis represents distance along the cell flow direction. The uni-directional profile is Gaussian in nature with a beam waist (1/e intensity) of 35.8 ± 0.3μm. The radial optics intensity values have been multiplied by a factor of six to compensate for the proportion of the light cylinder which was blocked by the wedge-aperture element. Once more, this profile is generally Gaussian in form but also displays an asymmetric tail which can be explained by Fresnel diffraction effects (Section 4.3.6). The beam waist of the radial focus (along the flow axis) is 96.7 ± 0.5μm. The peak intensity values of both profiles are similar. However, since the same laser power level was applied for both results, the broader

profile of the radial optics suggests there will be a narrower lateral profile than that of the uni-directional focus. This is investigated further in Section 4.5.2.

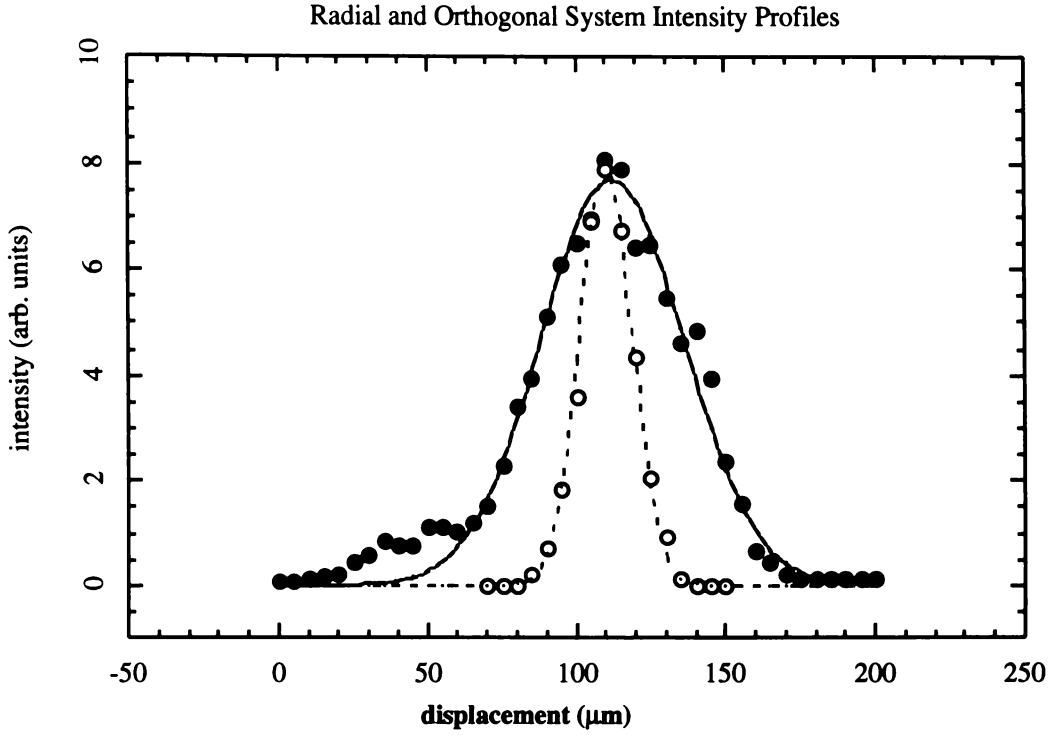

Figure 4-13. Intensity variation experienced by a 5μm diameter particle as it flows through the inspection point of uni-directional (dashed) and radially symmetric (solid) illumination systems.

The radial optics provides a peak excitation intensity at the inspection point approximately equivalent to that delivered by a uni-directional system. The radial optics profile is longer (96.7μm compared to 35.8μm) so that the cells would be exposed to a greater total irradiation when travelling through the focus. The width of this profile could be reduced by inserting a convex lens between the laser and the axicon.

4.5.2 Focal Spot Size

An experiment was performed to determine the focal volumes of both optical configurations. The purpose of this work was to compare the dimensions and proposed operational characteristics of the two designs.

The experimental apparatus was configured as illustrated in Figure 4-12 previously, but with the pinhole detector replaced by a CCD element. For each optical geometry, the CCD chip (a matrix of 192 × 165 pixels each measuring 13.75μm in height, by 16μm in width) was positioned at the focus by minimising the area of the focal region as viewed by the element. Once more, the same laser source was used on both optical geometries to provide consistent intensity comparisons. The wedge-aperture was also in place, restricting the light cylinder to a 60° illumination sector in order to reduce the effects of acute incidence angles, which can produce measurement errors over the detector element surface.

The measured intensity profiles of the uni-directional and radial systems are presented in Figure 4-14. The uni-directional beam is ellipsoidal in profile with a 56 ± 7μm vertical and 144 ± 18μm horizontal beam waist (the position at which the intensity falls to a value which is 13.5% of the maximum). The disparity between the vertical dimension measurement using the CCD element, and that obtained using the 5μm pinhole in Section 4.5.3 could be because of a loss of resolution with the large pixel size compared to the focal area, or from detector positional variation for the two measurements. The two-dimensional slice of the radial focus displays an elliptical profile which lies with its longest dimension along the flow axis and 13.5% intensity contour dimensions of 91 ± 9μm (vertical) by 58 ± 3μm (horizontal). The implications of this observed narrow radial profile to the measurement of bull sperm are discussed in Section 4.5.3.

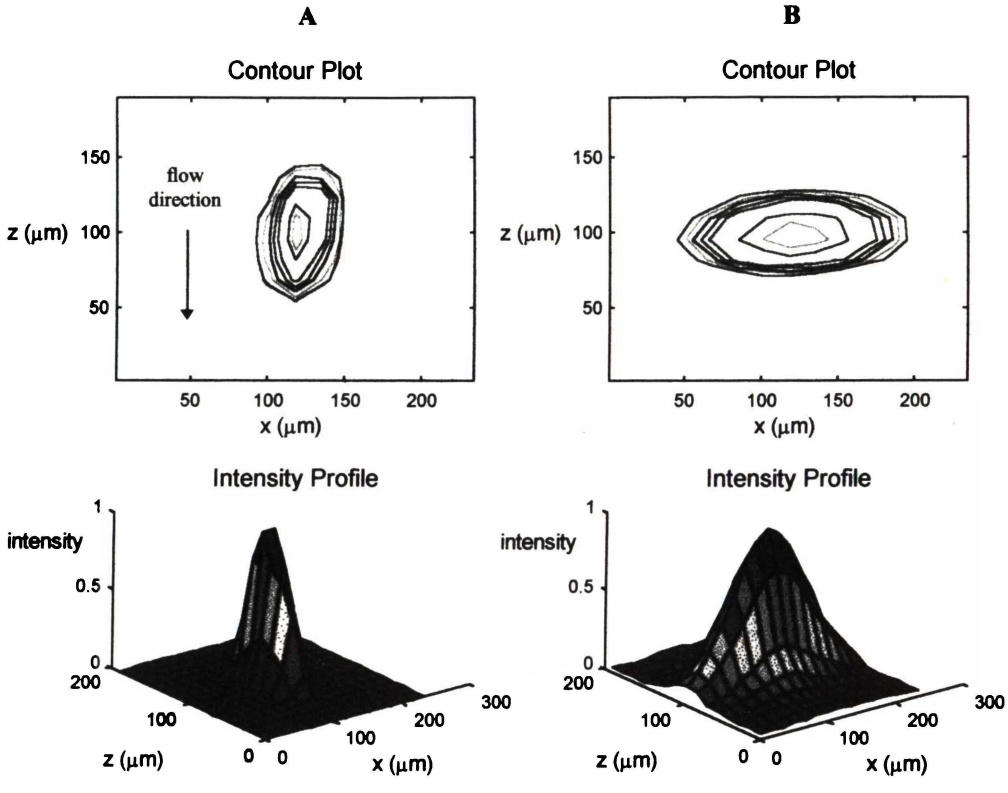

*Figure 4-14. Two-dimensional contour plots and focal region intensity profiles for each of the **A:** orthogonal, and **B:** radial optics geometries.*

This analysis does not include the possible refractive effects of the jet on the final illumination area seen by the cells as they flow through a flow cytometer (see Section 4.5.4). Therefore, these results give an indication of the general focusing characteristics of both systems, rather than representing the true light intensity that a cell would be subjected to as it passed through the focus.

4.5.3 Lateral Broadening of the Radial Focus

The differences between the focal regions of orthogonal (uni-directional), and radial (omni-directional), illumination geometries have been outlined in Section 4.5.2. These differences are also highlighted in the experimentation for bull sperm analysis in Chapter 5. In this experimentation, it was found that an increase in sample to sheath differential pressure resulted in a significant increase in CV. It is suggested that this effect is due to an increased positional uncertainty of cell to cell trajectories through the focus, which results in a difference in illumination, and therefore fluorescence emission.

In conventional flow cytometers, cell illumination differences are overcome by broadening the laser focus laterally using a pair of cylindrical lenses. A focal spot is created which is ellipsoidal in profile and which has its shortest dimension parallel to the cell flow direction. Thus, the difference in intensity experienced by a cell which passes through the centre of the focus and a cell which passes at a lateral displacement from the centre of the focus will be minimised. Positional variations along the optical axis of the uni-directional illumination beam do not have a significant effect on cell illumination.

The radial optics delivers a convergent disk of light at the excitation wavelength to the inspection point. Adjusting the vertical dimension of the radial focus is relatively simple if a concave or convex element is positioned in the laser beam in front of the axicon. However, broadening the focus laterally, while retaining sufficient light intensity at the focus for stain excitation and fluorescence, is not trivial.

The normal operation of the paraboloidal reflector to focus the light cylinder in a radially symmetric fashion is illustrated in Figure 4-15A. To laterally broaden or defocus the radial focus requires that the illumination light cylinder be altered to cause divergence tangentially around its circular cross-section as illustrated in Figure 4-15B. This would result in a lateral displacement of the incoming light disk thereby broadening the intensity distribution of the focal area. Two optical elements were proposed to perform this function. The first optical element would take the form of a radially etched diffraction grating (Figure 4-15B). Such a component would successfully achieve the goal of lateral displacement with a minimal dispersive effect in the vertical profile of the focus. The expense of custom manufacturing such a device was prohibitive to our research. The second optical element is a light shaping diffuser element, the operation of which is illustrated in Figure 4-15C. Implementation of this element into the radial optics design would result in both vertical and lateral focus broadening.

A light shaping diffuser (0.5° diffusion angle, Physical Optics Corporation, Torrance, CA) was incorporated into in the radial optics in an attempt to broaden the radial focus. The optics were aligned and configured with a CCD element located at the focus as described in Section 4.5.2. The focal region was measured both with and without the diffuser element in place. The element was positioned at a distance of 100mm from the paraboloidal reflector.

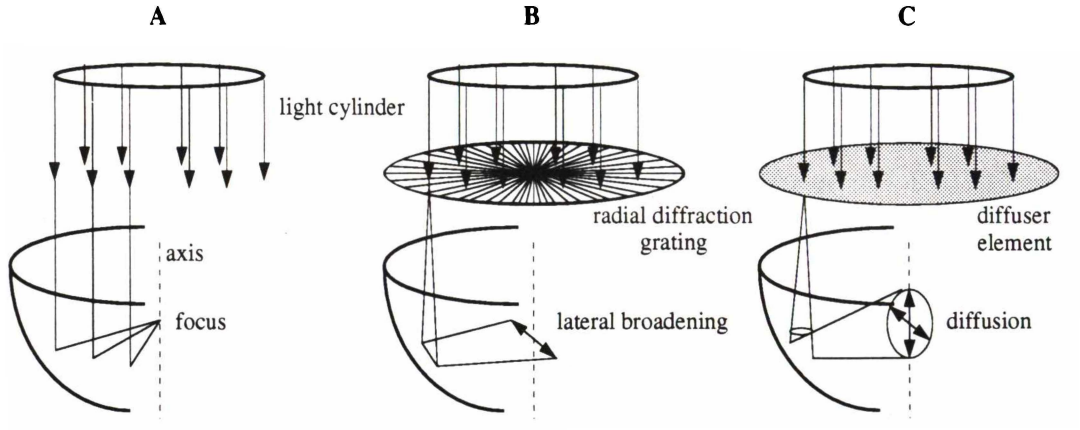

*Figure 4-15. An illustration of the required effect on the light cylinder to achieve lateral broadening of the radial focus. **A:** Radially symmetric illumination, **B:** operation of a proposed radial diffraction grating, and **C:** operation of a diffuser element.*

Intensity contour results, without and with the diffuser, are presented in Figures 4-16A and 4-16B respectively. Introducing the diffuser element resulted in a lateral broadening of the focus from 58 ± 3μm to 167 ± 30μm and an increase in the vertical dimension from 91 ± 9μm to 120 ± 8μm. There was a significant decrease in intensity at the focus. The peak intensity, I_0, of the broadened focus dropped to 10% of the original value. This drop in I_0 is consistent with a three-fold increase in the radial dimension r, according to the equation for an irradiance distribution of a Gaussian beam

$$I(r) = I_0 e^{-2r^2/w^2} = \frac{2P}{\pi w^2} e^{-2r^2/w^2} \qquad (4\text{-}14)$$

where P is the power in the beam, and w is the waist radius.

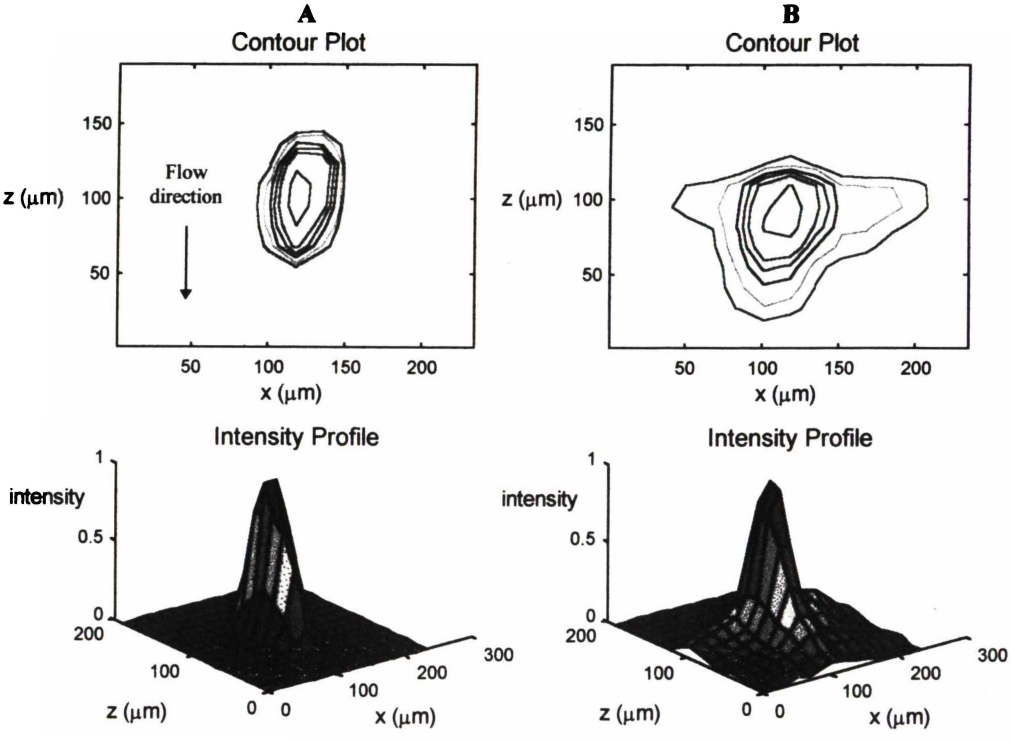

*Figure 4-16. Contour plots and intensity surface profiles of the radial focus as viewed by a 2D CCD element for the **A:** standard radial optics, and **B:** after introducing the 0.5° light diffuser element.*

A diffuser element has successfully been used to laterally broaden the radial focus produced by the paraboloidal reflector. This technique may be useful for reducing the effects of positional variations of cell trajectories on cell illumination and fluorescence. Future work should be carried out using a radial diffractive element to eliminate broadening of the focus in the vertical direction. If successful, implementation of such a device in the radial optics may enable higher sample to sheath differential pressures and therefore higher analysis rates of sperm cells without compromising measurement accuracy.

4.6 Radial Optics Efficiency Considerations

Light with a wavelength in the UV region is required for the excitation of the Hoechst 33342 stain (peak absorption at 365nm). The optical components implemented in the final radial configuration used for testing were primarily stock optics, and as such, were not matched to UV use.

The total losses incurred in the radial optics mean that 85% reflection for the first 45° steering mirror, 69.2% for the axicon combination, and 75% for the rhodium paraboloidal reflector surfaces produce a final illumination delivery efficiency to the jet of 44.1%.

Calculations of component transmittances for the collection optics were performed for a 450nm wavelength, which corresponds to the fluorescence peak of the Hoechst 33342 dye. The collection optics include the same paraboloidal reflector which is used for illumination (77%), a 45° apertured steering mirror (87.6%), and an aspheric lens (92%). Thus, the expected transmittance for the combined system is 62.0%.

The combined radial optics transmittance efficiency of the illumination and collection sections of the configuration (prior to the microscope objective) is 27.3%. Therefore in its present state, this system will deliver approximately one quarter of the expected cell fluorescence to the PMT housing for detection. This compares with approximately 90% for the conventional system, for which the delivery optics (a pair of cylindrical lenses) are optimised for UV transmission.

One further consideration must be given to the selection of optical component materials for UV transmission in flow cytometry, in cases where fluorescence measurements of cells are made. Glass (such as BK7) can absorb in the UV and produce considerable fluorescence (Shapiro, 1995). Thus, these fluorescent signals may interfere when performing high resolution measurements. It is unclear whether such fluorescence was detected in our experimentation.

The transmittance efficiency of the radial optics could be increased significantly by utilising optical components more suitable for UV transmission. Fused silica or fluorite materials produce low fluorescence and have higher UV transmittance than glasses, and would therefore be more desirable. In particular, by implementing a reflective axicon design, and by finding a better suited reflective coating for the paraboloidal reflector, illumination losses could be substantially reduced.

4.7 Discussion

A new radially symmetric optical configuration has been designed specifically for the analysis of aspherical cells. This configuration delivers excitation wavelength light to cells, and collects scatter and fluorescent signals from them over a 360° angle around the flow axis.

The radial optics design meets the objectives of increased efficiency, orientation independent operation, and electrostatic sort capability previously discussed. The new system has been described, its alignment outlined, and its characteristics compared to several previous optical configurations for measuring bull sperm. Design considerations made in selecting light delivery components have also been outlined. Manufacturer specifications and component performance have also been considered.

The focal volume of the radial optics has been measured and compared with the uni-directional focus of an orthogonal optics system. Results have shown that the inherent three-dimensional light delivery characteristic of the radial focus result in a narrow lateral intensity profile compared to the uni-directional system. A narrow focus coupled with positional uncertainty of cells can lead to illumination variations and a loss in measurement resolution. An investigation has been performed in an attempt to overcome this problem by using a diffuser element to laterally broaden the radial focus.

Efficiency considerations highlight the need to reduce transmission and reflection losses in future designs. This would be achieved by incorporating component materials and coatings which are better suited to the UV wavelength range.

5. Experimentation

The flow cytometric experiments performed for this thesis have been categorised into three main areas; preliminary experiments on a conventional flow cytometer using bull sperm, comparative experiments between the conventional (orthogonal optics) system and the new (radial optics) design for a variety of test particles and flat cells, and finally, further modifications to the radial optics configuration to investigate aspects of its performance.

The instrumentation used for the experiments is described in Section 5.1. Section 5.2 outlines sample preparation and staining of the various test particles and cells analysed. In Section 5.3 the preliminary experiments are discussed in detail. Experiments which compare the two optical configurations of interest in this thesis (orthogonal and radial) are described in Section 5.4. and relative merits of the two systems are discussed. Section 5.5 examines the results of several modifications that were carried out on the radial optics to measure aspects of scatter from sperm and to emulate operation characteristics of an orthogonal system.

5.1 Instrumentation

Experiments were performed using a commercial flow cytometer, a FACStar Plus (Becton Dickinson Immunocytometry Systems, BDIS, San Jose, CA). The manufacturer specifies the resolution of a FACStar Plus instrument to be less than 2%, with a recommended sample concentration of 10^5 to 10^7 cells ml^{-1} and a sensitivity of 2000 molecules of fluorescein per cell. The instrument had previously been modified for flow sorted sperm sexing as described by Johnson *et al.* (1986) and uses a jet-in-air flow chamber. This sorting flow cytometer is fitted with an Ar^+ laser (5W Innova 305, Coherent Lasers Inc., Palo Alto, CA) for ultraviolet (UV, 351-364nm, 150mW multiline) light excitation of cells. A 400LP long pass filter was used to block UV scatter and stray light while passing fluorescence transmission to the photodetector.

For live-dead sperm studies, the laser optics were modified to produce a 488nm line suitable for the absorption bands of the stains used. In addition, a pair of high pass filters (BP530/30 and BP585/42) were used to select wavelength regions specific to each of the stain excitation wavelengths.

The new radial optics platform was located alongside the FACStar and utilised the same laser, fluidics and acquisition electronics, to facilitate direct comparison between the two optical systems. Unless otherwise stated, sample to sheath differential pressure was regulated for sample flow, and therefore analysis rates, of 1000 events s^{-1}. Data were captured and acquired for each of 10 000 cells through LYSIS software run on a Hewlett Packard (HP) 320 computer. Further graphical analysis was performed on the data using PC LYSIS, Kaleidagraph, and Matlab (after transferring data from HP to PC format).

5.2 Sample Preparation and Staining

A variety of test particles were used in our experiments. The methods for their preparation are outlined below. Figure 5-1 displays videomicroscope fluorescence images for several of the test particle types analysed. These images were captured using a Nikon Labphot Biological Research Microscope.

Beads

Several beads were analysed in our experiments. They included blank (non-stained) 6μm, 10μm, and 20μm beads (Duke Scientific Corp., Palo Alto, CA), 6μm calibration fluorescence beads (Spherotech Inc., Libertyville, IL), 4.5μm Calbrite microspheres (Fluorescebrite carboxy BB, Polysciences, Inc., Warrington, PA), and 9μm Hoechst 33342 beads (Flow Cytometry Standards Corp., Research Triangle Park, NC). Each of these samples was supplied in solution. Prior to analysis, each microsphere sample type was extended in 3ml sheath fluid (Dulbeccos's Phosphate Buffered Saline (DPBS), Sigma Biosciences, St. Louis, MO) to a concentration of 10^6 ml^{-1}.

Chicken Red Blood Cells (CRBCs)

Blood was collected from live chickens. Red blood cells were isolated and fixed in 0.5% glutaraldehyde. Cells were extended in 3ml DPBS to a concentration of 10^6 ml^{-1}. This suspension was then stained with 9μl ml^{-1} Hoechst 33342 (Calbichem-Behring, La Jolla, CA) and incubated at 35°C for 60 minutes prior to analysis.

Chinchilla Sperm

Pre-stained Hoechst 33342 chinchilla sperm samples (provided by GR Welch and LA Johnson, USDA, Beltsville, MA) were fixed in 15% formaldehyde (to meet New Zealand Customs requirements).

Bull Sperm

Fresh samples of semen from several bulls were used for this study. The method of sperm preparation and staining is similar to that described by Johnson *et al.* (1986). The sperm were extended in 3ml of a lactose-citrate diluent (pH = 6.9) to a concentration of 10^6 ml^{-1}. As with the CRBCs, sperm were then stained with 9μl ml^{-1} Hoechst 33342 and incubated at 35°C for 60 minutes prior to analysis.

Ram Sperm

Fresh ram sperm were stained and treated in the same manner as the bull sperm preparation procedure described above.

Live-Dead Stain Procedure for Bull Sperm

Sperm membrane integrity (for live-dead ratio analysis) was determined using a Fertilight Sperm Viability Kit (Molecular Probes, Eugene, OR). Sperm were dual-stained with propidium iodide (PI) and SYBR-14 to final concentrations of 100nM and 12μM respectively (Gurnsey *et al.* 1997). SYBR-14 enters live cells and fluoresces green (494/521, excitation/emission) when bound to DNA. PI will only

enter sperm and other nucleated cells if there is membrane damage (i.e. the cell is dying or is dead). Those sperm which allow PI entrance, fluoresce red (536nm/623nm, excitation/emission).

Diatoms

Sea-water diatoms were provided by Julie Hall of the National Institute of Water and Atmospheric Research (NIWA, New Zealand). These particles are nucleated and were stained with 9µl ml^{-1} Hoechst 33342 as for the bull sperm. It was hoped that their disk-like morphology could also be used to test the radially symmetric optics. Unfortunately, the small size, low stain uptake and consequent low relative fluorescence intensity limited our analysis of diatoms using both optical systems.

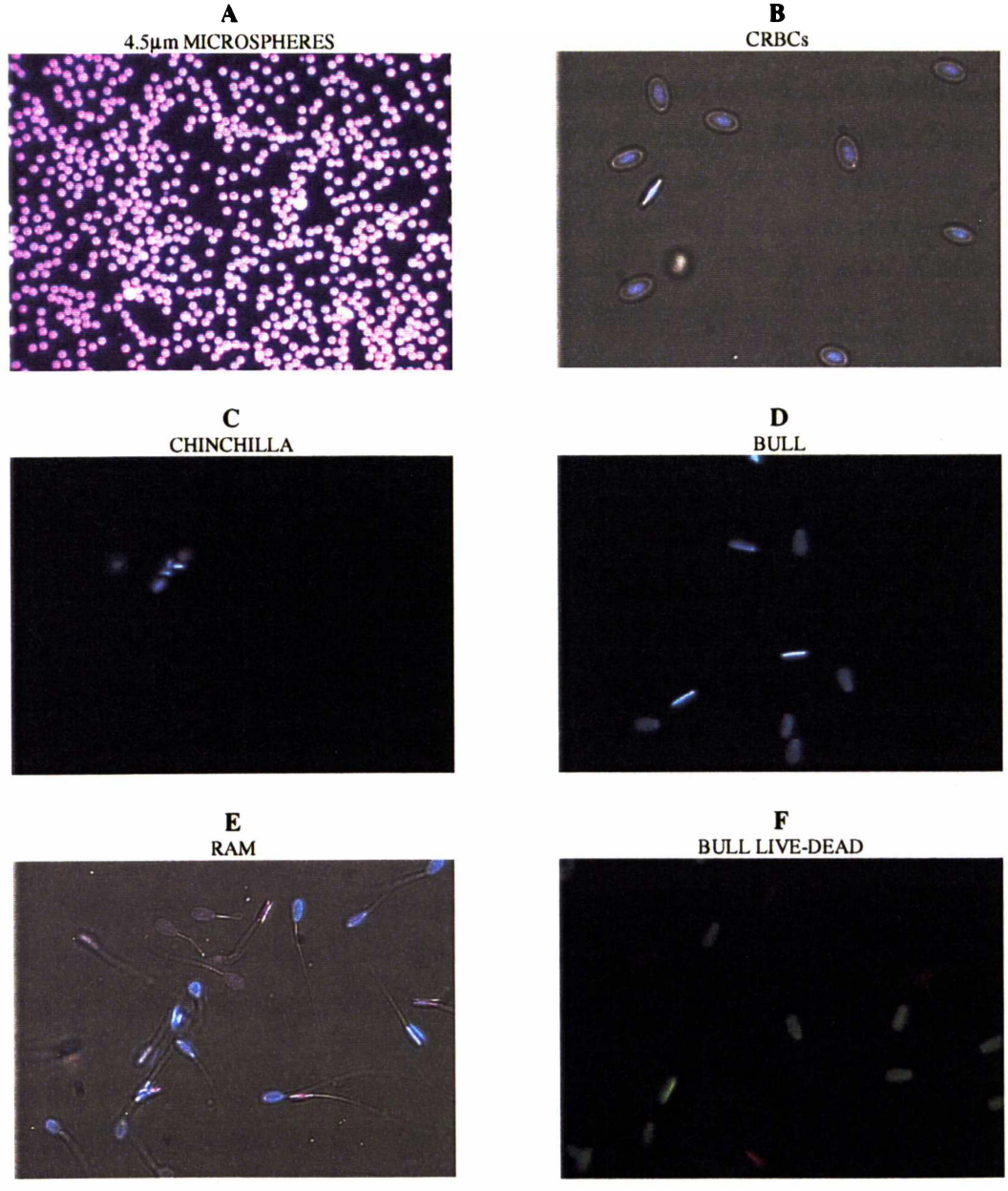

Figure 5-1. Videomicroscopic images of ***A****: Fluorescebrite (4.5µm) microspheres,* ***B****: chicken red blood cells,* ***C****: chinchilla sperm,* ***D****: bull sperm,* ***E****: ram sperm, and* ***F****: dual-stained (PI - SYBR-14) bull sperm for live-dead analysis.*

5.3 Preliminary Experiments on Conventional Flow Cytometer

Several studies were carried out in order to determine the orientational dependence of fluorescence emission from sperm using a conventional, orthogonal optical geometry flow cytometer that had been modified for sperm sexing.

5.3.1 Sperm Sexing Technique

The flow cytometric method, according to Johnson *et al.* (1986,1995) for staining, histogram interpretation, gating, and sorting sperm by X-Y DNA content is outlined in Chapter 3. Essentially, the process uses a combination of fluidic orientation of cells and orientation detection to increase the proportion of sperm which can be measured and subsequently sorted into X and Y fractions. The fluidic orientation serves to increase the proportion of cells for which DNA content can be accurately measured and the orientation detection determines which cells have been successfully oriented.

5.3.2 Cell Orientation as a Function of Sample to Sheath Differential Pressure

The method of Johnson *et al.* for sperm sexing uses hydrodynamic orientation to bias the orientation of cells towards one plane as they pass through the inspection point (Chapter 2). This technique increases the proportion of cells for which DNA content can be accurately measured. Optical artifacts which affect measurements, and which are present if cells pass through the focus at random orientations, are overcome using this technique because only cells oriented within a desired angle range are accepted for measurement.

The aim of this experiment was to investigate the effect of sample to sheath differential pressure on cell orientation, and therefore to determine the fraction of cells appropriately oriented as a function of sample to sheath differential pressure. Tests were carried out using Hoechst 33342-stained bull sperm. Test results were used to determine the effect of cell orientation on maximum sort rates of X and Y sperm.

The bevelled injection needle was positioned for planar flow perpendicular to the laser beam axis. The sample to sheath differential pressure, as monitored by the cell event rate, was varied from a minimum of 200 events s^{-1} to a maximum of 5000 events s^{-1}. Forward and side detector fluorescence intensity histograms and contour plots were obtained for each of the flow rate settings. Data were captured for each of 10 000 cell events. Each contour plot was analysed, using pre-set quartile cross-hairs, to determine the proportion of cells which fell into the lower right (LR) region of the L-shaped population distribution illustrated in Figure 5-2. The cells which fall into the LR region are considered to be oriented toward the side detector and it is the ratio of the number of cells in this region, to the number of cells in the lower left (LL) and upper left (UL) regions, which determines the fraction or percentage of cells which are deemed to be oriented and can be assessed for DNA content.

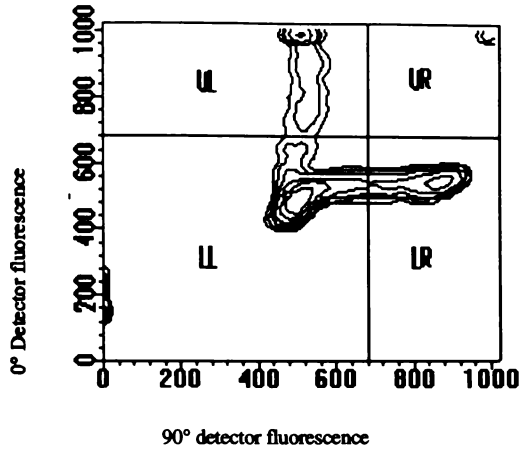

Figure 5-2. Bull sperm contour plot with oriented cells in the lower right (LR) quartile.

The effect of sample to sheath differential pressure on the ratio of aligned to non-aligned sperm cells is illustrated in Figure 5-3. The graphs display 39.2% and 19.3% appropriate orientation in the LR region for flow rates of 400 cells s^{-1} and 3500 cells s^{-1} respectively.

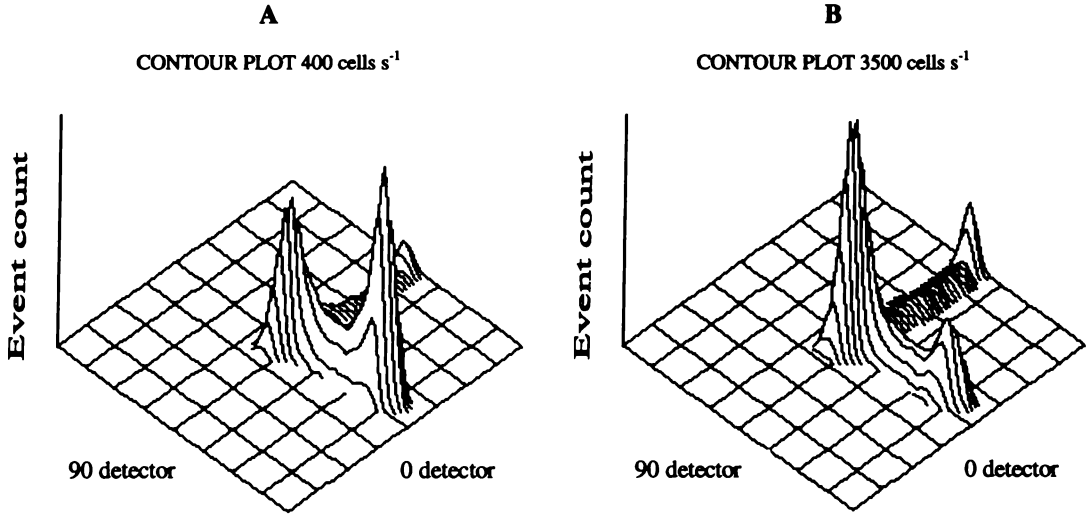

Figure 5-3. Contour plots displaying change in sperm alignment within the LR region for event rates of A: 400 cells s^{-1}, and B: 3500 cells s^{-1}.

A graph depicting proportion of cells aligned vs. cell event rate is illustrated in Figure 5-4. For the sperm sample studied, a maximum of 41.2% were aligned at an event rate of 200 events s^{-1}. The proportion of cells that were aligned decreased steadily with increased flow rate, until reaching an approximate limit of 18% for event rates exceeding 3500 events s^{-1}. This baseline corresponds to the situation where the fluidic forces provided by the bevelled injection needle are no longer capable of aligning sperm in planar flow. A figure of 18% alignment approximately represents the minimum proportion of cells with their edges aligned within the acceptance angle of the side detector. This situation is illustrated in Figure 5-3B by an equal proportion of cells located in the UL and LR regions of the profile.

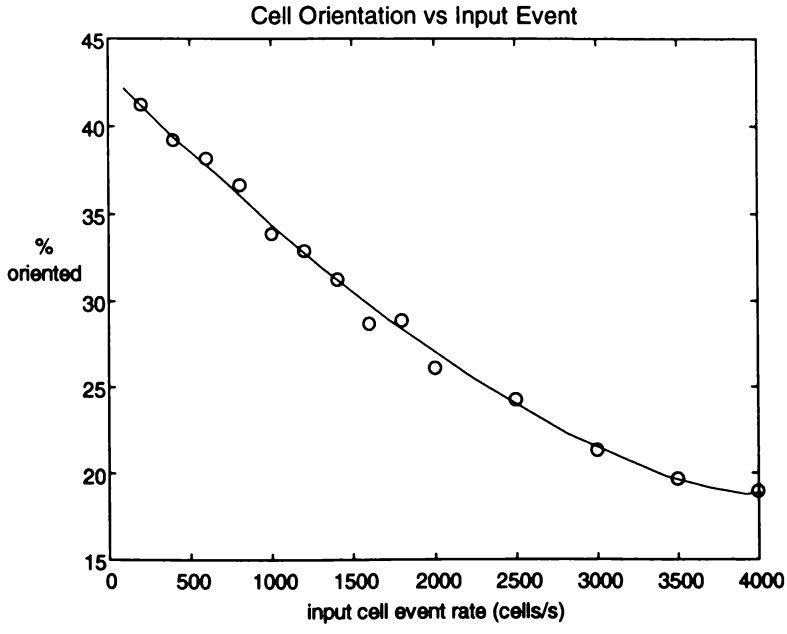

Figure 5-4. Graph of proportion of cells aligned as a function of input cell event rate.

Results from this study show that the proportion of cells which can be considered to be oriented toward the side detector, and can be reliably measured by the forward detector, decreases steadily with increased flow rate. This decrease continues until an event rate of 3500 cells s^{-1} is reached, at which point the fluidic orientation is no longer provided by the bevelled injection needle (for this sperm sample concentration), and statistical equilibration of random sperm orientation about the flow axis has been reached.

An ability to sort X and Y sperm must be considered for the purposes of sperm sexing. One could speculate that an increase in the input event rate well beyond the bounds of the graph would yield an equivalent increase in possible sort rates. However, there are several limiting factors, such as, CV broadening, instrument analysis and sort rate constraints, and cell damage effects which restrict possible input rates. In addition to these instrumental constraints, the economic importance of sample waste must also be considered.

The application of sperm sexing to flow cytometry and subsequent *in vitro* or *in vivo* fertilisation requires that sperm be sorted into X and Y subpopulations with high enrichment, at a maximum possible rate. In addition, for expensive sperm samples from top breeding sires, minimum sample waste must be ensured. The efficiency of the flow cytometric sperm sorting process is heavily dependent upon cell orientation, which is in turn dependent upon sample to sheath differential pressure. Thus, a trade-off exists between sorted output rate at a given purity, and sample to sheath differential pressure. To obtain a highly enriched X or Y sorted sperm fraction requires a low sample to sheath differential pressure which in turn results in a low net output. By increasing the sample to sheath differential pressure the possible sorted output rate will increase at the expense of increased sample waste.

In this experiment the effect of sample to sheath differential pressure on appropriate cell orientation has been determined for the orthogonal optics flow cytometric technique of sperm sexing. These results serve as a basis for comparing the efficiency of this system with the radial optics investigated in Chapter 7.

5.3.3 Stain Fluorescence Saturation as a Function of Laser Power

The aim of this study was to determine how fluorescence intensity saturates as laser power is increased. This is helpful in determining whether cells are saturated in routine sperm sexing and hence whether the fluorescence intensity is independent of cell orientation with respect to the excitation beam. These results are applied in Chapter 6 where a theoretical model of sperm fluorescence and detection is proposed.

A sample of sperm cells was analysed using the flow cytometer with laser power ramped from 20mW to 500mW (as measured by the laser power control module). The mean fluorescence intensity of the lower left peak of the characteristic L-shaped contour plot was calculated for both the forward and side detectors for each laser power setting[1].

Figure 5-5 displays a graph of fluorescence intensity as a function of laser power. The forward and side detector curves both exhibit the exponential form characteristic of stain saturation where the number of dye molecules (bound to the DNA of the cell) in the excited state, approaches that of the number of dye molecules in the ground state and further net transition between states is not possible.

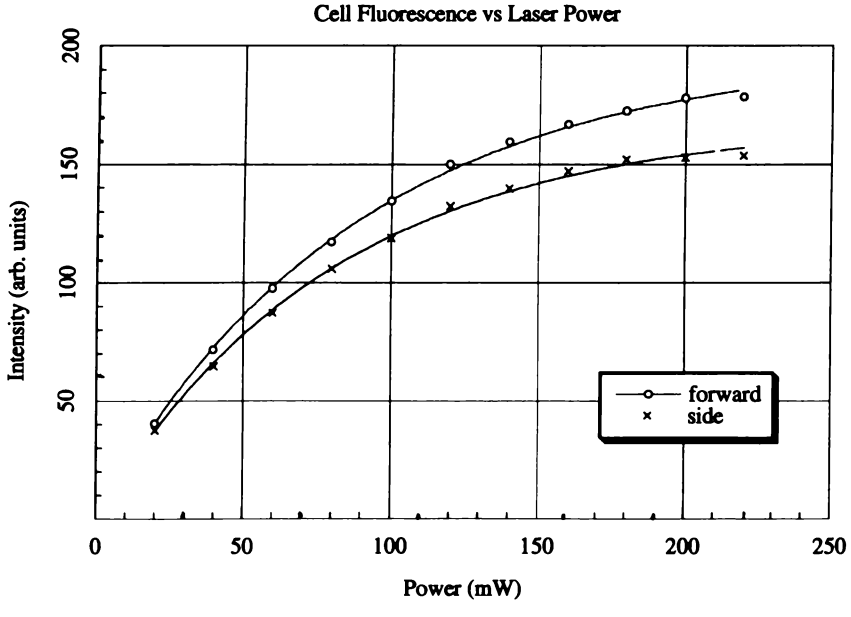

Figure 5-5. Graph of laser power vs. sperm fluorescence intensity.

[1] Because our laser had insufficient power to reach the intensity levels required for this test, this study was performed by Glenn Welch of the USDA according to our specifications.

The fluorescence intensity profile I, as a function of the operation power P, for each of the forward and side detectors is of the form

$$I = I_0\left(1 - e^{-P/k}\right), \tag{5-1}$$

where k is the saturation constant. The fluorescence intensity asymptotically approaches the saturation value I_0. This function was fitted to the experimental results for each of the forward and the side detector. The saturation constants k were 87mW and 80mW respectively and represent the power where the fluorescence intensity has reached 63% of I_0. A mean value of k = 83.5mW was chosen for our theoretical model in Chapter 6.

If high enough laser powers are applied to the sperm cells so that regardless of orientation, the stain in a sperm cell is saturated with wavelength excitation light, then, the directional effects of illumination on the flat cells would cease to be a problem. There would only remain the optical effects of cell orientation on fluorescence collection to consider. However, to minimise UV irradiation and therefore DNA damage, sperm sexing analysis is usually carried out at power levels of approximately 100mW. At these power levels, the stained sperm are only partially saturated with excitation wavelength light. The cell cross-sectional area presented to the uni-directional laser beam will have an affect on light collection and subsequent emission. For flat cells such as bull sperm, this cross-sectional area can vary by a factor of four. Thus, when operating at low laser power levels, cell orientation may complicate DNA content measurements. Implications of this effect are discussed further in Section 5.5.2.

5.4 Comparative Measurements of Orthogonal and Radial Optics

Several studies were performed to compare the new radial optics results with those from a conventional flow cytometer for several particle and cell types. These tests were carried out to determine the base-line resolution of both optical systems for spherical particles, to determine how successful the new optical configuration was at overcoming the optical artifacts associated with aspherical and flat cells, and to assess the multiwavelength analysis capability of the radial optics.

5.4.1 CV Baseline Measurement - Fluorescent Microspheres

Calibration fluorescent microspheres were analysed to determine baseline instrument CVs for both orthogonal and radial optical geometries. The same FACStar laser source and data acquisition electronics were utilised with both systems so that direct comparison between the optical configurations could be made. This approach allowed us to differentiate between the effects of the optical systems and other components of the instrument.

Figure 5-6 compares fluorescence measurements made on 4.5μm calibration microspheres using the FACStar optics to those made using the radial optics. The FACStar produced single-peaked fluorescence histogram distributions from both the forward (0°) and side (90°) detectors with CVs of 2.3% and 2.5%

respectively. Analysing the microsphere sample with the radial optics yielded histograms of similar shape and CV to those obtained with the FACStar. Figure 5-6C displays the resulting histogram which has a CV of 2.2%. From this result we can conclude that both optical systems have similar measurement resolution for spherical fluorescent beads.

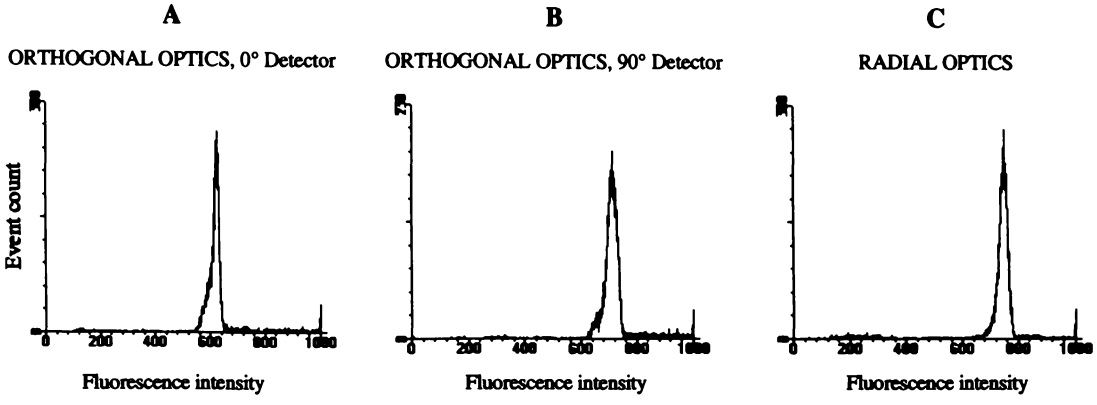

Figure 5-6. Histograms for calibration microspheres produced by A: FACStar forward detector, B: FACStar side detector, and C: radially symmetric optics single detector.

5.4.2 Broad Distribution Characteristics - Hoechst 33324 beads

In preparation for tests on stained cells, a sample of Hoechst 33342 calibration beads was analysed using both optical systems to determine the fluorescence collection efficiency of the two optical geometries. In addition, the broad CV of these beads was utilised to determine if any disparity in histogram form existed between the two optical configurations, for particles which fluoresce over a broad intensity range.

Histogram distributions for Hoechst 33342 beads, as measured using both optical configurations, are presented in Figure 5-7. The side detector of the orthogonal optics of the FACStar produced a broad distribution with a CV of 8.86% and a peak channel count of 89 (and a matched forward detector CV of 8.63%). The radial optics result, with a CV of 8.82% and a peak channel count of 92 is consistent with that of the orthogonal FACStar optics. These results show that, for a population of cells which has a broad intensity profile, both optical configurations measure this variation in intensity with similar precision.

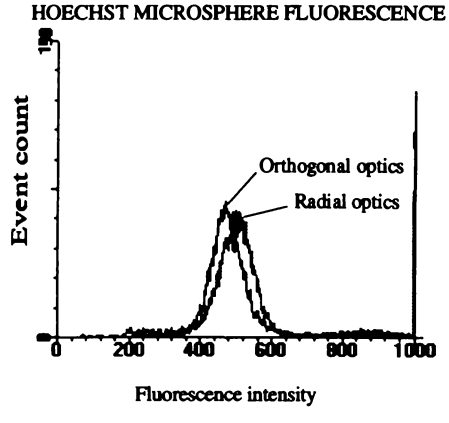

Figure 5-7. Fluorescence intensity histogram for Hoechst 33342 microspheres as measured by a FACStar forward detector and radially symmetric optics single detector.

5.4.3 Cell Orientation Effects - CRBCs

In this test, Hoechst 33342 stained CRBCs (which are moderately flat) were analysed to confirm orientation dependence of the orthogonal optics and independence of the radially symmetric optics. The orthogonal light collection system on the FACStar introduces an optical artifact in fluorescence measurement as a function of cell orientation. DNA analysis of CRBCs using orthogonal optics flow cytometers typically yields dual-peaked histogram distributions, corresponding to cells which pass flat-face toward or edge-on to the detector. If the radial optics are orientation independent, a single-peaked fluorescence histogram will be produced for the entire randomly oriented population of cells.

Figure 5-8 displays histograms acquired for the analysis of CRBCs using both optical configurations. The effect of orientation dependence for the orthogonal optics is displayed for the forward detector in Figure 5-8A as a bimodal histogram of fluorescence intensity. The proportion of cells in the left and right peaks of the histogram is dependent on flow rate because of the orienting capabilities of the bevelled sample tube. The radial optics produced a unimodal peak which represents orientation independent measurement of the CRBC fluorescence (Figure 5-8B). The CV of the entire population as measured by the radial optics is 7.6%, which may be compared to the orthogonal optics result of 14.6% for the entire double-peaked population and 7.5% for the 61% of cells which fall into the left-peaked portion of the histogram. This study has proven the orientation independence of the radial optics when measuring CRBCs.

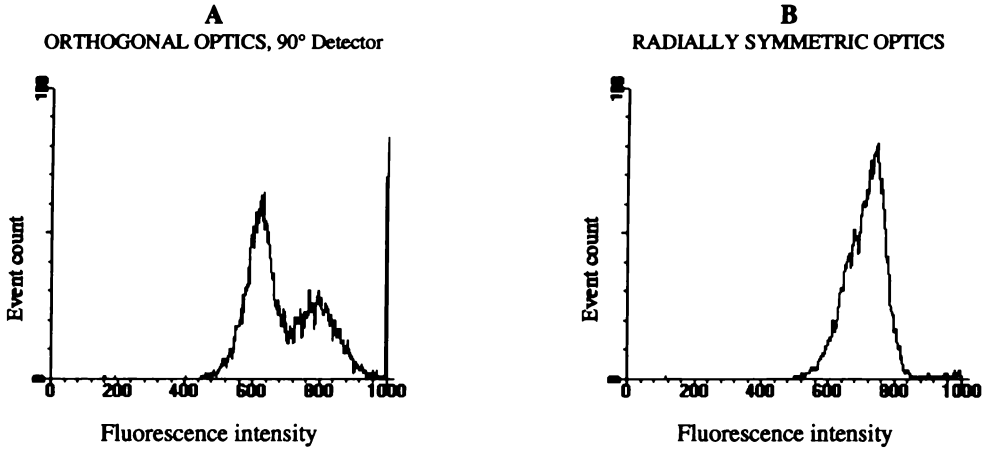

*Figure 5-8. Hoechst 33342 stained CRBC fluorescence histograms displaying **A**: a lateral extension to higher intensity values for the FACStar, and **B**: a unimodal population result from radial optics showing orientation independence.*

5.4.4 DNA Content - Chinchilla Sperm (X-Y > 5%)

In this test, we investigated the capability of both optical systems to resolve X- and Y-chromosome-bearing sperm. Hoechst 33342 stained sperm from the mammalian species *chinchilla langier* were analysed. The flat, disk-like shape of chinchilla sperm heads introduces optical artifacts which make accurate DNA content measurement difficult. There is a 7.5% difference in total DNA content, stain uptake, and therefore fluorescence between X and Y chinchilla sperm. Conventional flow cytometers require alignment selection or gating of cells to produce a dual X- and Y-peaked histogram with sufficient resolution to set sort gates for reliable enrichment of an X or Y sperm population.

Figure 5-9 compares measurements of chinchilla sperm DNA content using orthogonal and radial optics. The contour plot of side vs. forward fluorescence (Figure 5-9A) displays a characteristic L-shaped DNA content distribution for flat sperm cells. Sperm which are considered to be edge-on with respect to the side detector are located in the lower right LR region of the contour plot. Sperm which are oriented face-on to the side detector fall within the intensity values of the upper left region of the L, with intermediate positions lying between the two extremes. The effect of hydrodynamic orientation of the cells is demonstrated by the increased proportion of cells which are in the lower right region of the plot. A gate (R2) is positioned over the LR region and is applied to the forward detector histogram to obtain a fluorescence distribution of the oriented cells (Figure 5-9D). The X and Y sperm populations can be distinguished in this figure as two overlapping Gaussian-like curves separated by 8.6% in intensity. This gated fraction (40%) of the original population has a CV of 5.2%.

The radial optics (Figure 5-9E) produced a fluorescence histogram which shows two overlapping populations representative of X- and Y-bearing sperm with a peak intensity separation of 8.3% and a population CV of 5.4%. This data includes measurements from all the sperm independent of their orientation with respect to the detection optics. No lateral extension was observed in this histogram, confirming the orientation-independent measurement performance of the radial optics.

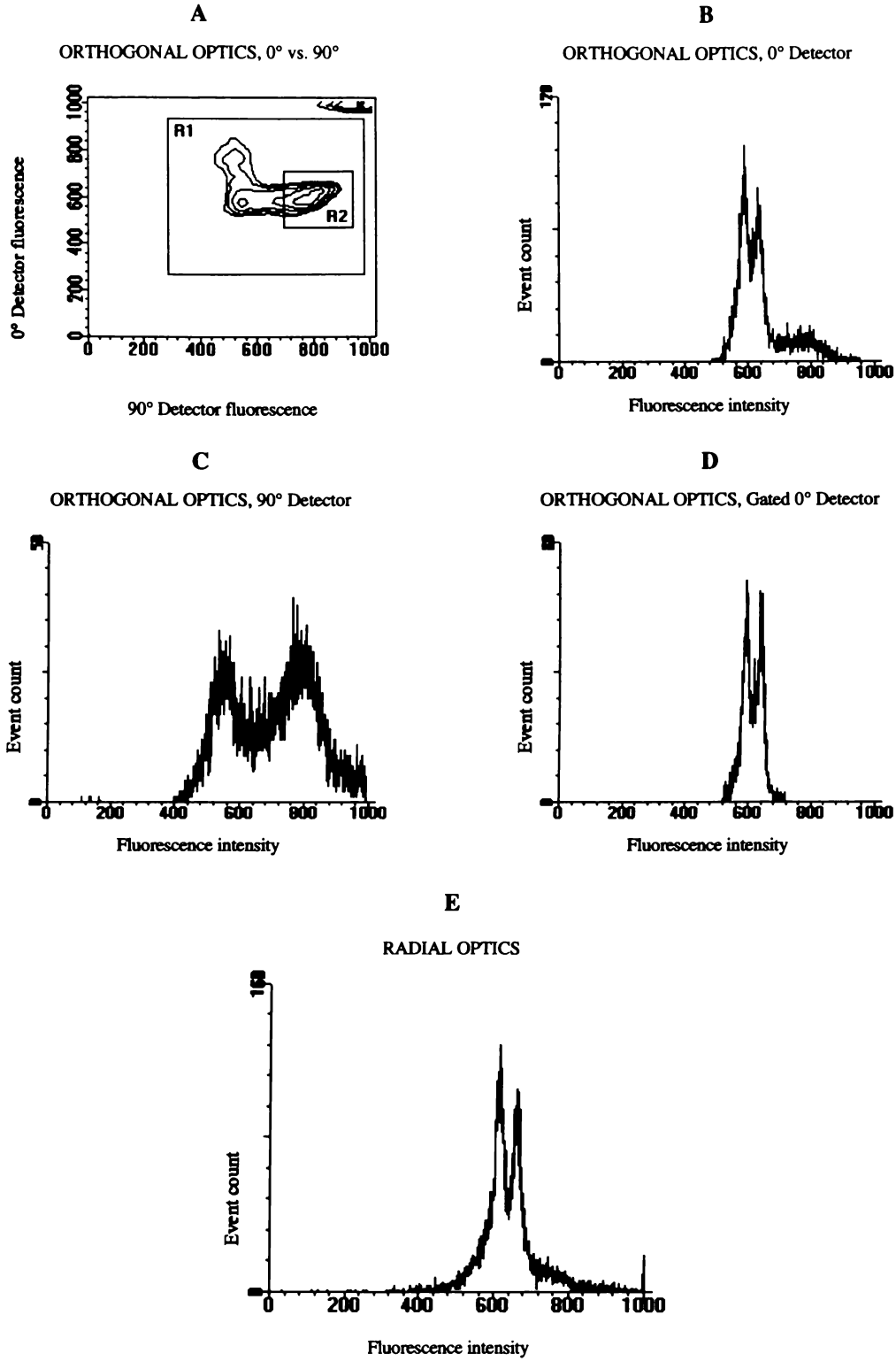

Figure 5-9. Contour plots and histograms for Hoechst-stained chinchilla sperm. A: Contour plot displaying gate (R2) over aligned sperm. B: Forward detector histogram of population. C: Side detector histogram. D: R2 gated forward detector histogram clearly showing X and Y peaks. E: Radially symmetric optics single detector histogram displaying X and Y peaks with no lateral extension to higher intensity values.

5.4.5 DNA Content - Bull Sperm (X-Y < 5%)

Resolution of both optical systems was further examined with bull sperm which exhibit a 3.9% X-Y difference in total DNA content. This small X-Y difference, coupled with the very flat ovoid shape of bull sperm heads means that greater instrument resolution is required than for chinchilla sperm.

Contour plots and histogram results for the analysis of bull sperm using both optical configurations are displayed in Figure 5-10. As with chinchilla sperm, the orthogonal optical system produced an L-shaped contour plot. Once more, the proportion of cells oriented toward the forward detector is increased by fluidic forces from the bevelled sample injection needle. The R1 gated forward detector histogram (Figure 5-10D) displays a dual-peaked population with a peak separation of 3.9%, consistent with the difference in DNA content between X- and Y-sperm. This gated population has a CV of 4.0%. By setting sort gates on the left and right hand side of this profile, samples enriched with Y and X sperm may be sorted. It is important for this process that the CV be low to minimise X-Y sperm overlap and maximise enrichment.

Bull sperm results for the radial optics are displayed in Figures 5-10E and 5-10F for two sample-to-sheath differential pressure settings which gave event rates of 200 cells s^{-1} and 1000 cells s^{-1} respectively. In both cases a single, symmetric peaked intensity distribution was observed with no evidence of the bimodal distribution measured by the FACStar. A low sample-to sheath differential (Figure 5-10E) produced a population CV of 4.2%. Increasing the sample-to-sheath differential pressure to obtain an event rate of 1000 cells s^{-1} yielded broader population distributions (Figure 5-10F). However, the uni-modal histogram form was retained throughout these flow rate adjustments, demonstrating that orientation independent fluorescence collection was retained. An X-Y split can be observed in Figure 5-10F which has a CV of 6.8%. The effect of sample to sheath differential pressure on population CV is discussed further in Chapter 7.

5.4.6 DNA Content - Ram Sperm (X-Y < 5%)

Ram sperm were also analysed using both optical geometries, because cattle and sheep have comparable agricultural (and commercial) significance. These cells exhibit a 4.2% X-Y DNA content difference and are similar in shape and form to bull sperm. The contour, forward, and side detector plots exhibit similar characteristics to those obtained for bull sperm in Section 5.4.5 above. Again, the R1 gated region (Figure 5-11D) displays an X-Y DNA content split which is separated by 4.1% in intensity. The radial optics histogram of the entire sperm (Figure 5-11E) clearly displays a uni-modal population which has a CV of 5.2 and shows some evidence of an X-Y split.

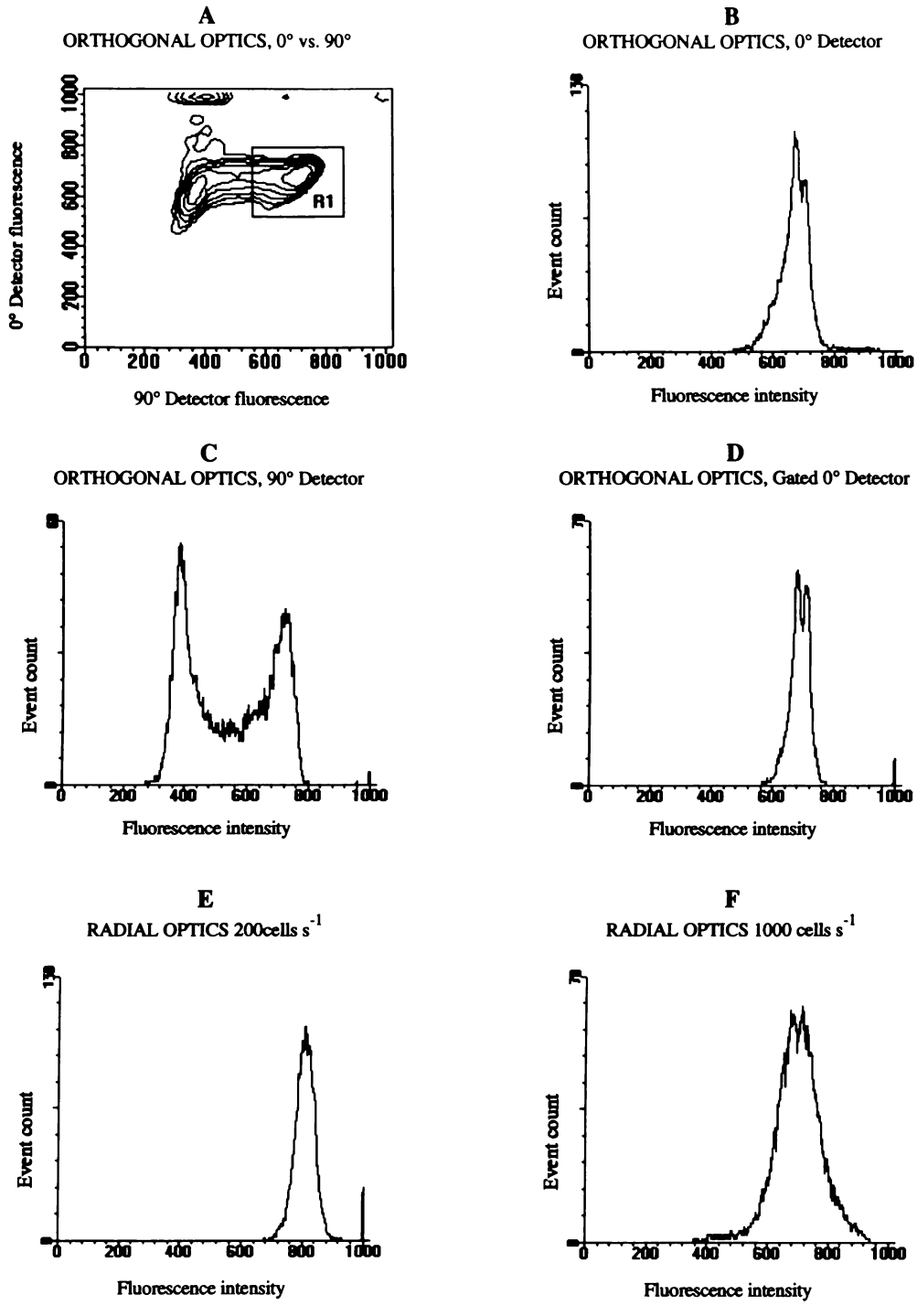

Figure 5-10. Hoechst 33342 stained bull sperm fluorescence histograms displaying A: contour plot, and histograms of B: forward detector, C: side detector and D: R1 gated side detector for oriented cells. E: Radial optics histogram clearly showing a single peak for the entire sperm population (sample rate 200 events s^{-1}). F: Radial optics histogram for a different sperm sample which displayed an X-Y split at a rate of 1000 events s^{-1}.

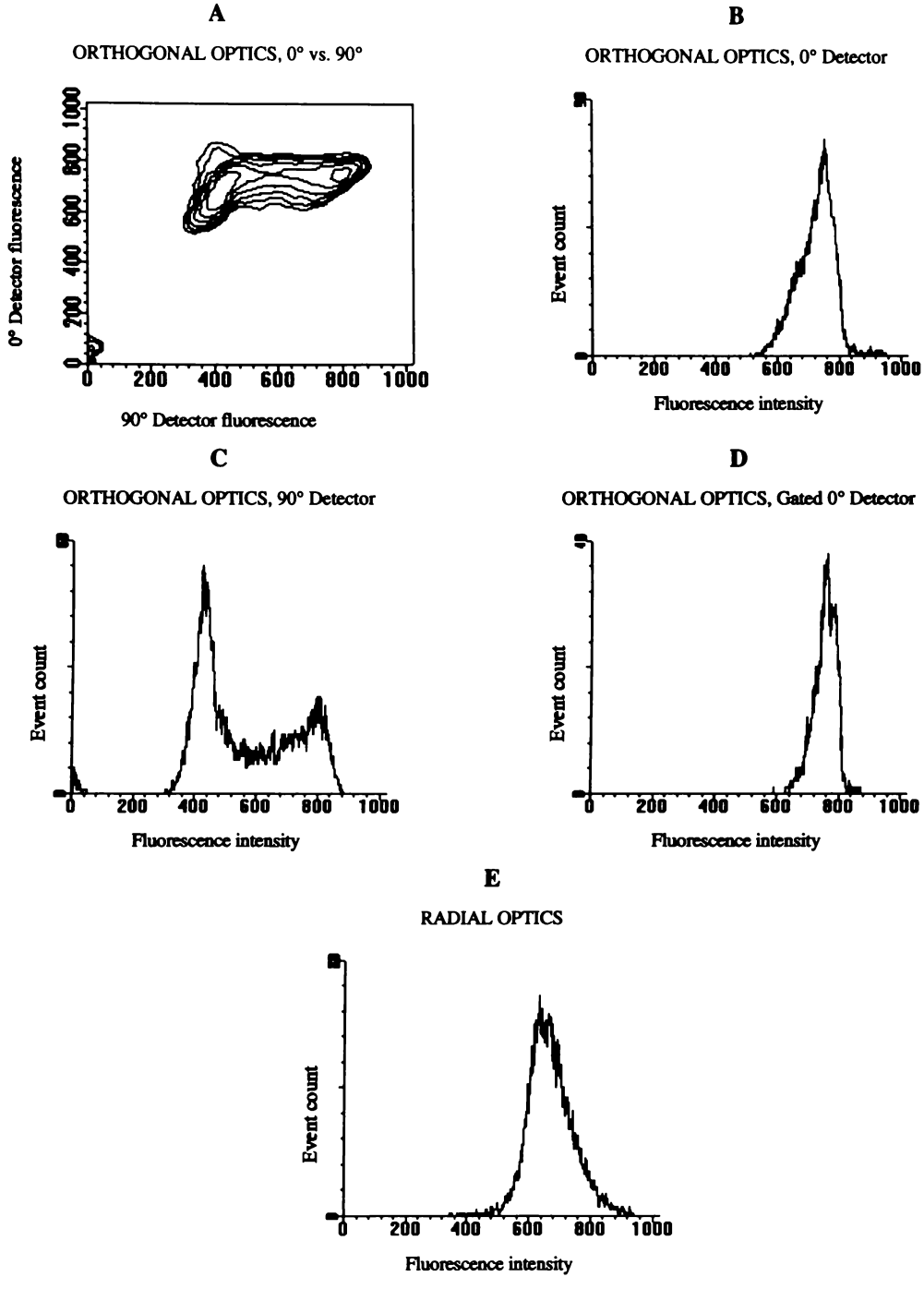

Figure 5-11. Ram sperm results showing A: contour plot of entire sperm population, B: forward, C: side, and D: gated side detector data which displays an X-Y split. E: Radial optics result showing a uni-modal population with no extension to higher intensity values.

5.4.7 Extension to Multi-Wavelength Live-Dead Sperm Analysis

The purpose of this study was to determine if the radial optics could be used to perform multiparameter (i.e. multi-wavelength) analysis. Live-dead ratio analysis was carried out on a population of dual-stained bull sperm.

Figure 5-12 displays green SYBR-14 (live, *x*-axis) vs. red PI (dead, *y*-axis) fluorescence intensity contour plots for both optical systems for the same sperm population. The logarithmic scale is due to logarithmic gain settings which were used to cover the entire dynamic intensity range, allowing both dim and bright fluorescence of the cells to be viewed within the window. An acceptance region (R1) was positioned on both plots to remove unwanted noise events in the LL region.

The ratio of live (UL) to dead (LR) sperm was measured to be 1:4.2 for the orthogonal optics case and 1:8.8 for the radial optics case. Analysis was performed on the radial optics prior to the orthogonal optics, after first treating the sperm (by adding saline) to kill some of the cells. The increase in dead sperm for the orthogonal optics result is consistent with further sample degradation during the time taken to switch the instrument from one configuration to the other (a few minutes).

The FL2 gain setting (of 560V) was identical for both tests, however the FL1 gain was adjusted from 579V (orthogonal optics) to 679V (radial optics) to maintain the live sperm population position on the *x*-axis. The logarithmic scale of these plots makes comparisons between the two contour profiles difficult. However, the relative positions of live and dead fractions is consistent between the plots. The upward extension of the live orthogonal optics population is not evident in the radial optics plot, suggesting that the orientation independence of the radial optics can separate populations of asymmetric cells more effectively than orthogonal optics.

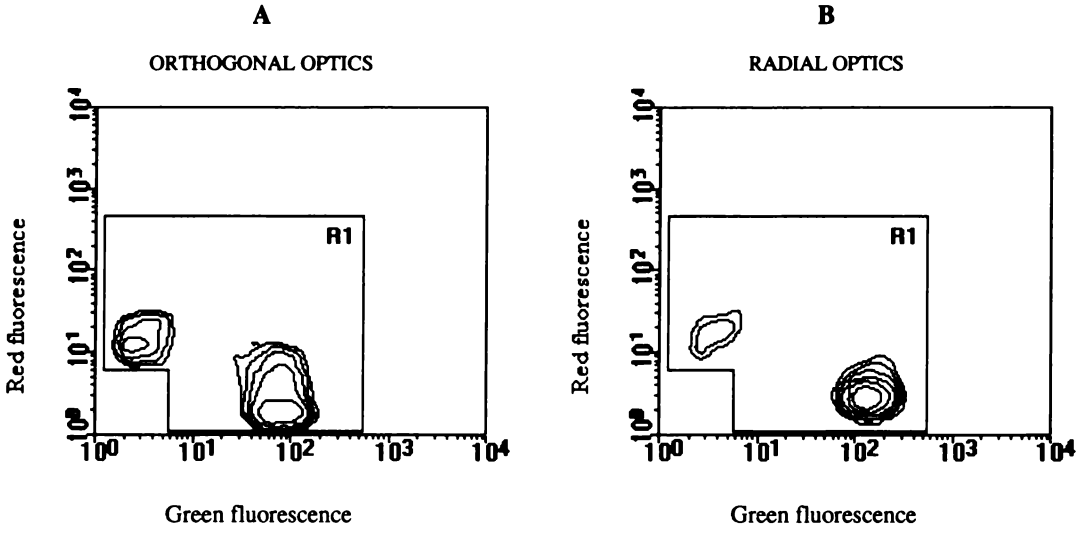

*Figure 5-12. Dual live-dead sperm analysis contour plots using **A**: conventional orthogonal optics and **B**: radial optics.*

5.5 Radial Optics Modifications

The physical arrangement of the radial optics readily allows modifications. Such modifications may take the form of additions to the experiment, or alterations to the geometric configuration of the optical components.

Two separate experiments were performed using modified radial optics. In the first experiment, the geometry was altered to provide fore and aft (fluorescence) detection from cells as they passed through the focus. From this experiment, two-parameter contour plots could be obtained. In the second experiment, further modifications were made so that the orthogonal collection geometry of a conventional flow cytometer could be mimicked, while retaining radial illumination.

5.5.1 Modified Radial Optics I: Fore-Aft Cell Detection

The radial optics collect light over a large solid angle in a radially symmetric fashion from above and below the plane of laser excitation. In the preferred configuration, all of this light is focused onto a single detector. The consequence of measuring the light with a single detector is that data is presented on a single dimensional plot or histogram, rather than a two-parameter plot as obtained with the forward-side detector geometry of an orthogonal instrument.

In this study, the radial optics collection geometry was modified to provide two-detector (single wavelength) fluorescence collection (see Chapter 4 for an optical description). This meant that two-parameter plots could be produced for visual comparison of the results of orthogonal and radial optics. The radial optics were partitioned to provide fore and aft detection of cells as they flowed through the inspection point while retaining radially symmetric light collection.

Figure 5-13 displays the results for 4.5μm calibration microspheres, chinchilla sperm, and bull sperm as measured by both orthogonal and radial optics. Figures 5-13A and 5-13B show that the microsphere calibration particles produced contour plots with matched characteristics, as expected for spherical particles.

The flat chinchilla and bull sperm produce L-shaped contour plot population distributions using orthogonal optics as previously shown in Section 5.4.4 (Figures 5-13C and 5-13E). The orientation independent nature of the radial detection system is again confirmed (Figures 5-13D and 5-13F) by single populations on the fore vs. aft contour plots. Both sperm samples yield populations which are elongated along an $x = y$, 45° line which represents a measured DNA content difference. A perpendicular variation from the 45° line represents a cell which has not been measured in an orientation independent manner by both fore and aft detectors and may be due to cells not travelling down the focus with their longest axis perfectly aligned with the direction of flow, thereby presenting a different fluorescence intensity to each of the fore and aft detectors.

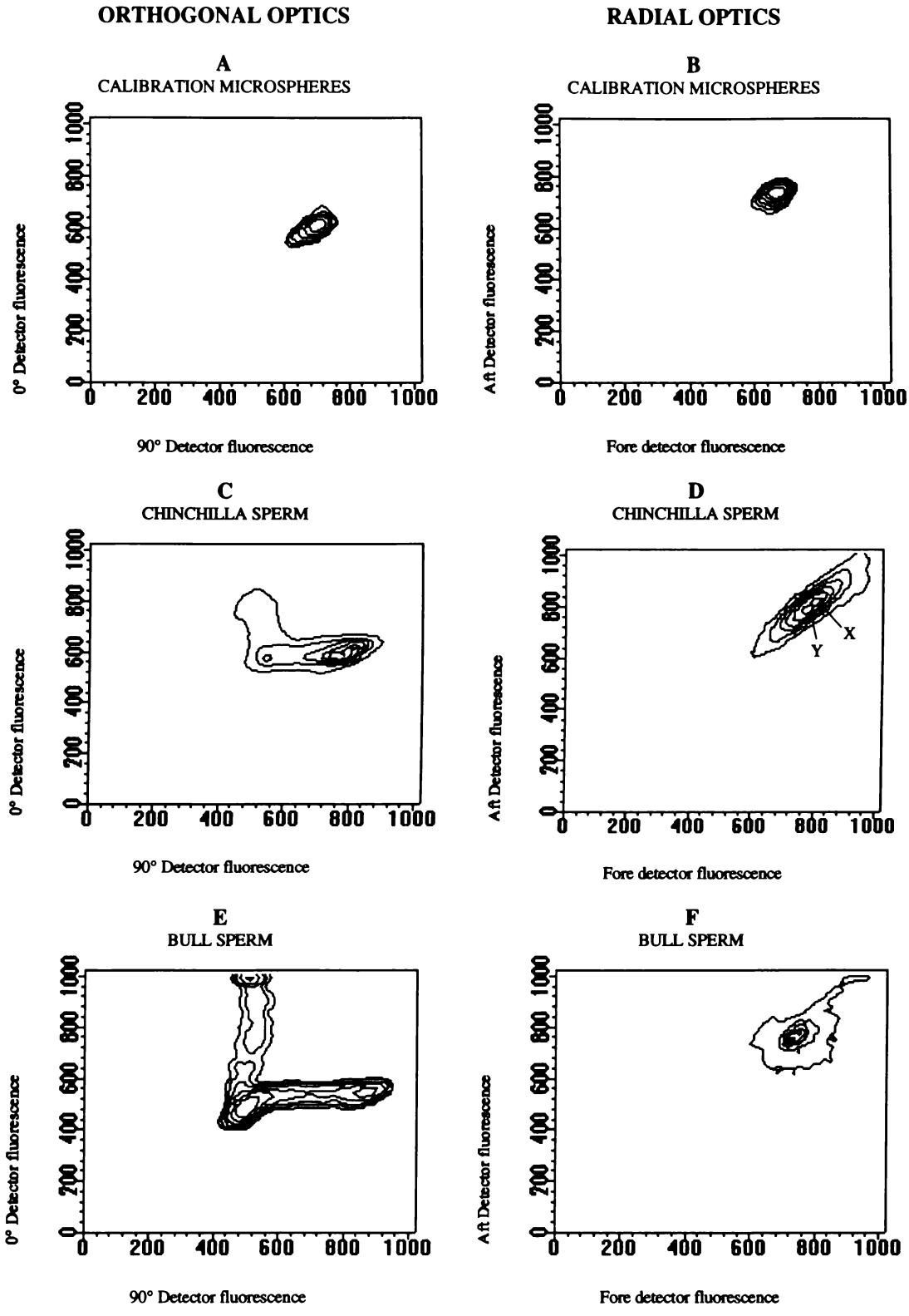

Figure 5-13. Contour plots for samples of A,B: Calibration microspheres, C,D: chinchilla sperm, and E,F: bull sperm obtained using orthogonal and modified radial optics.

An X-Y split is evident in the chinchilla sperm plot (Figure 5-13D). The magnitude of the X-Y difference in each of the x and y axes is approximately 7.5%. X-Y Splits for the chinchilla and bull sperm results are masked by a broad CV (Figure 5-13F). However, a general extension of the populations exists along the diagonal. If instrument errors and therefore CVs can be reduced, an X-Y split may become more evident.

In this study, the radial optics system has been modified to provide fore-aft detection while retaining radially symmetric fluorescence collection about the cell flow axis. This two-detector geometry has allowed a comparison to be made between forward vs. side detector plots of the orthogonal optics, and the fore vs. aft detector data of the radial optics. Symmetry about the 1:1 axis shows that sperm seem to fluoresce equally fore and aft, suggesting approximate symmetry about the equator of the cell.

5.5.2 Modified Radial Optics II: Orthogonal Optics Simulation

The aim of this study was to investigate the effect of sperm cell orientation (with respect to the excitation source) on the forward vs. side detector contour plot data. In conventional orthogonal systems, it is difficult to separate the effects of orientation on illumination with the effects on emission.

In conventional flow cytometers, cells are exposed to a uni-directional excitation source such as a laser beam as they pass through the inspection point. Thus, for a flat cell, the cross-sectional collection area and therefore possible collection of excitation light will depend on its orientation with respect to the beam direction. This may add a further degree of uncertainty to the interpretation of fluorescence data from a population of randomly oriented cells.

In this experiment, the radial configuration was modified to determine if such an orientation dependent illumination effect does in fact exist when measuring flat cells such as bull sperm. A sectored fore-aft detector arrangement was used to reproduce the forward and side light collection geometry of an orthogonal flow cytometer while preserving the orientation independent light delivery system of the radial optics design (see Chapter 4 for an optical description).

Contour plots were obtained for ten thousand events on each instrument and are presented in Figure 5-14. Experimentation using the orthogonal optics was performed with the bevelled injection needle (which could not be removed) in place and thus the figure shows a greater proportion of cells in the LR region than the UR region (Figure 5-14A). Orientation of the bevelled needle about the flow axis to orient more cells edge-toward the forward detector only adjusts the relative proportion of cells in each of the UL and LR regions and does not does not alter the form of the footprint or the LL region of the contour plot. The flow nozzle used for the modified radial optics did not have a bevelled sample injection tube and therefore cells were presented to the inspection point at random orientations about the flow axis. This is demonstrated by a similar number of cells in each of the UL and LR regions (Figure 5-14B).

A pair of x and y cross-hairs are located on each of the contour plots to bisect the UL and LR regions of the L population. It is expected that the cross-sectional area, the total light incident on, and therefore fluorescence from a sperm as it flows through the uni-directional focus of a conventional cytometer, will depend on its orientation with respect to the incident beam (Section 5.3.4). This may be observed in the uni-directional illumination plot (Figure 5-14A) by a reduction in intensity for cells which are in the LL region. This effect could be caused by cells which do not present their full flat face to the laser source. In contrast, Figure 5-14B shows that the radial optics system exhibits no drop-off of intensity in the LL region, suggesting that by providing radially symmetric illumination to the cells, consistent light delivery is maintained irrespective of cell orientation and the LL region drop-off is removed.

Histograms of the R1 gated regions in each of the contour plots are presented for DNA content analysis in Figures 5-14C and 5-14D. The greater event count on the orthogonal optics histogram is due to hydrodynamic orientation of the sperm heads using a bevelled injection needle. The orthogonal optics result displays a 3.9% X-Y peak separation. The apertured orthogonal optics result also exhibits an X-Y split with a value of approximately 4.3% for those sperm contained within the gated region.

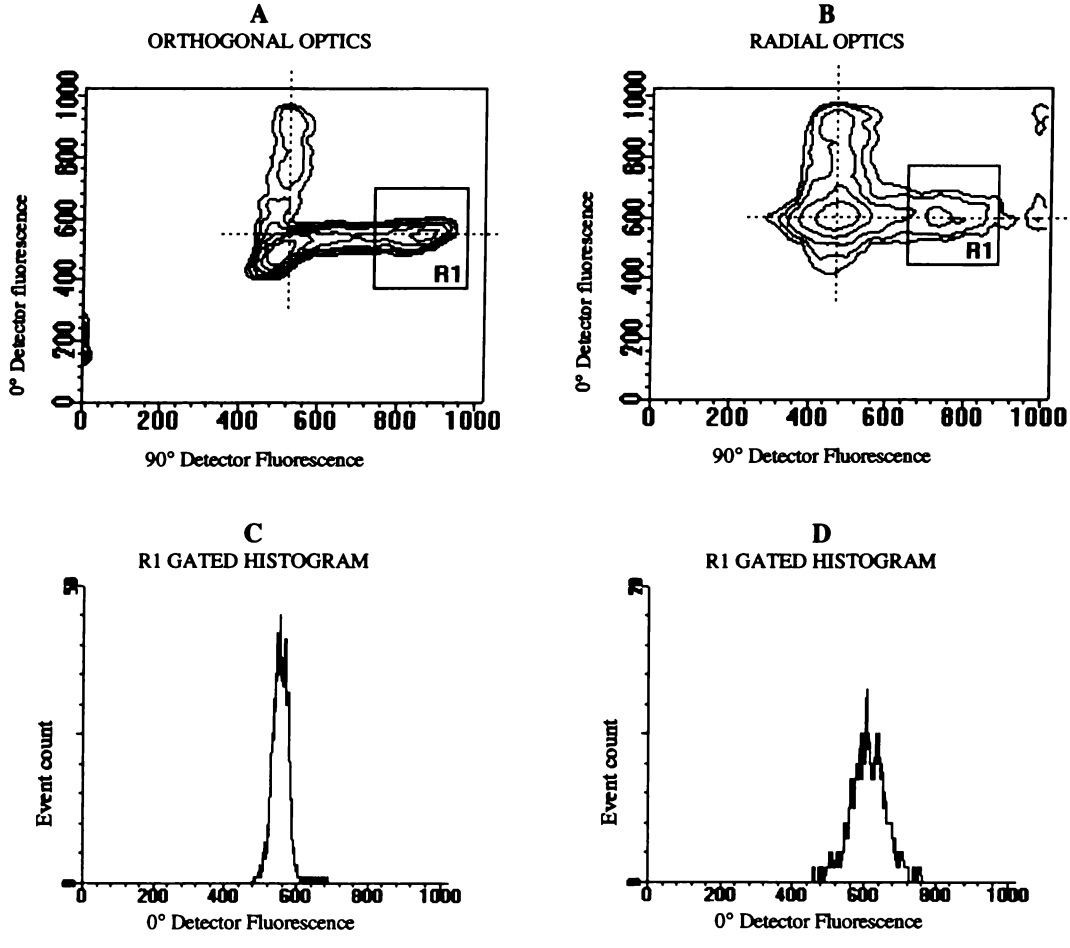

Figure 5-14. Comparison of contour plots produced for orthogonal collection geometries for a sample of Hoechst 33342 stained bull sperm using A: conventional uni-directional illumination and B: radial illumination optics. Gated portions of the contour plots are also given for C: orthogonal, and D: modified radial optics data.

The radial optics allowed us to separate the effects of illumination and fluorescence when using orthogonal optics on flat cells. These results demonstrated the problems faced with uni-directional illumination of flat cells.

5.6 Discussion

In this Chapter flow cytometric experimentation was carried out in three main areas; preliminary experiments on a conventional flow cytometer, comparative measurements on cells between orthogonal and radial optics, and radial optics modifications.

Preliminary Measurements Using Orthogonal Optics

The preliminary experiments using a conventional, orthogonal optics configuration, were performed to gain a full understanding of the sperm sexing process. A study of the efficiency of cell orientation using hydrodynamic alignment revealed the conditions that are necessary for maximum cell orientation. For cell event rates exceeding 3500 cells s^{-1}, random orientation was found to ensue whereby fluidic orientation of cells was no longer provided. Thus a trade-off existed between possible sort rates and efficiency (sample waste).

Comparative Measurements of Orthogonal and Radial Optics

Direct performance comparisons were made between the radially symmetric optics and the orthogonal optics of a FACStar Plus flow cytometer for several particle types and geometries including calibration microspheres, CRBCs, chinchilla sperm, bull sperm and ram sperm. Tests for both optical configurations used the same fluidics, laser excitation source, filter sets, photodetectors, and data processing equipment of the commercial instrument.

Microsphere calibration particles were analysed on both systems and produced equivalent CVs suggesting that the radial optics has comparable resolution to that produced by the orthogonal optical geometry of the FACStar Plus. The broadening of fluorescence intensity distributions normally observed with orthogonal optics for aspherical cells such as CRBCs was not present when using our system, demonstrating that radially symmetric optics can be used to remove geometrical artifacts from measurements on ovoid cells.

DNA content analysis of Hoechst 33342-stained flat chinchilla sperm by the radial optics system, produced unimodal histogram populations with clear X-Y peak separation. This result is in contrast to the bimodal histogram generated by the orthogonal optics which required orientation gating to yield histograms with similar CVs and X-Y distinction.

Bull sperm are larger and flatter than chinchilla sperm and show extreme optical artifacts of measurement in orthogonal cytometer optics. At low sample to sheath differential pressures the radial optics system gave a unimodal population with CVs which matched those for a gated fraction of the bimodal population measured by the FACStar. In our investigations on large cells such as bull sperm we found that increasing the sample to sheath differential pressure, and therefore the event rate, resulted in

an increase in the CV of the population. It is suggested that fluidic instability, combined with a focal region which is narrow compared to those commonly used with orthogonal optics, may have resulted in variations in cell illumination. Future work will be carried out to reduce fluidic instability and to broaden the excitation focus laterally in an attempt to reduce variations in cell illumination. Analysis on ram sperm yielded similar results to those obtained with bull sperm.

The study of sperm viability is an area where radial optics may be useful. This system has been successfully used for dual parameter, live-dead analysis of bull sperm. Population resolution is increased, since this orientation independent optical system is not prone to the optical artifacts of measurement associated with flat cells with orthogonal geometry flow cytometers. Additional applications may also be found for this system using other types of aspherical particles or cells.

Radial Optics Modifications

The geometry of the radial optics enabled several modifications to be made in an effort to emulate data visualisation and geometric aspects of an orthogonal system. Fore-aft detection of the cells showed that fore and aft emission were strongly correlated, suggesting sperm are approximately symmetrical about the equator of the head.

The second modification involved aperturing the fore and aft detectors in a way which emulated the orthogonal collection geometry of a conventional sperm sexing flow cytometer. With this modification it was possible to reproduce the L-shaped population inherent to analysis of bull sperm using the orthogonal system. It was also possible to distinguish an X-Y DNA content split which was consistent with the orthogonal optics result by locating an orientation acceptance gate around the oriented (LR) population. In addition, the effect of cell orientation with respect to the excitation source was investigated. Preliminary comparative measurements between the uni-directional illumination of the orthogonal optics and the omni-directional (radially symmetric) optics resulted in a difference in the LL region of the contour plot, which suggests that there is a cell orientation effect on the light absorbed by cells as they pass through a flow cytometer for sperm sexing.

6. An Optical Model of Bull Sperm

The morphological and physical properties of mammalian, and in particular, bovine sperm, and the method by which they can be differentiated according to DNA sex content, has been outlined in Chapter 3. The determination of sperm DNA content has been hampered by the flat shape of sperm heads which give rise to optical measurement artifacts in orthogonal flow cytometer geometries. In this chapter, the optical properties of flat biological cells such as sperm are investigated by a Monte-Carlo ray tracing model, the results of which are compared to the experimental findings of Chapter 5.

In Section 6.1, previous attempts at modelling fluorescence emission from bull sperm are outlined, and the aim of our modelling work is discussed. The optical effects that are included and the Monte-Carlo ray trace algorithm used to monitor the path of fluorescence emission from sperm are described in Section 6.2. The results of this model are presented and compared with experimental data in Section 6.3. In Section 6.4 several other physical techniques are investigated which lend support to the findings of our model. Finally, results from this work are discussed in Section 6.5.

6.1 Background

The first flow cytometric measurements of sperm yielded unexpected results (Gledhill *et al.* 1976, Van Dilla *et al.* 1977). Fluorescence intensity histograms showed a uni-modal peak contained most of the population, but that some of the population was also contained within a lateral extension to higher intensity values. A flow cytometer was used to sort sperm into low and high intensity populations. However, re-analysis of each of the sorted fractions yielded the same characteristic histogram distributions (i.e. laterally extended) once again. It seemed that the fluorescence collected from a sperm cell was dependent on the cell orientation with respect to the detector. It was proposed that the effects of total internal reflection resulted in preferential emission of fluorescence from the narrow edge of the sperm. It was suggested that those cells contained in the lateral extension of the histogram passed through the inspection point edge-toward the detector while cells in the main peak were oriented flat-face toward the detector. Van Dilla presented a two-dimensional mathematical model of sperm optical properties in an attempt to explain this effect.

Computation of the angular distribution of fluorescent light emission produced a theoretical distribution qualitatively similar to those found experimentally, that is, with a peak due to sperm heads oriented with their flat faces toward the detector, and a lateral extension toward higher fluorescence values due to heads oriented with their edges toward the detector. However, it was noted that the computed distribution was too narrow, and the area of the peak was too small compared to experimental data. The model of Gledhill *et al.* considered fluorescence from a uniformly illuminated cell, neglecting any effect of cell orientation with respect to the laser excitation beam.

In Chapter 5 an experiment was carried out to investigate the effect of cell orientation on the level of fluorescence emission. This experiment demonstrated the problems faced with uni-directional illumination of flat cells in orthogonal flow cytometers. For the uni-directional illumination (orthogonal) system, there was a characteristic intensity fall-off for cells which were in the LL region of the plot. It was found that this drop-off could be removed by implementing the radial illumination-orthogonal collection geometry. We explain this effect by simulating the optical artifacts that are associated with the measurement of sperm cells using a Monte-Carlo optical ray trace model.

6.2 Optical Model of a Sperm Cell - Description

A physical model has been developed to explain observed fluorescence emission artifacts when measuring flat cells using flow cytometry. The sperm cell is modeled as a lens-like element and optical phenomena such as reflection, refraction, transmission, and total internal reflection are taken into account. The effects of cell illumination, absorption, and fluorescence, as a function of orientation with respect to the excitation source are considered. Stain saturation for high laser powers is also considered. Cells are assumed to contain a uniform stain distribution throughout their volume.

6.2.1 Cell Geometry

Four model geometries were investigated and are pictured in Figure 6-1. These geometries are 2D rectangle, 2D (semi-circle) capped rectangle, 2D ellipse, and 3D ellipsoid. The rectangular geometry implemented by Van Dilla was modeled (2D rectangle) and extended to the capped rectangle case to investigate cell end effects on the modeled fluorescence output. The 2D ellipse geometry was chosen in an attempt to provide a more realistic biological shape and served as a prelude to the 3D model.

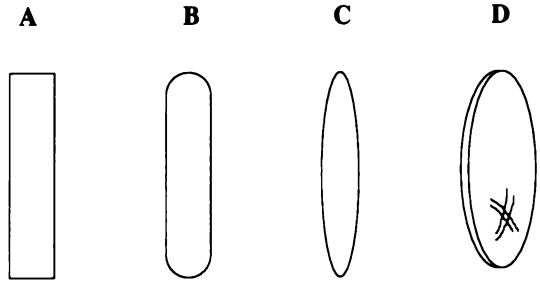

Figure 6-1. The four cell geometries modeled; A: rectangle, B: capped rectangle, C: ellipse, and D: 3D ellipsoid.

For the 3D model, an ellipsoid cell geometry was chosen. The ellipsoid cell has semi-major dimensions a, b and c, is centred on the x, y and z axes, and points on its surface obey

$$\frac{x^2}{a^2}+\frac{y^2}{b^2}+\frac{z^2}{c^2}=1. \qquad (6\text{-}1)$$

The dimensions of a bull sperm head were taken as 10μm x 4.5μm x 1μm (length x breadth x thickness) and are consistent with those measured in Chapter 3. A cell (n_1) to jet (n_2) refractive index ratio of 1.33:1.42 was used in our analysis. The value of n_2 for the DPBS sheath fluid was assumed to be

equivalent to a saline solution containing 9 g l^{-1} NaCl (CRC Press 1975). The n_l of 1.42 was obtained from the value calculated for live bull sperm by Van Duijn (1971).

6.2.2 Cell Illumination

Cell illumination (and therefore fluorescence) as a function of orientation with respect to a uni-directional excitation source was considered via three calculations; the effect of cross-sectional area presented to the source, the effect of incidence angle on transmittance of excitation wavelength light into the cell, and finally, the effect of saturation of the DNA-bound stain.

Cross-Sectional Light Collection Area

As a cell travelling in a liquid stream passes through a uniform, collimated beam of light, the collected portion of the total beam will be directly proportional to the cross-sectional area the cell presents to the beam. We can determine this cross-sectional area by considering the cell to be an ellipsoid and projecting the area A seen by the light beam, as a function of cell orientation θ.

Transmittance of light into the Cell

The proportion of light which is transmitted into (and absorbed by) a cell is dependent on the mean angle of incidence θ_1 across the cell surface, the refractive index mismatch at the stream-cell interface, and therefore the angle of refraction θ_2, according to the Fresnel formula

$$T = 1 - \frac{1}{2}\left(\frac{\sin^2(\theta_1 - \theta_2)}{\sin^2(\theta_1 + \theta_2)} + \frac{\tan^2(\theta_1 - \theta_2)}{\tan^2(\theta_1 + \theta_2)}\right). \tag{6-2}$$

Stain Saturation

A study was conducted in Chapter 5 to determine what effect increased excitation power has on the saturation of DNA-bound stain in sperm. The fluorescence intensity profile I, as a function of the operation power P, for each of the forward and side detectors was proportional to $1 - e^{-P/k}$, where P is the input laser power and k is a constant. The illumination effects of cross-section C, transmittance T, and saturation were combined according to

$$I = I_0\left(1 - e^{-CTP/k}\right) \tag{6-3}$$

to obtain an expression for light captured by a stained sperm as a function of orientation. A mean value of k was determined from the dye saturation measurements of Chapter 5 to be 83.5mW for Hoechst 33342 using the specified staining procedure for bull sperm.

6.2.3 Cell Fluorescence Emission

The spatial emission profile of fluorescent light from a stained sperm cell was determined by combining the effects of reflection, refraction and absorption.

Fluorescence Emission, Reflection and Refraction

As discussed in Chapter 3, the sperm staining (Hoechst 33342) process is stoichiometric, and therefore

fluorescence emission within the sperm was assumed to be homogeneous. This homogeneous distribution of fluorescent light from within the cell was modeled by selecting a large number of random stain molecule locations within the cell, and selecting a random photon (ray) emission start direction for each location. The path of each ray is followed through the cell until it intercepts with the cell-stream interface. Once the interface is encountered, the incidence angle and transmission criterion are assessed. Provided the incidence angle θ_1 does not exceed the critical angle given by

$$\theta_{crit} = \sin^{-1}\left(\frac{n_2}{n_1}\right) \tag{6-4}$$

the ray will be transmitted through the stream-cell interface at an angle θ_2, corresponding to refraction according to Snell's law. If $\theta_1 > \theta_{crit}$ the ray is totally internally reflected.

Absorption

The path of a total internally reflected ray is monitored until a threshold number of total internal reflections is exceeded. If the ray escapes before this threshold is exceeded, its attenuation is calculated from the path length l, according to the Beer-Lambert law for the final intensity I

$$I = I_0 e^{-\alpha l}, \tag{6-5}$$

where α is the absorption coefficient for the bull sperm head ($\alpha = 0.346\mu m^{-1}$, calculated from the optical density of a sperm in Section 3.2.4) and I_0 is the original ray intensity. If the threshold is exceeded the ray is no longer studied and is considered to have been attenuated or absorbed within the cell. Re-absorption of fluorescent light by the dye is not considered for this calculation.

6.3 Monte-Carlo Ray Trace Routine

6.3.1 Algorithm

The general ray trace algorithm for the bull sperm model is outlined in the flow chart of Figure 6-2. This algorithm traces the path of an emitted photon as it travels through a cell and interacts with one or more cell-jet interfaces before being absorbed or transmitted.

The program begins with the selection of dimensions and refractive index values for the cell model. It then repeatedly traces rays from a random location within the cell and in a random direction. When a ray meets the first cell-fluid interface, the incidence angle is calculated and the transmission criterion assessed. The path of this ray is traced until it escapes, or until it has undergone a maximum number of internal reflections (estimated from the absorption coefficient α) at which point the ray can be considered to have been absorbed within the cell. If the ray escapes, the angle of emission is recorded.

Once ray tracing is completed for an appropriate number of fluorescent molecule starting points, results are collated to produce an intensity distribution polar plot around the flow axis. This data is also binned to obtain theoretical 0° and 90° detector histograms and a contour plot for a population of cells randomly oriented about the flow axis. The path of one ray, traced for the 2D ellipse model, is illustrated in Figure 6-3. In this figure the effect of total internal reflection is shown.

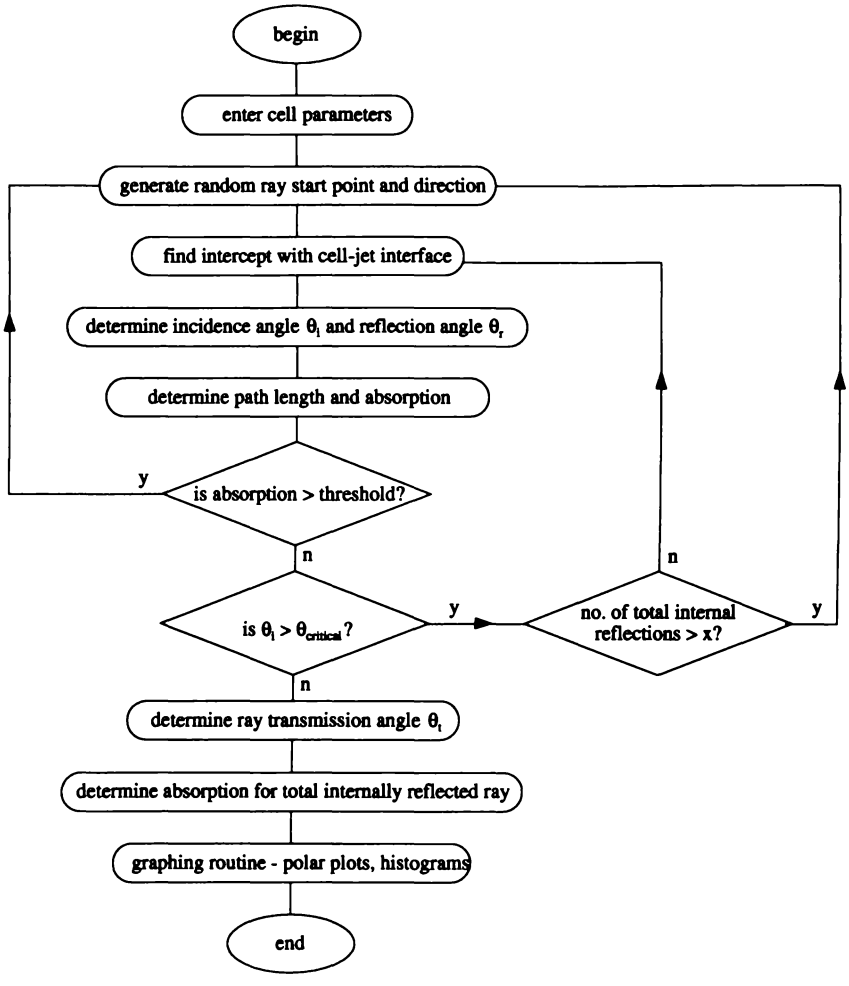

Figure 6-2. Flow chart of ray tracing routine

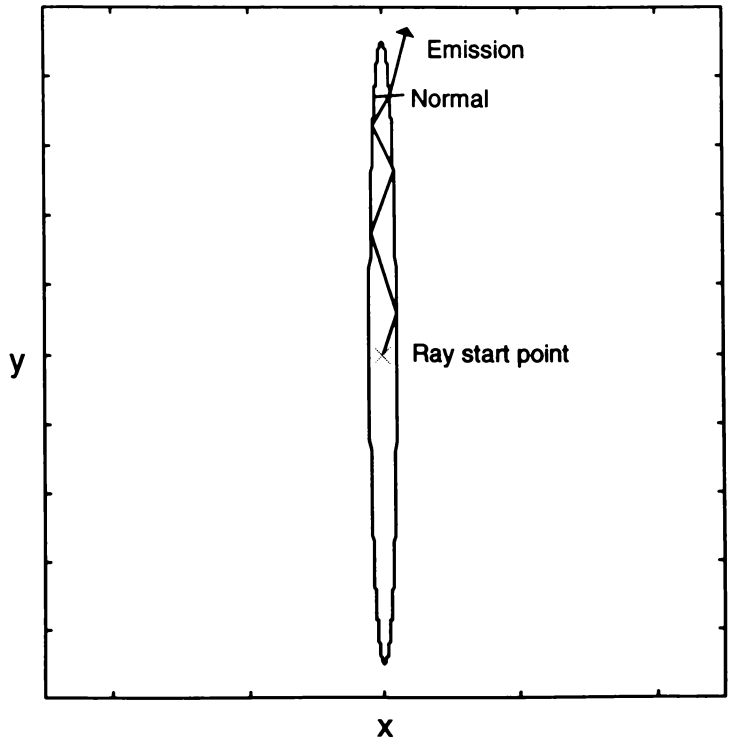

Figure 6-3. The path of a total internally reflected ray (flow axis is into page).

6.3.2 Computational Considerations

The Monte-Carlo ray trace program was written in the Matlab (v4.1c) environment with development on a 486 DX2/100 PC and execution of large jobs on a Dec Alpha. The Matlab random number generator (rand()) function was utilised to obtain the random ray start positions and directions of the Monte-Carlo algorithm. The rand() function is based on the linear congruential method described in Park and Miller (1988). The basic algorithm used is seed = $(7^5 \text{seed}) \bmod(2^{31} - 1)$. This generator complies with warnings often given which relate to random number generators displaying distinctly non-random characteristics, as outlined in Park and Miller (1988).

A run of fifty thousand ray start points gave sufficient resolution to observe the general effects of the model. However, up to one million ray start points were chosen to obtain smooth plots. To reduce run time, cell symmetry was utilised to restrict ray start positions to within one quadrant for the 2D models, and within one octant for the 3D model. Matrix manipulation was then used to map results for the single quadrant (octant) onto the remaining quadrants, to produce a fully rendered fluorescence intensity distribution in one quarter (one eighth) of the time necessary if each quadrant (octant) were rendered individually.

In a further effort to reduce unnecessary computations, the model assumed 100% transmission for a refracted ray, and 100% reflection for a total internally reflected ray. This assumption was considered to be valid on investigating the magnitudes of reflection and transmittance on a graph of incidence angle vs. transmittance and reflectance for a 1.33:1.42 refractive index interface.

6.4 Results

Results from the modelling work are presented in three sections. First, data from each of the 2D models are presented in polar plot form. The emission profile for the 3D ellipsoid model is presented as a 3D surface plot, with intensity $x = 0$, $y = 0$, and $z = 0$ cross-sectional slices. Finally, the radial emission data has been used to generate theoretical histograms and contour plots for comparison with experimental results from Chapter 5.

6.4.1 Two-Dimensional Model Geometries

Figure 6-4 shows polar fluorescence intensity plots (around the cell circumference) for each of the 2D cell geometries modeled. Each of the geometries displays an intensity profile which has a relatively constant intensity across the front face of the sperm head, with an increase to higher intensity values toward each end of the cell.

The rectangle model result displays a sharp intensity increase at approximately 20° from the vertical. This effect can be explained by considering the condition for total internal reflection to take place at the jet-cell interface and the square geometry at the end of the cell. The capped rectangle emission profile is similar in form to the rectangle result. In this instance, it is clear that the addition of semi-circular caps to the ends of the rectangle has smoothed the sharp intensity transition near the end of the uncapped cell. The 2D ellipse geometry again displays a uniform intensity profile around the flat side of the sperm. However, the intensity peak is narrower and taller than for the rectangular model. There is a considerable decrease in intensity in the direction 0° from the end of the cell, which is due to the geometry of the ellipsoid. As a ray which is totally internally reflected propagates toward the end of the cell, the narrow elliptical cell walls become increasingly tapered and the likelihood of the ray being transmitted is increased. Therefore, the ray will be refracted by a small angle which is defined by the cell-jet refractive index ratio. This draws the rays toward the two lobes evident in Figure 6-4C.

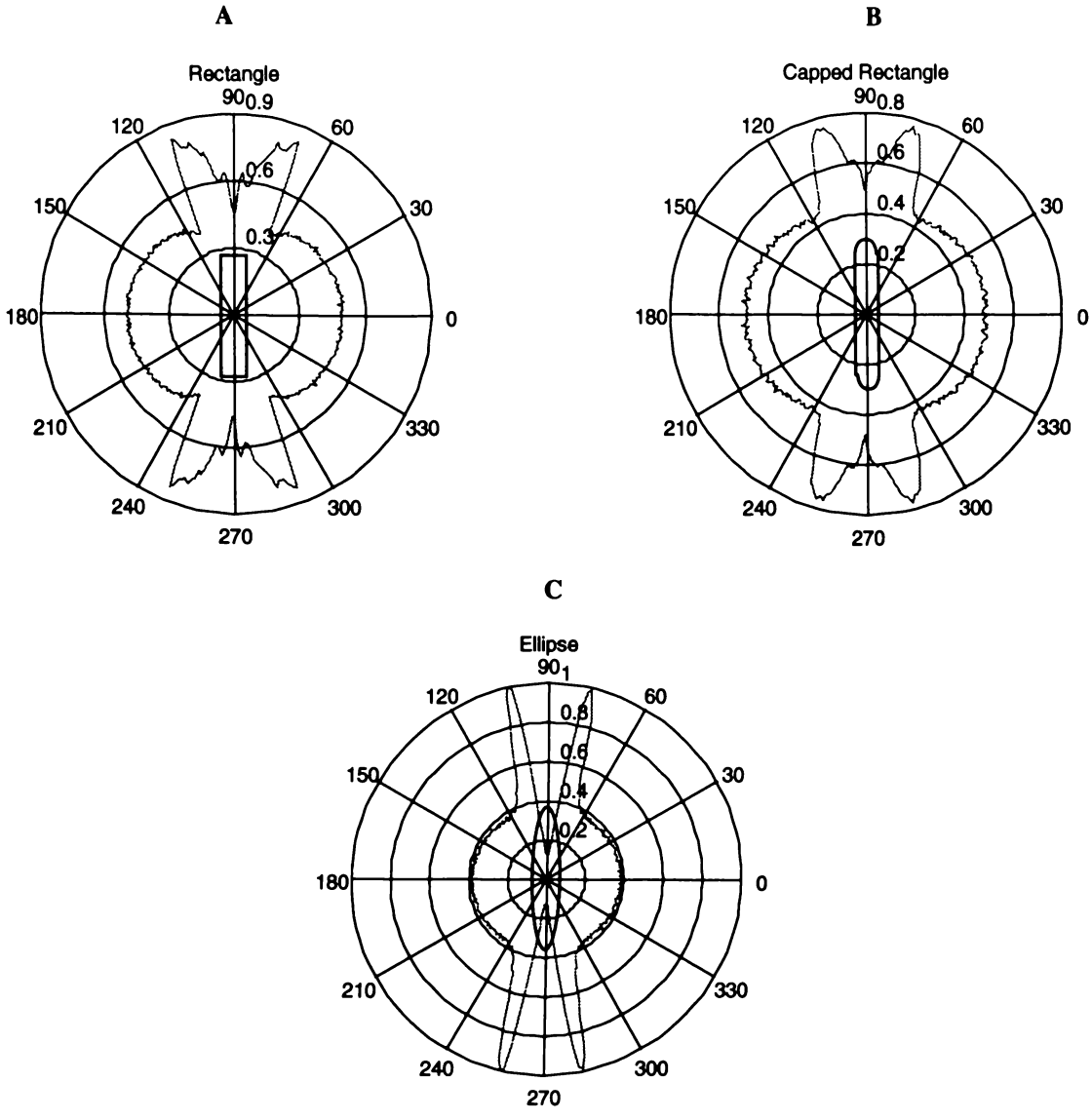

*Figure 6-4. Output fluorescence distribution for **A**: rectangle, **B**: capped rectangle, and **C**: ellipse geometries.*

6.4.2 Three-Dimensional Ellipsoid Geometry

Figure 6-5 displays the radial intensity result for the 3D ellipsoid geometry on a spherical polar plot. The intensity information emitted from the cell was collected in spherical coordinates. The matrix size required to store intensity over a 3D spherical area was restricted to 36 x 36 elements (10° square bins) to keep graphing of the results tractable. A near-spherical intensity profile exists out the flat face of the sperm head. Once more, there is a pair of intensity lobes that extend around the edge of the cell. These features can be seen more clearly if slices are taken through each of x, y and z planes (Figure 6-6).

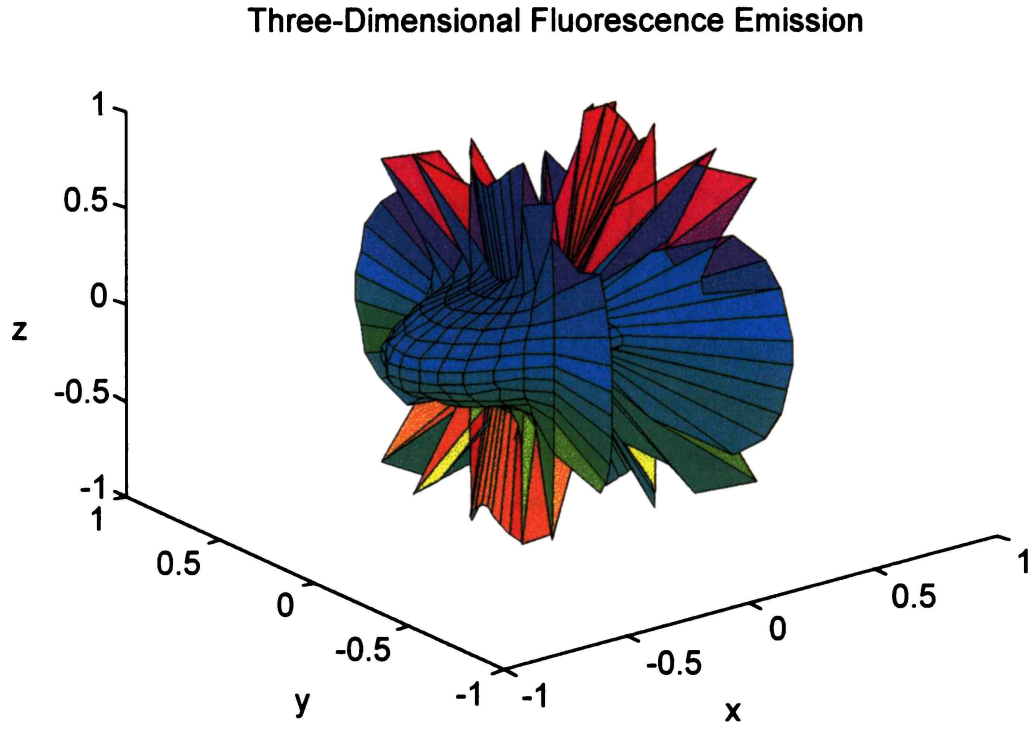

Figure 6-5. Modelled fluorescence intensity distribution for a 3D ellipsoid sperm cell. The direction of flow is along the z-axis.

General agreement exists between the 2D ellipse data and the 3D ellipsoid results for the $z = 0$ plane (around the flow axis which is into the page). For the $x = 0$ plane, which gives intensity information for a slice across the broadest dimension of the cell, a small amount of waveguiding is evident. For the $y = 0$ plane, which represents a vertical slice through the narrow section of the cell, there is no significant change in the intensity profile for angles less than ± 60° from the horizontal. Flow cytometers that utilise orthogonal optical geometries collect fluorescence from an angle of approximately ± 30°. Therefore, we propose that the 2D geometries we have modeled are adequate to approximate the fluorescence distribution that would be seen by an orthogonal optics detector. However, if a different collection geometry which collected a large proportion of light from other angles were to be modeled, the effects of this three-dimensional profile would have to be considered.

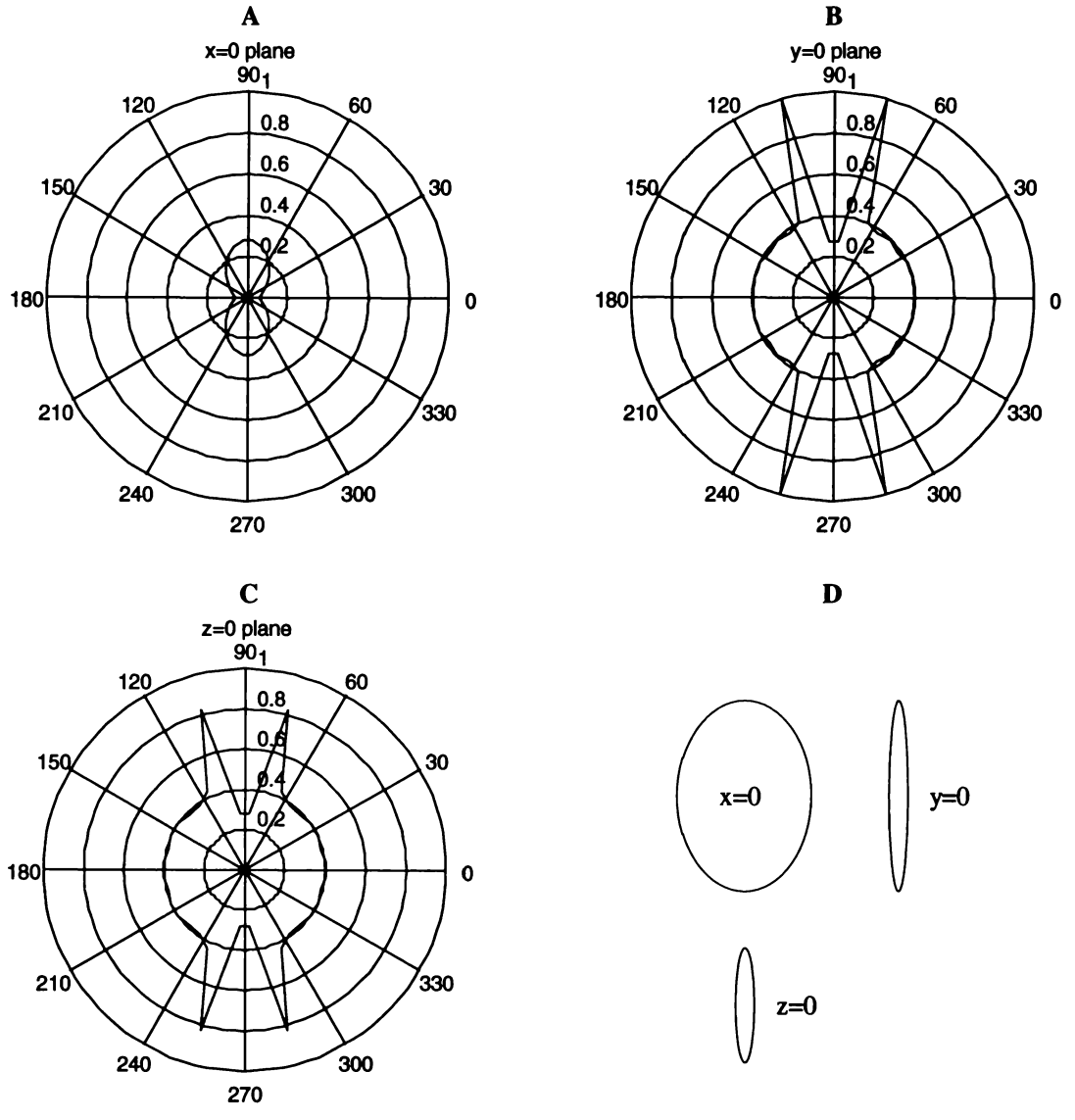

Figure 6-6. Intensity profile slices for 3D ellipsoid cell geometry showing A: x = 0 plane cross-section, B: y = 0 cross-section, and C: z = 0 cross-section. D: Cell orientation for each plane is illustrated.

6.4.3 Histograms and Contour Plots

The following models of the effect of cell orientation on illumination and fluorescence detection use the 2D ellipse geometry which was selected as most closely representing real sperm cells. The notation for cell angle θ, with respect to the laser and detectors is shown in Figure 6-7.

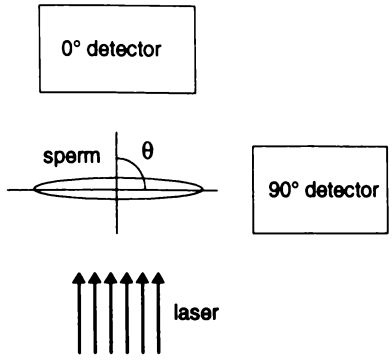

Figure 6-7. Illustration of cell orientation with respect to the laser, 0° and 90° detectors.

Figure 6-8 illustrates the sequence of steps that were carried out to obtain a fluorescence distribution for a sperm angle variation of 0° to 180° with respect to the laser beam axis. Cross-sectional area and transmittance curves (Figure 6-8A,B) show the effect of sperm orientation on proportionate light collection with respect to the laser beam axis. As expected, the cell presents a maximum collection area when it is oriented flat face toward the laser. The mean transmittance of light into the cell is also maximised when the incidence angle of light on the flat surface of the cell approaches the normal. The data of both 0° and 90° detector plots are identical. The profiles of Figures 6-8C and 6-8D show the combined result of cross-section C, transmittance T, and saturation constant k, in accordance with Equation (6-3). Fluorescence emission as a function of θ for each of the 0° and 90° detectors is illustrated in Figures 6-8E and 6-8F respectively. The 0° detector plot has been phase shifted along the sperm orientation axis to produce the 90° detector result. These curves illustrate the situation of orientation independent illumination of cells.

The intensity profiles of Figures 6-8G and 6-8H were generated by multiplying cell illumination effects (Figures 6-8C,D) by the emission profiles (Figures 6-8E,F), and show the situation of uni-directional cell illumination. In this situation a sperm cell that passes through the inspection point edge-toward the laser will collect less light and will therefore fluoresce by a lesser amount than a cell that passes with a flat face toward the laser.

Intensity histograms analogous to those measured by orthogonal flow cytometers can be generated from the data (Figures 6-8G,H) by assuming random cell orientations and using the data to estimate the probability density function for illumination. Contour plots can also be generated by plotting intensity values on the 90° detector. Similarly, the intensity histogram generated by using radial illumination and orthogonal detection (Chapter 5) and the associated contour plots can be generated from Figures 6-8E,F.

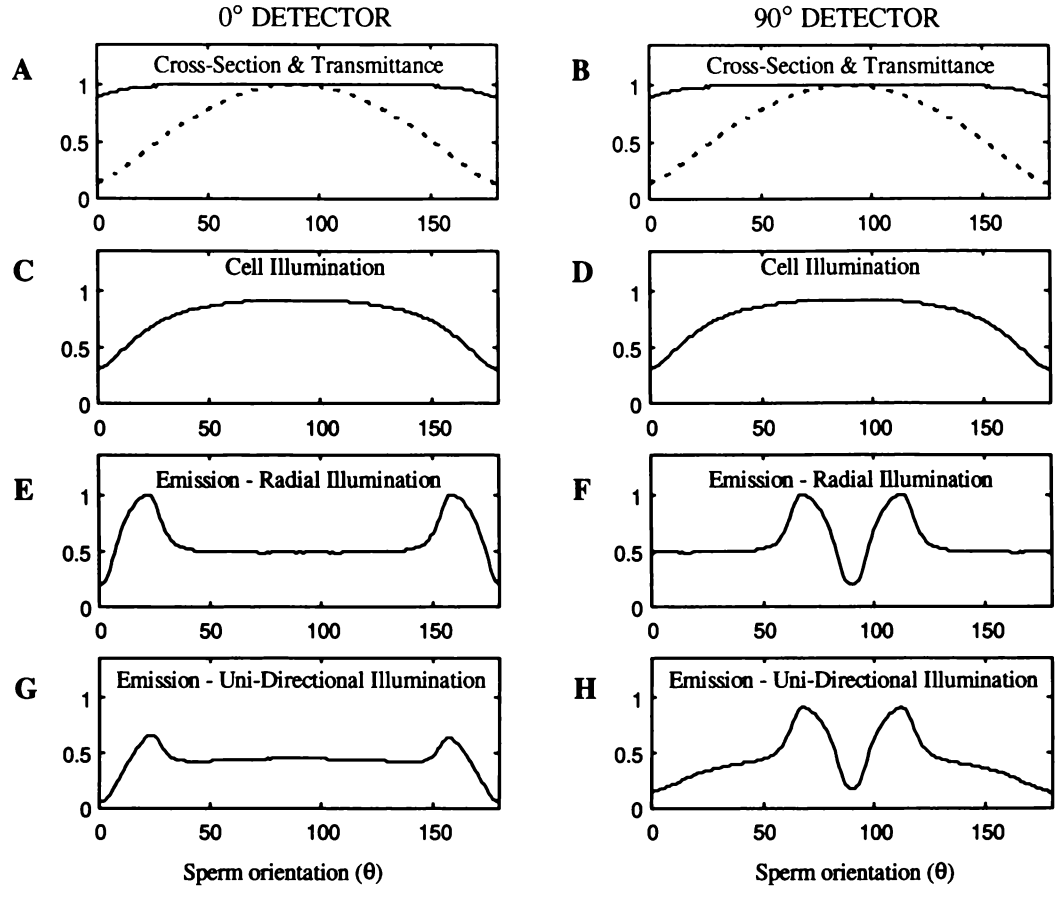

Figure 6-8. Series of plots that demonstrate the effect of each model component on the fluorescence collected at each of the 0° and 90° detectors as a function of sperm orientation about the flow axis. ***A,B:*** *Transmittance (solid line) and cross-sectional area presented to the excitation source (dashed line).* ***C,D:*** *Combined transmittance, cross-section and saturation curve.* ***E,F:*** *Emission profile produced for the 2D ellipse model.* ***G,H:*** *Combined emission profile for uni-directional illumination.*

Theoretical histograms and contour plots for both the radially symmetric, and uni-directional, illumination geometries are presented along with experimental data in Figures 6-9 and 6-10 respectively. Histograms for the 0° and 90° detectors were generated by binning the emission data (from Figures 6-8E to 6-8H) for a detector (bin) angle of 20°. Contour plots were generated from the data of Figures 6-8E and 6-8F by determining the 90° detector and 0° detector intensity for each value of θ. A narrow spacing of data points on the theoretical contour plot represents a large number of cells.

The 2D ellipse model produces identical 0° and 90° histograms with a large proportion of cells around channel 0.5 corresponding to sperm being flat face toward each detector, and a lateral extension to higher intensities for cells oriented edge toward the detector. This model shape also displays some fluorescence intensity data to the left of the main peak. This is generated by the intensity dip (between the lobes) that this model produced directly out the narrow edge of the cell (Section 6.4.1). The corresponding contour plot shows an L-shaped population which is consistent with the experimental data obtained for radially symmetric illumination and orthogonal fluorescence collection.

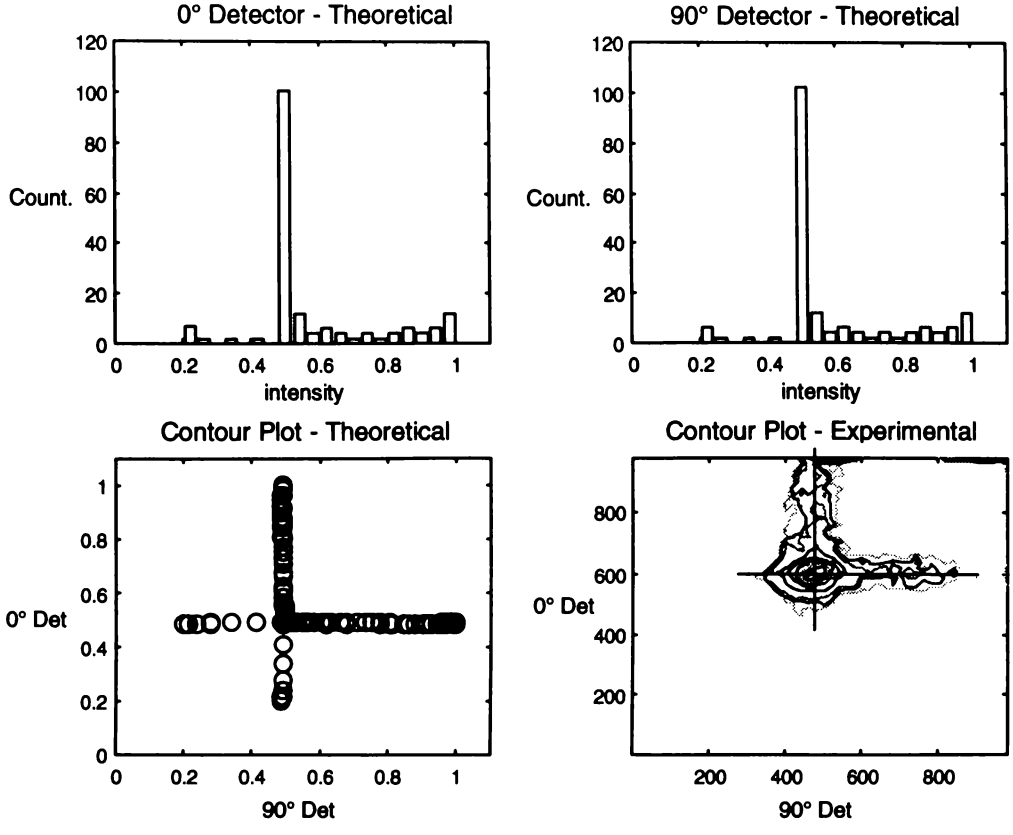

Figure 6-9. Model results and experimental data for radially symmetric illumination with orthogonal fluorescence detection. A narrow spacing between data points represents a high channel count.

Figure 6-10 shows 0° and 90° detector histograms generated for the unidirectional system. Both display the general form of a main population corresponding to sperm being oriented flat face toward each detector with a lateral extension to higher intensity values. The width of the 90° detector distribution is less than that of the 0° detector. This effect is illustrated in the theoretical uni-directional illumination contour plot. The contour plot generally displays the characteristic L-shape, where sperm oriented towards the forward and side detectors are positioned in the UL and LR regions respectively. However, there is an intensity drop-off in the LL region of the population. This drop-off is consistent with the experimentally observed effect.

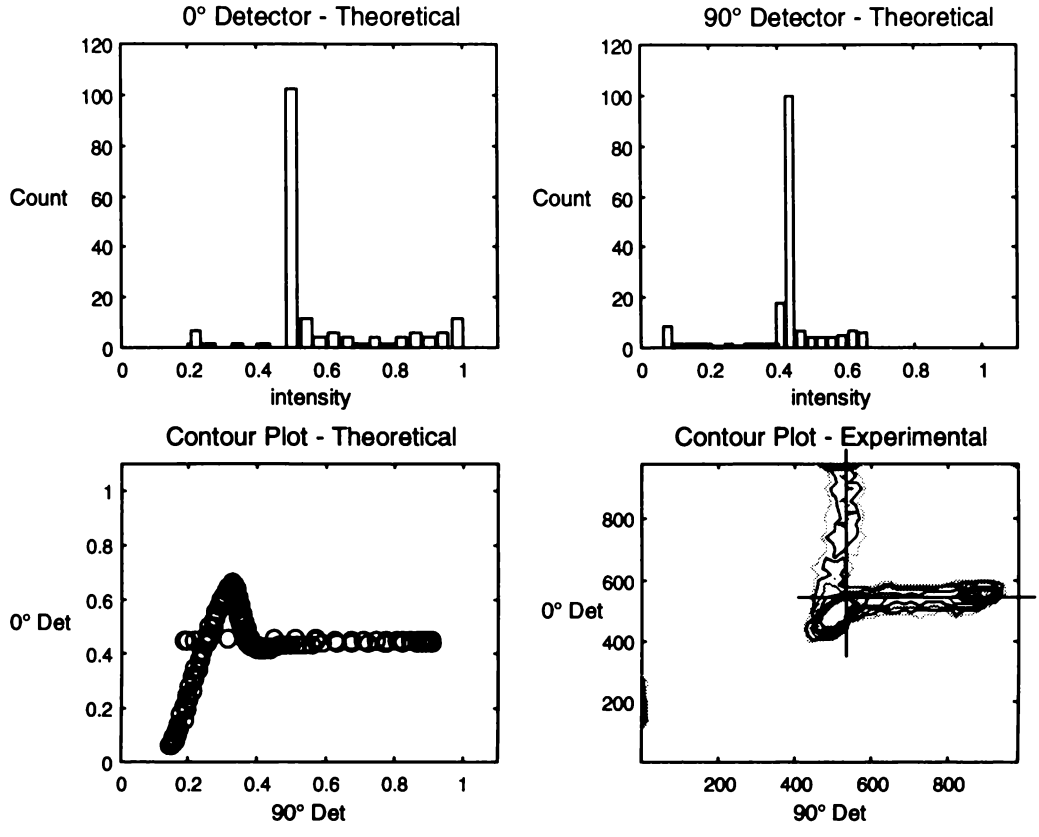

Figure 6-10. Model results for an orthogonal optics geometry showing theoretical histograms and a contour plot for comparison with experimental data.

These results support our hypothesis that varying cell orientation with respect to the excitation source in standard orthogonal geometry flow cytometers produces variations in fluorescence measurement. These variations become significant when the sperm cells are edge-toward both the excitation source and the forward detector. The implication of this effect to flow cytometers that operate with uni-directional cell illumination is that resolution may be reduced. In the case of sperm sexing, where it is necessary to measure a 3.9% difference in fluorescence intensity, this loss in resolution may ultimately limit the ability to resolve the X and Y populations outside of the LR window of the L-shaped population.

6.5 Other Optical Simulation Methods for a Sperm Cell

Two investigations were carried out to test and validate the assumptions of our geometric optics model. First, a scale-up experiment was carried out to test the validity of the geometric optics approach of waveguiding in a sperm cell whose dimensions approach the wavelength of fluorescence. This experiment was carried out in the microwave domain. Second, a calculation was performed to determine the likely number of propagation modes that a sperm cell, when contained within the sheath fluid of the jet, would support to further validate the assumptions of our geometric optics model.

6.5.1 Microwave Scale-Up

Usually, the assumptions of geometric optics hold provided the dimensions of the object that the light interacts with are much greater than the wavelength. The model that has been presented in this chapter assumes that simple geometric optics conditions apply. However, the dimensions of a sperm cell (1-10μm) are of the order of the optical wavelength (450nm). Therefore, the geometric optics assumptions of waveguiding may not be entirely valid.

This qualitative study was carried out in an attempt to verify the waveguiding properties of the sperm cell by uniformly scaling cell geometry and wavelength to the microwave domain. This scale-up allowed manageable cell orientation control while retaining the same wavelength to cell dimension ratio as for fluorescence in a sperm.

The sperm cell was represented by a sheet of perspex measuring 30cm x 30cm x 5cm (compare with 10μm x 4.5μm x 1μm for the bull sperm). The microwave emitter was a Gunn effect diode with a centre frequency of 10.5GHz (λ = 2.86cm). Therefore, a wavelength to cell thickness ratio of approximately 1:2 was maintained (as for the actual sperm thickness to fluorescence wavelength ratio). A Schottky barrier diode (sensitive to the frequency range 1GHz to 12GHz) was used for microwave detection. Measurements of field intensity from the microwave emitter were obtained over an angle of 180° at a radial distance of 2m from the source.

Results of the microwave intensity with and without the perspex slab are presented in Figure 6-11. The source produced a Gaussian-like intensity profile as a function of receiver angle. When the dielectric slab was put in place appreciable waveguiding was observed. This is illustrated by the narrow profile with a peak intensity that has not dropped significantly from the initial value. Much of the microwave energy was attenuated by reflection at the air-perspex interfaces. The results from this qualitative investigation support the use of geometric optics to model sperm fluorescence.

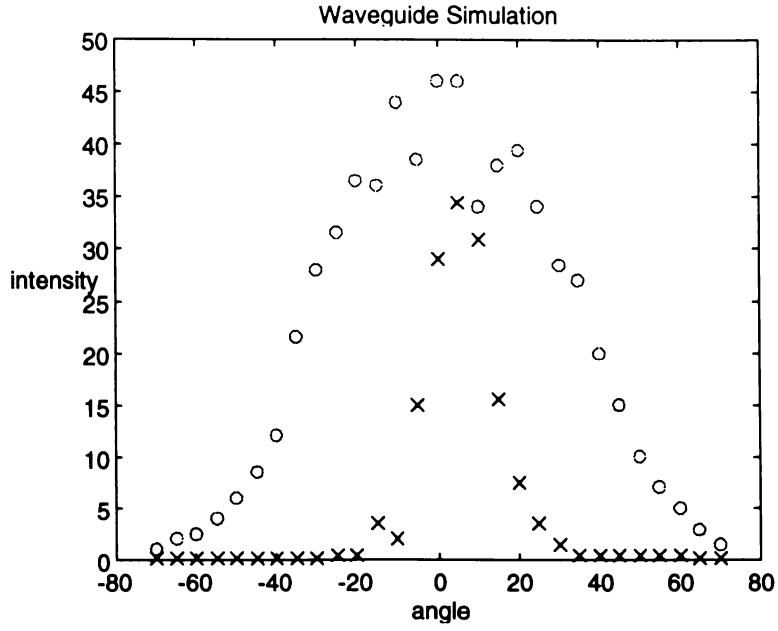

Figure 6-11. The radial field intensity distribution around a microwave emitter, without (o) and with (x), a dielectric slab in place.

6.5.2 Waveguide Model - Mode Propagation

If we consider the preferential fluorescence emission effects of a sperm cell by considering it to be a planar dielectric waveguide, then we can determine an approximate estimate for the effectiveness of total internal reflection in a sperm cell in terms of the number of modes such an element will support. For this analysis, the cell core n_1, of thickness d, is sandwiched between the sheath fluid cladding n_2, of the dielectric waveguide. The fluorescent rays produced from stain molecules within the cell are emitted at random locations and in random directions. Those light rays which strike the cell-jet interface at an incidence angle less than the critical angle (given by Equation (6-4)) are refracted out of the cell. The remaining rays, which exceed the critical angle, undergo multiple internal reflections down the cell-jet (core-cladding) boundaries without loss of power.

The waveguide modes can be determined by Maxwell's equations and the appropriate boundary conditions. These modes can also be obtained in terms of transverse electromagnetic (TEM) plane waves bouncing between the cell boundaries which is also a result of Maxwell's equations (Saleh and Teich, 1991). The number of transverse electric (TE) modes supported by the waveguide cell model can be determined from the smallest integer greater than M such that

$$M = \frac{\sin(90 - \theta_{crit})}{\lambda/2d}. \qquad (6\text{-}6)$$

Substituting the values θ_{crit} = 69.5°, λ = 450nm, d = 1μm into this expression for the cell waveguide yields M = 1.556. The cell thus supports two TE modes. A similar expression can be obtained for the transverse magnetic (TM) case which is found to support two modes also. This result supports the geometric optics approximations for waveguiding in a cell whose dimensions approach the wavelength of emission.

6.6 Discussion

A Monte-Carlo ray trace model has been devised to simulate the possible effect of fluorescence waveguiding inside sperm cells. This mathematical model was developed as a check on experimental results for sperm fluorescence.

With this model it has been possible to produce radial intensity distributions for a range of cell dimensions and refractive index values. The effects of variations in illumination and preferential scattering from the narrow edge of sperm heads can be seen. The angular intensity distributions predicted by the model have been transformed into histogram and contour plot forms for comparison with experimental data produced using flow cytometry.

The possible limitations of geometric optics due to the small dimensions of sperm compared to the wavelength of light have been discussed and further experimental work has been carried out to justify the assumptions in the model. An experiment was performed to increase the dimensions of a model cell and the wavelength into the microwave domain. Here, the ability of a planar dielectric material to act like a waveguide when its thickness approaches the wavelength of transmission was investigated and confirmed. Waveguiding effects in the model have also been discussed in terms of mode propagation in a dielectric.

The geometric optics model has been developed to determine the intensity distribution of fluorescence emission from sperm cells. This information has been useful in explaining the optical artifacts associated with the analysis of aspherical particles using flow cytometry.

7. Prospects for Sperm Sexing

The ultimate aim of the sperm sexing process is to sort sperm by DNA sex content with sufficient purity to enable gender preselection following fertilisation. The possibility of carrying out artificial insemination on cattle with sexed sperm is currently inhibited by the sort time required to produce the two to ten million sperm for successful fertilisation of each egg. Sex preselection is possible by *in vitro* fertilisation because this technique requires a much smaller number of sorted sperm for success. However, this method is laborious and is economic only for animals of high genetic value. The goal of the research for this thesis was to improve the economics of routine gender selection of domestic animals by developing a new optical configuration that could be used to differentiate and sort bovine sperm by sex at a faster rate, and with higher efficiency, than present flow cytometric techniques. In this chapter the performance of orthogonal optics is compared with radial optics results.

In Section 7.1 the method for setting gates to sort X and Y sperm based on intensity histogram data is outlined. Sorting performance of the orthogonal optics system is determined and compared with that of the radial optics in Section 7.2. In Section 7.3 the effect of CV broadening with increased sample to sheath differential pressure is investigated and possible sources of errors are suggested. The potential effect of laser noise in our experimental results is discussed in Section 7.4. Suggestions for future work on the radial optics are presented in Section 7.5.

7.1 Background

The current technique for high resolution analysis of bull sperm is outlined in Chapter 3. In this section the analysis is extended to the positioning of sort gates for the sperm, which can, within known confidence levels, be reliably separated into X and Y fractions using the electrostatic sort function of the flow cytometer.

A stylised fluorescence intensity histogram for a population of X- and Y-chromosome bearing sperm is shown in Figure 7-1. A double peaked population is evident in the figure, which, using conventional least squares methods, is fitted with a pair of Gaussian curves. The amplitudes and widths of each curve are constrained to be identical, and consistent with peak separations measured by others. The relative width of each Gaussian, and therefore the existence of an X-Y split or gap between the curves, is dependent on statistical fluctuations in measurement. These variations can be caused by instrument errors such as laser or electronic noise, fluidic instability, or detection constraints of the optical geometry. Statistical variation can also be caused by actual cell differences due to inconsistent stain uptake, or, by inherent cellular features. In the analysis that follows, the sort gate positions are set (somewhat arbitrarily) at the peaks of each of the X and Y peaks as illustrated in Figure 7-1. The positioning of the gates at the peaks is not necessarily the best for maximum purity, or sort rates. However, these gate positions are used for consistency with published results in the analysis that follows.

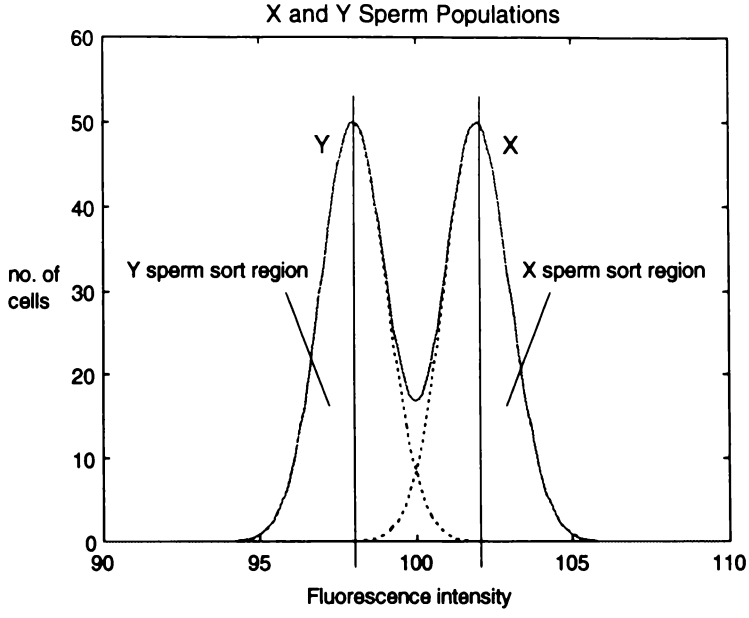

Figure 7-1. A stylised illustration of a pair of Gaussian profiles to represent Y and X sperm populations separated by 3.9% intensity.

In routine sorting it is important to achieve a low population CV (i.e. a tight or narrow curve) so that the overlap of the X and Y populations is minimised. Figure 7-2 illustrates the effect of CV on overlap for a pair of Gaussian curves with means separated by 3.9% and for four different CVs. This data was generated for a population of 10 000 sperm with an X to Y ratio of 1:1. Therefore, the area under the graph is equal in each plot. From this figure it can be seen that there is significant overlap for CVs exceeding 1.5%.

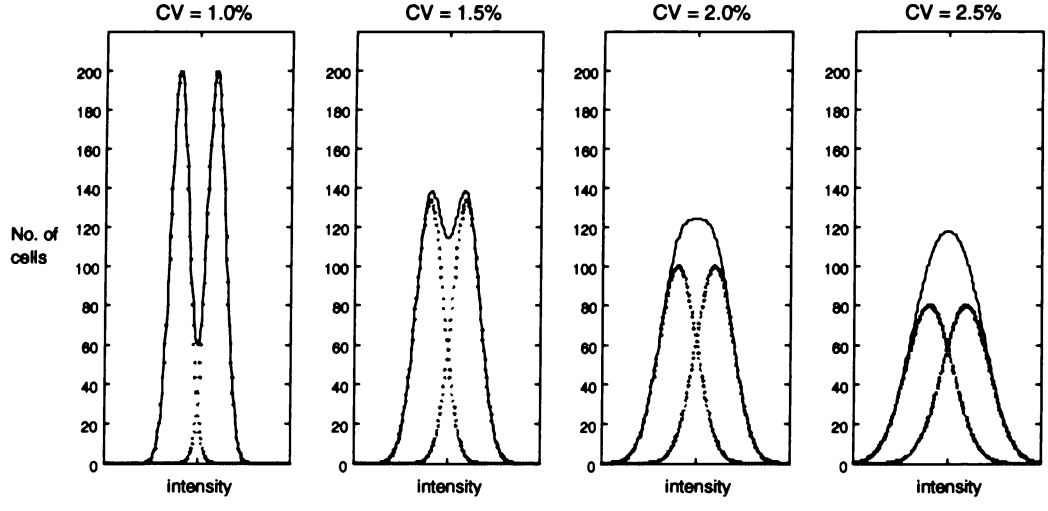

Figure 7-2. Theoretical distributions obtained by summing two equal Gaussian distributions with means separated by 3.9%. The total number of cells in each curve is equal.

7.2 Sort Performance Orthogonal vs. Radial Optics

This section compares levels of sort purity, sort rate, and sample waste for the orthogonal and radial optics. Experimental histogram data from Chapter 5 were utilised for this study and included a gated (oriented) population of sperm measured on the orthogonal system at an event rate of 1000 cells s^{-1}, and radial optics results for event rates of 200 cells s^{-1} and 1000 cells s^{-1}.

For each of the histograms, a double Gaussian curve fit routine was used to determine the amplitude, mean and standard deviation for a pair of theoretical X and Y sperm curves separated by 3.9% in intensity. These graphs are presented in Figure 7-3. For the orthogonal optics data, the gated (33.4%) fraction of sperm produced a population with a distinct X-Y split. However, when all of the data points were included, the curve fit was poor around the peaks as the Gaussian curves were broadened to fit the non-zero shoulders in the data bordering the peaks. To obtain good agreement between the double Gaussian fit and the experimental data, the curve fit routine was applied only to the data within a window defined by the full width half maximum (FWHM) of the peak. This results in a disparity between the position of the experimental points on the graph, and the fitted curve outside the FWHM window.

A FWHM window was also used for generating the radial optics curves. There is an increased number of cells (along the *y*-axis) of the graph for an event rate of 200 cells s^{-1} since there is no gating of cells according to orientation. An X-Y split was not evident with this sperm population and this resulted in greater X-Y curve overlap than for the orthogonal data set.

At an increased sample to sheath differential and therefore event rate of 1000 cells s^{-1}, the radial optics profile shows the effect of CV broadening (discussed in Chapter 5) on X-Y curve overlap. This graph gives further demonstration to the importance of low CV to obtain high sort purity. Once more, this data has not been gated by orientation.

Several sort performance parameters were determined for each of the data sets in Figure 7-3. These parameters included sample waste due to orientation gating, sort purity, and output sort rate of correctly sexed cells. Results from this analysis are presented in Table 7-1. A description of each performance parameter in the table follows.

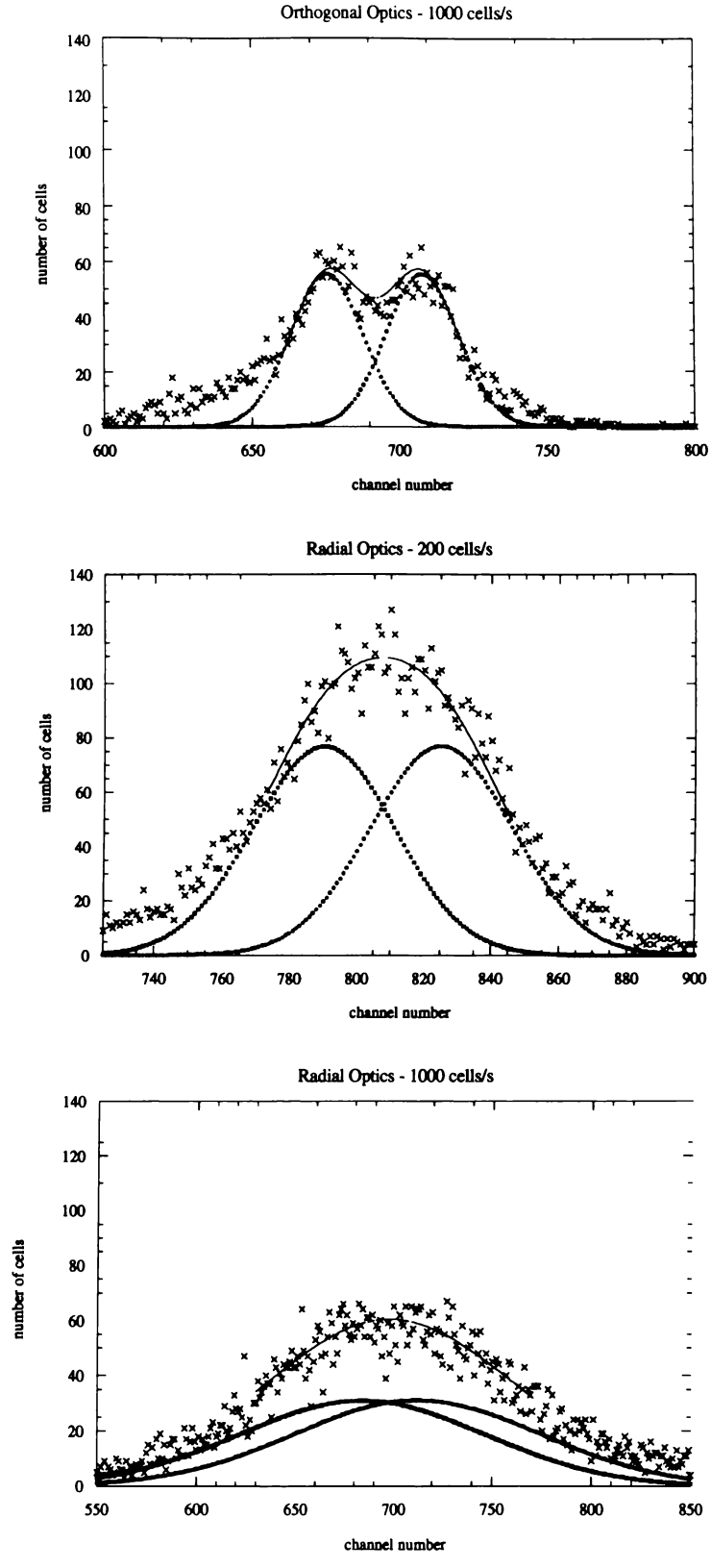

Figure 7-3. Experimental data and Gaussian curve fits for each of the optical configurations showing theoretical Y and X sperm populations and a summed result.

The input event rate was taken as the value displayed on the flow cytometer console during cell analysis and is the rate at which cells passing the inspection point cause photomultiplier voltages to exceed a prescribed minimum threshold. This parameter is proportional to sample to sheath differential pressure since cell concentration was maintained at 10^6 ml^{-1} throughout our experiments. The CV was calculated as the ratio of the standard deviation to the mean of the fitted Gaussian. Values for sample waste due to orientation gating were obtained from analysis of flow rate vs. number of cells oriented (Chapter 5). Radial optics sample waste is set to 0% since this system does not use cell orientation gating. This figure does not include sample waste due to cells falling outside the sort gate which is equivalent for both optical systems (50% because of the prescribed method used for X and Y gate settings).

It is important that the purity of a sorted fraction of X or Y sperm be sufficient to successfully (i.e. statistically) predetermine the sex of offspring. Sort purity was determined from the theoretical ratio of Y:X cells sorted. The ultimate goal of the sperm sexing process is to sort sperm at maximum possible rates (within the limits of damage and with minimum sample waste), using flow sorting electrostatic technology. An output sort rate of desired sperm cells was determined for each input event rate. For this calculation the sort process is assumed free of errors due to coincidence, incorrect charging, or unreliable droplet capture. The sort rate value does not include unwanted cells and has a theoretical maximum of half of the event rate, due to the method used to set gating values.

Table 7-1. Current and projected sort rates of X and Y bearing sperm using a flow cytometer fitted with orthogonal and radial optics.

Optical system	Input event rate (cells s^{-1})	CV (%)	Sample waste due to orientation gating (%)	Sort purity (%)	Output sort rate (Y+X cells s^{-1})
Orthogonal	200	3.1*	58.8	99.2	42
	1000	3.1	66.6	99.2	164
	3000	3.1*	78.4	99.2	324
Radial	200	5.5	0	83.8	98
	1000	8.6	0	60.5	470

* For the orthogonal optics, the CV of 3.1% obtained at the event rate of 1000 cells s^{-1} was assumed constant over the range 200 cells s^{-1} to 3000 cells s^{-1}

Table 7-1 emphasises that two factors are central to the comparison of sort rate which may be achieved using orthogonal and radial optics. The first factor is the waste due to orientation gating and the second is the waste due to sort gating.

The primary advantage of the radial optics system is that there are no losses due to orientation gating, whereas the orthogonal optics system suffers increasing orientation gating losses as sample rate is increased. However, although data were not available to demonstrate it for the orthogonal system, both systems suffer an increase in CV as sample rate is increased. It is thought that this may be because of an increased variation of cell location within the sample stream due to a lower differential between sample

and sheath flow rates. Variations in particle location can be partly reduced by broadening the illumination and detection foci, which is already practiced in orthogonal systems. Potential for improving this aspect for the radial optics design is discussed in Section 7.5.

The sort purity of the orthogonal system suggests that a population of X or Y sperm could be separated from populations of near 100% enrichment. In practice, this level of purity is difficult to achieve.

CVs must ultimately be reduced if the radial optics are to outperform the orthogonal optics system. Radial optics analysis of chinchilla sperm (Chapter 5) yielded fluorescence histograms with clear 7.5% X-Y splits and CVs that matched orthogonal optics results, and did not exhibit the CV broadening that was present for the bull sperm. If the effect of CV broadening with increased sample to sheath differential pressures can be overcome, radial optics may provide improved performance over orthogonal systems.

7.3 CV Broadening with Increased Sample to Sheath Pressure

During experiments which were performed on bull sperm, it was found that increased sample to differential pressure had a considerable effect on population CV. While the histogram still displayed a uni-modal population of sperm demonstrating orientation independent measurement, the population broadened considerably with increasing sample to sheath differential pressure. Figure 7-3 demonstrates histograms for two flow rate settings of 200 cells s^{-1} and 2000 cells s^{-1}. Also displayed is a plot of CV vs. input event rate, which is related to pressure differential, for the range 50 cells s^{-1} to 3000 cells s^{-1}.

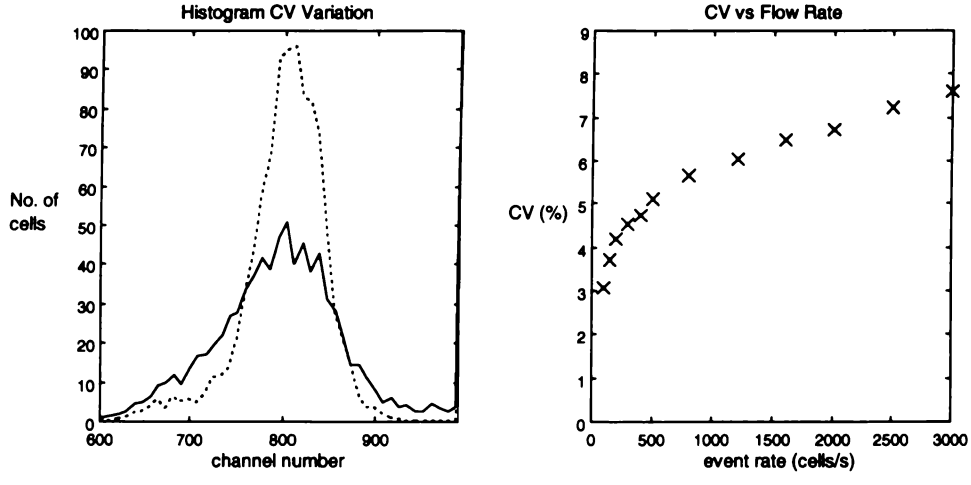

Figure 7-4. The effect of sample to sheath differential pressure on CV for bull sperm. A: A pair of histogram results for flow rates of 200 cells s^{-1} and 2000 cells s^{-1}. B: Graph of CV vs. event rate.

The effect of increased CV with increased sample to sheath differential pressure was inherent to bull sperm. Analysis of chinchilla sperm, which are smaller than bull sperm, did not produce the same effect. There are several factors of the design and operation of the radial optics which may have combined to produce the increased bull sperm population CVs.

The effective focal waist of the radial optics is narrower than that of the orthogonal system (Chapter 4). Therefore, in its present configuration, this system may be sensitive to positional variations of cells through the excitation focus. Fluidic instabilities caused by the nozzle, or by the long sample and sheath fluid lines that were used for the radial optics may also have contributed to CV broadening.

7.4 Instrument Noise

The experimentation for Chapter 5 was carried out on a comparative basis between the orthogonal and radial optical configurations and utilised the same excitation source, fluidics, and electronics. To obtain information about the relative resolution capabilities of each optical geometry, these tests would have to be repeated using a system with minimal fluidic instability, and electronics and an excitation source with optimally low noise. If such a study were carried out, we propose that the CV values would be improved considerably across all particle types measured, and that this would facilitate better X-Y sperm resolution capabilities for high purity sperm sorting.

Since conducting our experimentation, we have learnt that it is possible to obtain CVs approaching the value of 0.5 for the fluorescent calibration standard we used to determine the baseline CV for both instruments (Rens, 1997). The CVs obtained by us for these microspheres on both optical configurations (2.2% and 2.3% for the radial and orthogonal systems respectively) are much higher than this value. We suspect high laser output noise was responsible for the disparity between our CV measurements and those of others. The laser tube had a high number of operation hours which resulted in an increase current levels to obtain sufficient UV power for cell excitation.

One further source of noise on the radial optics may be due to the materials used for the optical components. The BK7 glass used for manufacture of the axicon is not ideal for UV transmission due to its high absorption and fluorescence (discussed in Chapter 4). Thus, the radial optics results may have been contaminated with background noise from the axicon.

7.5 Future Work

In future implementations of a radial optics configuration there are several possible improvements that may benefit the operation, resolution, or general performance of the system. If these implementations were successful they would undoubtedly provide an optical geometry which is useful for sperm sexing and other applications that require high speed analysis or sorting of aspherical cells or particles with minimal sample waste.

In its present configuration, measurement of large cells using the radial optics has been found to be sensitive to positional variations of cell trajectories through the inspection point. Further work is required to determine how significant this positional variation is. Improvements to the fluidic system should include the design or sourcing of a nozzle which provides increased fluidic focusing, and stable alignment of cells to reduce cell position variations. Investigations should also be carried out to shorten sample and

sheath lines to reduce possible fluidic pressure instabilities and blockages. To further reduce cell illumination variations, additional work should be carried out to integrate other optical components which can be used to laterally broaden the radial focus.

To increase the illumination and collection efficiencies of the system, UV grade optical components should be implemented into the design. This will reduce possible background fluorescence from optical components and may facilitate the introduction of a low powered UV source.

7.6 Discussion

In this chapter the technique for gating and sorting X and Y fractions of bull sperm has been described. The method of fitting a Gaussian curve to the data, and the operational characteristics of sort purity and sort waste and rate, have also been outlined. The performance of both the orthogonal and radial optics systems has also been evaluated. From this analysis we can conclude improvements are required if this system is to sort X and Y bull sperm at a rate and purity which approaches that of the orthogonal system. Sample waste is significantly reduced for the radial system since all the sperm are analysed, which is in contrast to the orthogonal system where only a gated, appropriately oriented sub-population of cells can be reliably measured and sorted.

The effect of CV broadening for the analysis of bull sperm has been investigated and several possible causes of this problem have been suggested. We propose that the main reason for this CV broadening effect (which is not seen for smaller species of sperm such as chinchilla sperm) is due to the relatively large size of the bull sperm compared to the radial optics focus and nozzle, which is coupled with poor hydrodynamic focusing of the sample within the core region of the jet for high sample to sheath differential pressures. In the long term, investigations should be carried out to improve the fluidic focusing of the nozzle. In addition, a lateral broadening of the radial focus in keeping with the investigations of Chapter 4 may provide an optical solution to CV broadening with increased sample to sheath differential.

It is suspected that the low overall sperm sorting performance of both optical systems compared to results published by others may have been because the laser that was used for this experimentation was inherently noisy. However, the analyses were performed on a comparative basis between optical geometries so that qualitative measurements could be made for each system.

The radially symmetric illumination and detection of cells provides a method for measurement of cellular fluorescence that is insensitive to cell orientation and has the advantage of low sample waste. With the above-mentioned improvements in mind, it may be possible to reduce the CV broadening problem to a level where analysis rates can be increased without loss of DNA measurement resolution. Thus, sort rates may be increased to provide a fast and efficient method for separating sperm by sex.

8. Conclusion

A successful technique for commercial gender preselection in cattle is reliant on the development of a fast and efficient method for sorting sperm according to sex chromosome DNA content. Flow cytometry can be used to differentiate and sort cattle sperm by sex. However, present analysis and sort rates are limited by constraints of the optical configurations they employ. Flow cytometers which use orthogonal illumination and collection geometries are inherently susceptible to optical artifacts of measurement for flat and aspherical particles such as bull sperm.

A new optical configuration for the flow cytometric analysis of aspherical cells has been presented. This geometry provides 360° radial illumination and orientation-independent fluorescence collection of a specimen under analysis. The design and operation of this system has been compared to that of an orthogonal flow cytometer for the analysis of several particle and cell types. The radial optics provide equivalent baseline CVs to the orthogonal system for calibration microspheres. Analysis of flat and aspherical particles such as chicken red blood cells and spermatozoa from several mammalian species clearly indicates that the radial optics system provides an orientation-independent optical measurement system.

Radial optics measurements on chinchilla sperm DNA content produce clear X- and Y-chromosome bearing populations with a 7.5% split which is consistent with published results. In contrast, orthogonal optics require orientation monitoring and gating of cells (that are considered to be appropriately oriented) for accurate DNA analysis. Radial optics analysis of bull sperm, which in an orthogonal optics system give rise to extreme optical artifacts of measurement, has at low sample to sheath differential pressures, produced CVs for the entire population matching those achieved by orthogonal optical systems for only an orientation gated fraction of the sample. At higher sample to sheath differential pressures the histogram populations retain a uni-modal peak, suggesting continued orientation independent fluorescence collection. However, there is a noticeable increase in CV as sample to sheath differential pressures are increased. This effect has been attributed to a combination of poor fluidic focusing, and the narrow radial focus of the radial optics design. Cells which do not pass directly through the centre of the flow axis may be subjected to a lower illumination intensity causing their fluorescence to be measured with insufficient resolution to provide clearly resolved X and Y sperm populations.

Historically, efforts to overcome the optical artifacts of measuring bull sperm have concentrated on fixing the cell orientation with respect to detector position. In our experimentation, we have considered the possible effect of cell orientation with respect to illumination and therefore fluorescence. The radial optics were modified to perform orientation independent cell illumination (light delivery) while simulating the orthogonal collection geometry of a conventional flow cytometer by blocking part of the paraboloidal reflector path. Results from this study suggested that there is a significant dependence of cellular

fluorescence on cell orientation with respect to the excitation source. Results from a Monte-Carlo ray trace model have confirmed this.

The prospects for using a new optical geometry for sperm sexing are largely dependent on operational factors such as sort rate, purity, and waste. We have investigated these prospects by comparing the operational characteristics of a conventional system with the radial optics. Further reductions in CV will be necessary if this system is to sort X and Y bull sperm at a rate and purity which approaches that of the orthogonal system. At current levels of efficiency this system provides a means for sorting sperm with low sample waste. Initial attempts to reduce cell to cell illumination at the inspection point by laterally broadening the focus have been successful. Further work is required to establish whether these modifications will be adequate to enable increased throughput of bull sperm. In addition, for future implementations of the radial optics, it is hoped that fluidic effects on CV may be minimised by using a more efficient flow chamber, and by using shorter sample line tubing.

In our analysis of a calibration standard, it was found that the base-line CV for the FACStar we used was considerably more than expected, possibly because of laser noise. If this problem were overcome (with a new laser), CVs may further decrease to provide better X-Y resolution and sort purity.

If UV grade optical components are integrated into the radial design, the high collection efficiency of the system may enable low powered UV sources to be used for cell excitation. The benefits of this are two-fold. Expenses associated with the type of UV source required are reduced, as is the potential for genetic damage of sperm cells due to UV irradiation.

The radially symmetric optics we have described can be used to overcome the optical artifacts which decrease the accuracy of optical measurements on aspherical cells. With the addition of electrostatic sort capability, this system can provide the high speed sort rates of conventional jet in air flow cytometers. If the fluidic and optical problems that presently limit low CV analysis at high event rates can be overcome, this optical configuration may provide a means for increasing throughput and accuracy for sperm sexing and other applications which require high resolution measurement and sorting of aspherical particles or cells.

9. References

Adimoelja FXA: *Sephadex Gel for Sex Preselection.* In: *New Horizons in Sperm Cell Research.* Mohri H (ed), Gordon and Breach Science Publishers, New York, 491-499, 1987.

Amann RP, Seidel GE (eds): *Prospects for Sexing Mammalian Sperm.* Boulder, Colorado: Colorado Associated University Press, 1982.

Baker FN, Bouters RA, Salisbury GW: *Optical Density Profiles in Feulgen-Stained Bovine Spermatozoan Nuclei.* J Dairy Science, 44:1104-1105, 1962.

Baker FN, Salisbury GW: *Nuclear Size of Live and Dead Bovine Spermatozoa.* Nature 197:820, 1963.

Beal WE, White LM, Garner DL: *Sex Ratio After Insemination of Bovine Spermatozoa Isolated Using a Bovine Serum Albumin Gradient.* J Animal Science 58:1432-1436, 1984.

Beaumont S: personal communication, AgResearch, Hamilton, New Zealand, 1997.

Bernie T, Hutcheon JM: *A Photoelectric Particle Counter for Use in the Sieve Range.* J Sci Instr 34:196-200, 1957.

Bhattacharya BC: *Guide to Pre-Arranging the Sex of Offspring.* Ralston, Nebraska: Action Press, 1977.

Bonner WA, Hulett HR, Sweet RG, Herzenberg LA: *Fluorescence Activated Cell Sorting.* Rev Sci Instr 43:404-409, 1972.

Bonner WA, Sweet RG, Hulett HR: *Particle Sorting Method and Apparatus.* US Patent 3 826 364, 1972.

Chandler JE, Tirado V, Adkinson RW: *Videomicroscopic Comparison of Bull Sperm and Leukocyte Chromosome Areas as Related to Gender.* J Dairy Science 73:2129-2135, 1990.

Coulter WH: *High Speed Automatic Blood Cell Counter and Cell Size Analyser.* Proceedings of the National Electronics Conference 12:1034-1042, 1956.

Cran DG, Johnson LA, Miller NGA, Cochrane D, Polge C: *Production of Bovine Calves Following Separation of X- and Y-Chromosome Bearing Sperm and In Vitro Fertilisation.* The Veterinary Record 9:40-41, 1993.

CRC handbook of Chemistry and Physics (55th ed) CRC Press, Inc., Ohio, 1975.

Crosland-Tayor PJ: *A Device for Counting Small Particles Suspended in a Fluid Through a Tube.* Nature 171:37-38, 1953.

Dean PN, Pinkel D, Mendelsohn ML: *Hydrodynamic Orientation of Sperm Heads for Flow Cytometry.* Biophys J 23:7-13, 1978.

Dittrich W, Göhde H: *Automatic Measuring and Counting Device for Particles in a Dispersion.* British Patent 1 300 585, 1968.

Dresser DW, Keeler KD: *Sorting Living Spermatozoa.* UK Patent Application GB 2 145 112A, 1985.

Ericsson RJ, Langevin CN, Nishino M: *Isolation of Fractions Rich in Human Y sperm.* Nature 246:421-424, 1973.

Fulwyler MJ: *Electronic Separation of Biological Cells by Volume.* Science 150:910-911, 1965.

Garner DL, Gledhill BL, Pinkel D, Lake S, Stephenson D, Van Dilla MA, Johnson LA: *Quantification of the X- and Y-Chromosome Bearing Spermatozoa of Domestic Animals by Flow Cytometry.* Biology of Reproduction 28:312-321, 1983.

Gledhill BL, Lake S, Steinmetz LL, Gray JW, Crawford JR, Dean PN, Van Dilla MA: *Flow Microfluorometric Analysis of Sperm DNA Content: Effect of Cell Shape on the Fluorescence Distribution.* J Cell Physiol 87:367-376, 1976.

Gledhill BL: *Selection and Separation of X- and Y- Chromosome-Bearing Mammalian Sperm.* Gamete Research 20:377-395, 1988.

Göhde W: *Automation of Flow Cytometry by Use of the Impulse Microphotometer.* In: Thaer AA, Sernetz M (eds): *Fluorescence Techniques in Cell Biology.* Springer-Verlag, Berlin, 79-88, 1973.

Göhde H, Schumann J: *Fluidic Cell Sorter.* European Patent EP 0177.718, 1987.

Gurnsey MP, Arlotto T, Beaumont S, Weilert L: *The Effect of Freezing on Viability of Bovine Sperm Sorted by Flow Cytometry.* Animal Reproduction Science, In Press.

Heavens OS, Ditchburn RW: *Insight into Optics.* John Wiley & Sons, Chichester, 1991

Jafar SI, Flint APF: *Sex Selection in Mammals: A Review.* Theriogenology 40:191-200, 1996.

Johnson LA, Pinkel D: *Modification of a Laser-Based Flow Cytometer for High Resolution DNA Analysis of Mammalian Spermatozoa.* Cytometry 7:268-273, 1986.

Johnson LA, Flook JP, Look MV, Pinkel D: *Flow Sorting of X and Y Chromosome-Bearing Spermatozoa Into Two Populations.* Gamete Research 16:1-9, 1987a.

Johnson LA, Flook JP, Look MV: *Flow Cytometry of X and Y Chromosome-Bearing Sperm for DNA Using an Improved Preparation Method and Staining With Hoechst 33342.* Gamete Research 17:203-212, 1987b.

Johnson LA, Clarke RN: *Flow Sorting of X and Y Chromosome-Bearing Mammalian Sperm: Activation and Pronuclear Development of Sorted Bull, Boar, and Ram Sperm Microinjected Into Hamster Oocytes.* Gamete Research 21:335-343, 1988.

Johnson LA, Flook JP, Hawk HW: *Sex Preselection in Rabbits: Live Births from X and Y Sperm separated by DNA and Cell Sorting.* Biology of Reproduction 41:199-203, 1989.

Johnson LA: *Gender Preselection in Domestic Animals Using Flow Cytometrically Sorted Sperm.* J Animal Science 70:8-18, 1992a.

Johnson LA: *Method to Preselect the Sex of Offspring.* United States Patent US 005 135 759A, 1992b.

Johnson LA: *Sex Preselection by Flow Cytometric Separation of X and Y Chromosome-Bearing Sperm Based on DNA Difference: A Review.* Reprod Fertil Dev 7:893-903, 1995.

Kachel V, Kordwig E, Glossner E: *Uniform Lateral Orientation, Caused by Flow Forces, of Flat Particles in Flow-Through Systems.* J Histochem Cytochem, 25:774-780, 1977.

Kachel V, Fellner-Feldegg H, Menke E: *Hydrodynamic Properties of Flow Cytometry Instruments.* In Melamed MR, Lindmo T, Mendelsohn ML (eds): *Flow Cytometry and Sorting.* Second Edition, Wiley-Liss, New York, 27-80, 1991.

Kamentsky LA, Melamed MR: *Spectophotometric Cell Sorter.* Science 156:1364-1365, 1967.

Kamentsky LA, Melamed MR: *Instrumentation for Automated Examination of Cellular Specimens.* IEEE 57:2007-2016, 1969.

Kaneko S, Iizuka R, Oshiro S, Nakajima H, Osho S, Mohri H: *Separation of Human X- and Y-Bearing Sperm Using Free-Flow Electrophoresis.* Proc Japn Acad 59B:276-279, 1983.

Kissane RJ, Tobey RA, Crissman HA: *Detailed FCM and Cell Sorting Studies of Dye-Binding Kinetics, Viability and Cell Growth of Cells following DNA Staining with Hoechst 33342.* Cell Tissue Kinetics 15:105, 1982.

Laufer N, May JY, Segal S, Grover NB: *Size of Rat Spermatozoa During Maturation Along the Epididymis.* Arch Androl 3:293-299, 1979.

Levin RJ: *Human Sex Preselection.* Oxford Review of Reproductive Biology 9:161-191, 1987.

Levinson G, Coulam, CB, Spence WC, Sherins J, Schulman JD: *Recent Advances in Reproductive Genetic Technologies.* BioTechnology 13:968-973, 1995.

McLeod JH: *The axicon: A New Type of Optical Element.* J Optical Society of America 44:592-597, 1954.

Meistrich M: *Potential and Limitations of Physical Methods for Separation of Sperm Bearing an X- or Y-Chromosome.* In: Amann and Seidel, 143-163, 1982.

Melamed MR, Lindo T, Mendelsohn ML (eds): *Flow Cytometry and Sorting.* Wiley-Liss, New York, 1991.

Melles Griot, *Optics Guide 5.* Irvine, CA, 1990.

Métézeau P, Cotinot C, Colas G, Azoulay M, Kiefer H, Goldberg ME, Kirszenbaum M: *Improvement of Flow Cytometry Analysis and Sorting of Bull Spermatozoa by Optical Monitoring of Cell Orientation as Evaluated by DNA Specific Probing.* Mol Reprod Dev 30:250-257, 1991.

Morrell JM, Keeler KD, Noakes DE, Mackenzie NM, Dresser DW: *Sexing of Sperm by Flow Cytometry.* The Veterinary Record 2:322-324, 1988.

Mukherjee DP, Dott HM: *Effects of Egg-Yolk-Citrate and Egg-Yolk-Glycine Dilutors on the Morphology of Bovine Spermatozoa.* J Agricultural Science 55:225, 1960.

O'Donnel JM: *Electronic Counting and Sizing of Mammalian Spermatozoa and Cytoplasmic Droplets.* J Reprod Fertil 19:263-272, 1969.

Otto FJ, Hacker U, Zante J, Schumann J, Gohde W, Meistrich ML: *Flow Cytometry of Human Spermatozoa.* Histochemistry 161:652-665, 1979.

Park SK, Miller KW: *Random Number Generators: Good Ones are Hard to Find.* Communications of the ACM, 31:1192-1201, 1988.

Peter AT, Jones PP, Robinson JP: *Fractionation of Bovine Spermatozoa for Sex Selection: A Rapid Immunomagnetic Technique to Remove Spermatozoa that contain the H-Y Antigen.* Theriogenology 40:1177-1185, 1993.

Pinkel D, Lake S, Gledhill BL, Van Dilla MA, Stephenson D, Watchmaker G: *High Resolution DNA Content Measurements of Mammalian Sperm.* Cytometry 3:1-9, 1982.

Pinkel D, Garner DL, Gledhill BL, Lake S, Stephenson D, Johnson LA: *Flow Cytometric Determination of the Proportions of X- and Y-Chromosome-Bearing Sperm in Samples of Purportedly Separated Bull Sperm.* J Animal Science 60:1303-1307, 1985.

Rahlmann DF: *Electron Microscopic Study of Mature Bovine Spermatozoa.* J Dairy Science 44:1104-1105 1961.

Rens W, Welch GR, Houck DW, van Oven CH, Johnson LA: *Slit-Scan Flow Cytometry for Consistent High Resolution DNA Analysis of X- and Y-Chromosome Bearing Sperm.* Cytometry 25:191-199, 1996.

Rens W: personal communication, US Department of Agriculture, Beltsville, MD, 1997.

Roberts AM: *Gravitational Separation of X- and Y-Bearing Human Sperm Using BSA Gradients.* Nature 262:223-235, 1972.

Rudak E, Jacobs PA, Yanagimachi R: *Direct Analysis of the Chromosome Constitution of Human Spermatozoa.* Nature 274:911-913, 1978.

Saleh BE, Teich MC: *Fundamentals of Photonics.* John Wiley & Sons, Inc., New York, 1991.

Sarkar S, Jones OW, Shioura N: *Constancy in Human Sperm DNA Content.* Proc Natl Acad Sci USA 71:3512, 1974.

Sarkar S: *Human Sperm Swimming in Flow.* Differentiation 27:126-132, 1984.

Shapiro HM: *Practical Flow Cytometry.* (3rd Edn). Wiley-Liss, New York, 1995.

Sharpe JS, Schaare PN: *Flow Cytometer.* New Zealand Patent Application No. 314 169, 1997.

Skogen-Hagenson MJ, Salzman GC, Mullaney PF, Brockman WH: *A High Efficiency Flow Cytometer.* J Histochem Cytochem 25:784-789, 1977.

Steeno O, Adimoelja A, Steeno J: *Separation of X and Y Bearing Human Spermatozoa with the Sephadex Gel-filtration Method.* Andrologia 7:95, 1975.

Stovel RT, Sweet RG, Herzenberg LA: *A Means for Orienting Flat Cells in Flow Systems.* Biophys J 23:1-5, 1978.

Sweet RG: *High Frequency Recording with Electrostatically Deflected Ink Jets.* Rev Sci Instr 36:131-136, 1965.

Van Dilla MA, Trujillo TT, Mullaney PF, Coulter JR: *Cell Microfluorometry: A Method for Rapid Fluorescence Measurement.* Science 163:1213-1214, 1969.

Van Dilla MA, Gledhill BL, Lake S, Dean PN, Gray JW, Kachel V, Barlogie B, Göhde W: *Measurement of Mammalian Sperm Deoxyribonucleic Acid by Flow Cytometry: Problems and Approaches.* J Histochem Cytochem 25:763-773, 1977.

Van Duijn C, Van Voorst C: *Precision Measurements of Dimensions, Refractive Index and Mass of Bull Spermatozoa in the Living State.* Mikroskopie 27:142-167, 1971.

Van Duijn C: *Mensuration of Spermatozoa.* Bibliography, Reproduction Information Service Ltd. Cambridge 121-128, 1974.

Van Vliet RA, Verrinder AM, Gibbins AM, Walton JS: *Livestock Embryo Sexing: A Review of Current Methods, With Emphasis on Y Specific DNA Probes.* Theriogenology 32:421-438, 1989.

Windsor DP, Evans G, White IG: *Sex Predetermination by Separation of X and Y Chromosome-Bearing Sperm: A Review.* Reprod Fertil Dev 5:155-171, 1993.

Zavous PM: Sperm Separation Attempts via the Use of Albumin Gradients in Rabbits. Theriogenology 23:875-879, 1985.

Errata

The reference "Johnson *et al.* (1986)" which appears on pages 41, 53, 69, 70 should read "Johnson and Pinkel (1986)".

Page 6 In the second paragraph "Kamentsky *et al.* (1969)" should read "Kamentsky and Melamed (1969)".

Page 30 A footnote should be added to Table 3.1 for turkey sperm which states "Turkey sperm are not mammal and the sex chromosome complement is ZZ since the avian species male is homogametic".

Page 32 In Section 3.3 the technique of PCR should be referenced to GR Welch, GC Waldbeiser, RJ Wall, LA Johnson: Flow Cytometric Sperm Sorting and PCR to Confirm Separation of X and Y Chromosome Bearing Bovine Sperm, Animal Biotechnology 6:131-139, 1995. Reanalysis should be referenced to Pinkel et al. (1995) and LA Johnson, Flow Cytometric Determination of Sperm Sex Ratio in Semen Purportedly Enriched for X or Y Bearing Sperm. Theriogenology 29:265, 1988. Relative to DNA probes in situ hybridisation the following reference should be included, LA Johnson, GR Welch, K Kevanfar, A Dorfmann, EF Fugger and JD Schulman, Gender Preselection in Humans? Flow Cytometric Separation of X and Y Spermatozoa for the Prevention of X-Linked Diseases. Human Reproduction 8:1733-1739.

Page 33 In Section 3.4 the word principle in the heading should be spelt principal.

Page 35 In the second paragraph of Section 3.4.8 "Johnson (1986)" should be replaced with "Johnson *et al.* (1987a)". and the last sentence of the paragraph should have the word "surgically" removed, and have the words "...but there was no significant skewing of the sex ratio in the offspring." added at the end of the sentence.

Page 40 In Section 3.5.6 the sentence "There was no significant skewing of the sex ratio from the sorted X and Y semen inseminated by this group, either in cattle or rabbits." should be appended to the end of the first paragraph.

Page 41 Line 4 (Rens 1996) should read (Rens *et al.* 1996).

Page 41 In Section 3.5.7 a sentence should be added to the end of **1)** stating "Although this bimodal profile is shown, it does not represent X and Y sperm as the authors projected, rather it represents living motile and dead sperm."

Page 41 In Section 3.6 the first line should include a reference to Johnson *et al.* (1989) as the key reference.

Page 43 In Section 3.7 a reference to Johnson *et al.* (1989) should be added at the end of the second paragraph.

Page 43 In Section 3.7 the last paragraph should have the reference "L.A. Johnson, *personal communication*" added.

Page 70 Under the "Chinchilla Sperm" heading, MA should read MD.

Page 77 The heading of Section 5.4.2 should have the 2 and 4 transposed to read Hoechst 33342.

Page 114 In Section 7.3 the first sentence has the word "sheath" missing before the word "differential", and line 4 should read "Figure 7-4 demonstrates...".

Page 120 Johnson 1992a should be 70:(Suppl. 2) 8-18 for the complete citation.